Southeastern Geology: Volume 34, No. 3 September 1994

Editor in Chief: S. Duncan Heron, Jr.

Abstract

Academic journal published quarterly by the Department of Geology, Duke University.

SOUTHEASTERN GEOLOGY

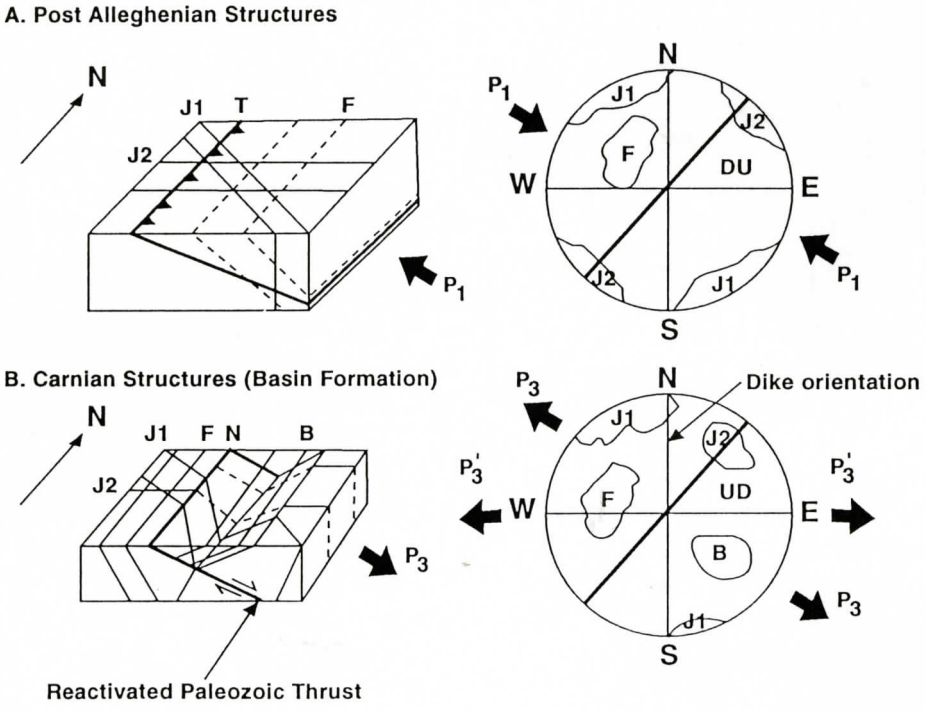

VOL. 34, NO. 3 SEPTEMBER 1994

SOUTHEASTERN GEOLOGY

PUBLISHED

at

DUKE UNIVERSITY

Editor in Chief:

Duncan Heron

This journal publishes the results of original research on all phases of geology, geophysics, geochemistry and environmental geology as related to the Southeast. Send manuscripts to **DUNCAN HERON, DUKE UNIVERSITY, DEPARTMENT OF GEOLOGY, BOX 90233, DURHAM, NORTH CAROLINA 27708**. Phone 919-684-5321, Fax 919-684-5833, E Mail heron@rogue.geo.Duke.edu. Please observe the following:

1) Type the manuscript with double space lines and submit in duplicate.
2) Cite references and prepare bibliographic lists in accordance with the method found within the pages of this journal.
3) Submit line drawings and complex tables reduced to final publication size (no bigger than 8 x 5 3/8 inches).
4) Make certain that all photographs are sharp, clear, and of good contrast.
5) Stratigraphic terminology should abide by the North American Stratigraphic Code (American Association Petroleum Geologists Bulletin, v. 67, p. 841-875).

Subscriptions to *Southeastern Geology* for volume 34 are: individuals - $15.00 (paid by personal check); corporations and libraries - $20.00; foreign $24. Inquires should be sent to: **SOUTHEASTERN GEOLOGY, DUKE UNIVERSITY, DEPARTMENT OF GEOLOGY, BOX 90233, DURHAM, NORTH CAROLINA 27708**. Make checks payable to: *Southeastern Geology.*

SOUTHEASTERN GEOLOGY is a peer review journal.

ISSN 0038-3678

SOUTHEASTERN GEOLOGY

Table of Contents

Volume 34, No. 3

September 1994

SOUTHEASTERN GEOLOGY
V. 34, No. 3, September 1994, p. 99-120

SYNERGISTIC INTERPRETATION OF MULTISENSOR GEOPHYSICAL DATA OF THE FARMVILLE TRIASSIC BASIN IN CENTRAL VIRGINIA.

ALI A. NOWROOZI AND C.G. JAMES

Department of Geological Sciences
Old Dominion University
Norfolk, Virginia 23529-0496

ABSTRACT

The Farmville Basin is one of many Triassic basins along the eastern coast of North America, and is the largest among the basins in central Virginia. Metavolcanic and metasedimentary rocks of the Paleozoic Chopawamsic Formation, as well as felsic intrusives, are the primary lithologies surrounding the basin, and Triassic sedimentary rocks occur within its trough. A detailed gravity survey was conducted along six roads that trend approximately NW-SE across the basin. In addition, aeromagnetic and aeroradiometric data from Virginia Division of Mineral Resources were used for interpretation. Geologic, gravity, magnetic, and radiometric data were used to develop a three dimensional geometry of the basin in the form of a fence diagram. All observed geophysical anomalies are the result of structures that lie within the upper few kilometers of crust. Detailed gravity modelling indicates that the basin's shape is controlled by several half-grabens with an east dipping listric border fault, and that the basin is relatively shallow. Maximum depth of the basin occurs along State Road 636 and is over 600 m. Modelling further suggests that the deepest portion of the basin is away from the western border fault, and is near the center as a result of a master fault lying underneath the basin rocks. Several igneous dikes with distinct gravity and magnetic signatures are detected which intrude the basin. The largest one is a diabase-granophyre dike observed on outcrop in the southern part of the basin with a maximum width of about 500 m.

INTRODUCTION

The Farmville Basin is one of the series of fault bounded through which were formed following the Appalachian orogeny in central Virginia. Figure 1 shows the entire Newark rift system as reported by Benson (1984). The sediments deposited in them are part of the Newark Supergroup of Early Triassic time (Cornet, 1977, Goodwin and others 1985). The Triassic basins may be suitable for oil and coal exploration, as well as, other mineral resources (Manspeizer, 1988). Several papers report on geology and geophysics of the Triassic basins in Virginia, (Wilkes, 1979, 1982, 1986; Weems, 1980; Goodwin and others, 1986; Johnson and others 1985; and Nowroozi and Wong 1989). Theories explaining the origin of the basins have been proposed by many authors (Russell, 1892; Lindholm, 1978; Ratcliffe and Burton, 1985; Swanson, 1986). Theories for the formation of smaller basins is based on the data from larger basins, such as the Newark-Gettysburg (Ratcliffe and Burton, 1985). Here, we present a three dimensional interpretation of the subsurface shape of the smaller Farmville basin based on field work and geophysical modeling and present a kinematic model for its formation.

The Farmville Basin is exposed in Buckingham, Prince Edward, and Cumberland Counties, Virginia; the basin exceeds 43 kilometers in length, and has a maximum width of 16 kilometers (Figure 2). Geologic mapping was conducted to obtain a general understanding of the lithologies and structures in the study area. The geophysical surveys provided data that were used to interpret the subsurface form and structural relationships between various

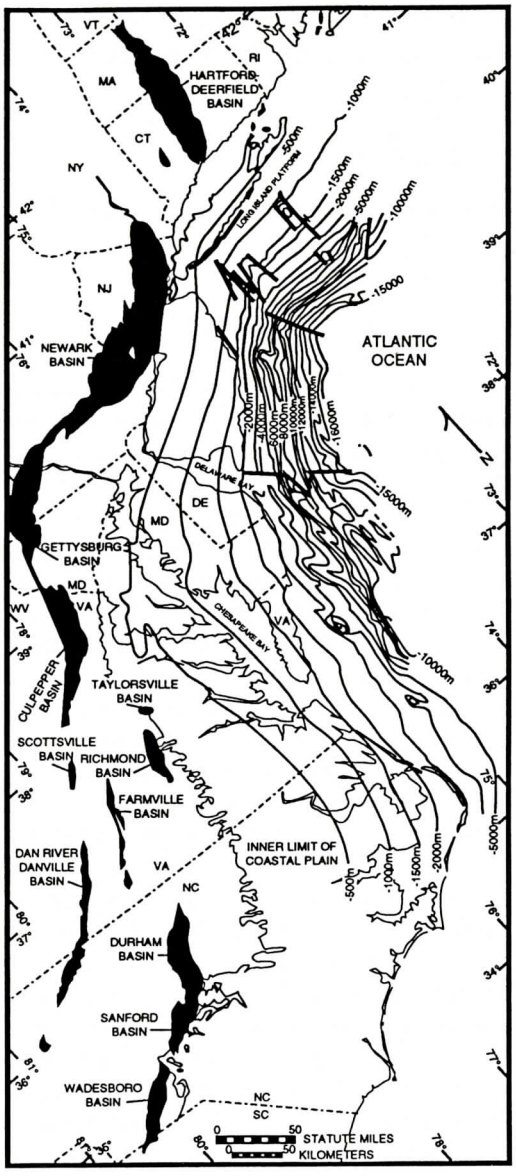

Figure 1: Map of the Exposed Newark Supergroup Basins in the Eastern United States, the basins are shown by solid black. State abbreviations are: CT= Connecticut, DE= Delaware, MA= Massachusetts, MD= Maryland, NC= North Carolina, NJ= New Jersey, NY= New York, PA= Pennsylvania, RI= Rhode Island, SC= South Carolina, VA= Virginia, VT= Vermont, WV= West Virginia; and C. H.= Cape Hatteras. Contours indicate depth of sedimentary section, (after Benson, 1984).

lithologies.

Our first objective in this work was to define the distinct shape, maximum depth, geologic structures, and geophysical features of the Farmville Basin. This was accomplished by detailed field mapping and gravity survey along six profiles on roads shown in Figure 2. Furthermore, we have used the aeromagnetic and aeroradiometric survey maps (Virginia Division of Mineral Resources, 1970a, 1970b ,1978a, 1978b) as additional constrains for interpretation. Our second objective was to develop a kinematic model for the Farmville Basin, and explain its evolution. The kinematic model presented is based on our field data, as well as information from previous studies (Johnson and others, 1985; Marr, 1980, 1981; Brown, 1969; Wilkes and Lasch, 1979).

GEOLOGICAL SETTING AND STRATIGRAPHY

The Farmville Basin as shown in Figure 1

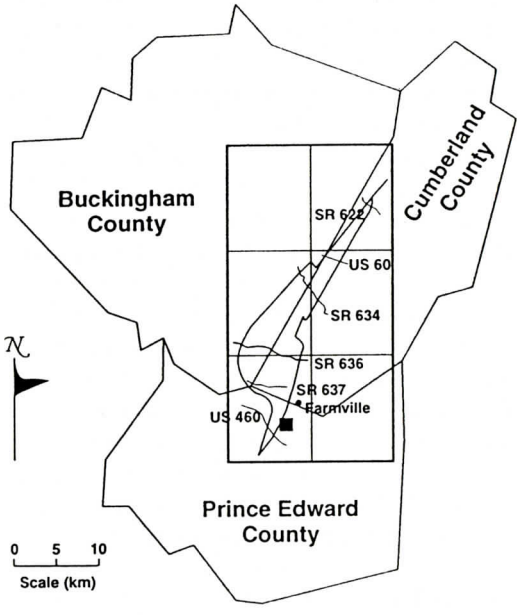

Figure 2: Farmville Basin is located in the Prince Edward, Cumberland, and Buckingham Counties in central Virginia. The positions of six gravity profiles are on the indicated highways.

Table 1: Tentative stratigraphic correlation of lithologies within the study area. The stratigraphic column used for this study is based on the work of Marr (1980, 1981), Brown (1969), and geologic mapping conducted during this investigation.

ERA	PERIOD	BROWN (1969)	MARR (1980)	Present Study
CENOZOIC	QAL	Alluvium	Alluvium	Alluvium
MESOZOIC	JR	Diabase Dikes	Diabase Dikes	Diabase/ Granophyric Diabase
	TR	Newark Supergroup	Newark Supergroup	Newark Supergroup
PALEOZOIC	ORD	Arvonia Formation	Arvonia Formation	Arvonia Formation
		Hatcher Complex	?	"Granitic" Gneisses (Hatcher Complex Equivalent ?)
	?	?	Pegmatite	Pegmatite
		Ultramafic Rocks & Hornblende Metadiorite	?	?
	C	Evington Group (?) & Rocks of Uncertain Age	Chopawamsic Formation	Chopawamsic Formation

Note: The letter abbreviations in this table are defined as follows: C-Cambrian, ORD-Ordovician, TR-Triassic, JR-Jurassic, QAL-Quaternary, and ? - Unknown

is the largest of five Mesozoic basins in central Virginia (Johnson, 1981, Goodwin and others, 1986). Rodgers (1840) was the first author to describe the various lithologies in and around the Farmville Basin. Since that time, some reconnaissance studies (Russell, 1892; Jonas, 1932; Espenshade and Potter, 1960) and more detailed work in this area (Brown, 1969; Marr, 1980) have been reported.

A geologic map of the Dillwyn 15-minute quadrangle that includes the Gold Hill 7.5 minute quadrangle was prepared by Brown (1969). A geologic map of the Willis Mountain quadrangle was prepared by Marr (1980). These two publications account for the majority of the known geology within the study area. However, the stratigraphic columns in these publications are different. Table 1 is a proposed stratigraphic column for the study area based on work of Brown (1969) and Marr (1980, 1981), as well as mapping conducted during this investigation. Rocks from oldest to youngest in the stratigraphic column are the Chopawamsic Formation, "Granitic" Gneiss Undifferentiated (Hatcher Complex), Arvonia Formation, Triassic Rocks, and Diabase/Granophyre dikes (Figure 3). These rock units are described below.

Chopawamsic

The type section of the Chopawamsic Formation lies along Chopawamsic Creek near Quantico, Virginia (Southwick and others,

Figure 3: Geology map of the Farmville Basin. This map is based on the work of Marr (1980, 1981), and Brown (1969) as well as field investigation conducted for this study.

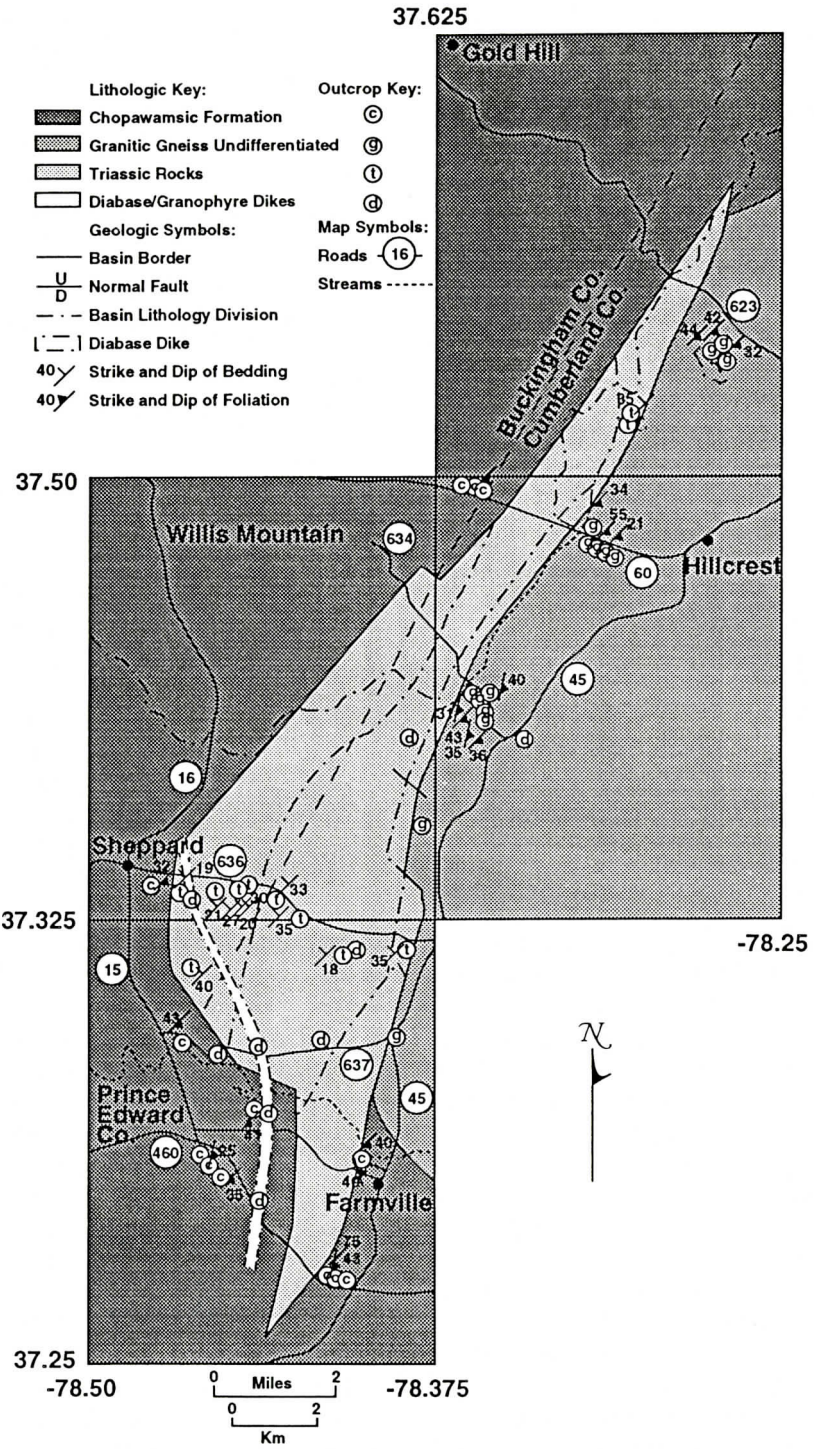

1971), and is estimated to be 1829 m thick. Conley and Johnson (1975) traced the formation from northern Virginia to the study area. Marr (1980) described the various lithologies within the Chopawamsic Formation, and defined a lower and a upper member. Only the upper member is found within the study area. The lower member has a maximum age of early to middle Cambrian, and is composed of metavolcanic and metasedimentary rocks (Tilton, 1970; Higgins, and others, 1977).

The upper member of the Chopawamsic Formation is a biotite gneiss that ranges in thickness from 3 to 31 m. The unit is interlayered with amphibolite gneiss. The biotite and amphibolite gneisses compose nearly 90% of this member. The remaining 10% of the upper member is comprised of felsic volcanics (rhyodacites), talc-tremolite schists, and ferruginous quartzites. These rocks are primarily found along the western margin of the basin, although numerous outcrops are found farther to the south. The following descriptions of the above rocks units are from Marr (1980, and 1981) with modifications based on field observation. The biotite gneiss is medium to fine-grained, moderately foliated, and light gray to gray. Quartzofeldspathic bands within this unit are interlayered with biotite layers. Some of the biotite layers contain amphibole. Composition of this unit ranges from granitic gneiss to biotite-quartz-feldspar gneiss. This unit is not resistant to weathering and occupies areas of low topography. Outcrop of the biotite gneiss is predominantly limited to the Willis Mountain and Farmville quadrangles. Fresh outcrops contain pegmatitic bands ranging in size from a few cm to nearly 0.5 m. The pegmatitic bands are a distinctive feature of this unit. A few quartz veins are concentrated in some areas. This unit usually displays low magnetic, intermediate gravity, and low radiometric values in comparison to the surrounding rocks (Johnson, 1981), and grades into an amphibole gneiss. Table 2 gives the geophysical characteristics of various lithologies.

The amphibole gneiss is medium to coarse-grained, banded, and greenish-black to black. The banding in this unit is composed of tremolite-cummingtonite or hornblende-cummingtonite and quartz calcic oligoclase, biotite, epidote, and garnet. Talc-tremolite schistose bodies range in composition form talc-tremolite schist to actinolite-chlorite schist. This unit is generally found west of the basin and is more resistant to weathering than the biotite gneiss occurring in areas of rolling topography. The outcrop of this unit is often resistant to weathering. Minor folds are common, but banding is not as distinctive in this unit as in the biotite gneiss. Light-green quartz-epidote lenses are present. High magnetic and gravity values, and low radiometric values are the geophysical characteristics of the unit.

Granitic-Gneiss Undifferentiated

This unit is thought to be the equivalent of the Hatcher Complex, and Mose (1980) assigns an Ordovician age of 454 $\pm$ 9 Ma to this unit. Surface exposures occur in the northern and eastern portions of the study area. Generally, these rocks are medium grained, with strong lineation, and light-gray to tan. The term "granitic" was used to describe a group of metaintrusive rocks ranging in composition from granite to quartz-diorite. The gneisses have low resistance to weathering, and are found in areas of low topography. In the field, the quality of outcrop of this unit ranges from highly weathered to fresh, and is strongly banded and foliated. When weathered, the unit looks very similar to the granitic gneisses of the Chopawamsic Formation. Geophysical characteristics include low magnetic and gravity values, and high radiometric values. Brown (1969) indicates that basal conglomerates of the Arvonia Formation uncomformably overlie the granitic intrusives, and therefore, the Arvonia is the younger of the two lithologies.

Arvonia Formation

Fossils indicate that the Arvonia Formation was formed during the Upper Ordovician and ranges in age from 440 to 460 Ma (Mose,

Table 2: Geophysical characteristic of various lithologies.

ERA	PERIOD	GEOPHYSICAL CHARACTERISTICS OF LITHOLOGIES WITHIN STUDY AREA
MESOZOIC	TR–JR	**DIABASE/GRANOPHYRIC DIKE** 1. High Magnetics 2. High Gravity 3. Low Radiometrics 4. density = 2.88 g/cm^3
	TR	**TRIASSIC ROCKS** 1. Low Magnetics 2. Low Gravity 3. Low Radiometrics 4. density = 2.55 g/cm^3
PALEOZOIC	ORD	**"GRANITIC GNEISS"** 1. Low Magnetics 2. Low Gravity 3. High Radiometric 4. density = 2.775 g/cm^3
	C	**CHOPAWAMSIC FORMATION** 1. High Magnetics 2. High Gravity 3. Low Radiometrics 4. density = 2.845 g/cm^3

Note 1: The letter abbreviations in this table are: C-Cambrian, ORD-Ordovician, TR-Triassic, and JR-Jurassic.

Note 2: The terms High, and Low are relative terms. In other, words they are relative to the surrounding rock units. For example, if Triassic rocks were in lithologic contact with the Chopawamsic Formation then magnetic, gravity, and radiometric readings of the two units would display the characteristics in this table.

1980; Mose and Nagel, 1983). Near the study area, this formation consists of: quartz-mica schist with interlayered micaceous quartzite and quartz mica conglomerate, quartzite and kyanite quartzite, and porphyroblastic garnet mica schist. These rocks are found in the extreme northwestern part of the study area. Marr (1980) described the conglomeratic quartz-mica schist as medium to coarse grained, moderately foliated and lineated, light-gray to gray schist with blue quartz found in some conglomerates. Kyanite occurs locally as massive lenses and can make up as much as 30% of the unit. The quartzite/kyanite unit is medium to coarse-grained, banded, and is light-yellow to gray (Marr, 1980). This unit is resistant to weathering and exposed along NE-SW trending linear ridges formed by isoclinal synclines. The highest magnetic values within the study area are found within this formation. The Arvonia Formation has intermediate radiometric and gravity values as compared to other lithologies within the study area. This formation is not used as a unit in the gravity models produced in this study, because it lies outside the surveyed area.

Newark Supergroup

Unconformably overlying the metamorphic basement are the Triassic rocks of the Newark Supergroup. Basal strata are Carnian in age as determined by Robbins (1985). This age is based on pollen and spore data found in the basin. This places rocks of the Farmville Basin, along with rocks in the Richmond and Taylorsville basins, as the oldest rocks in the Newark Supergroup (based on palynological

data; Cornet, 1977). The rocks show a general fining away from the basin perimeter. According to Smoot (1985), this is an indication of a closed basin, where all surface drainage and groundwater entering the basin evaporates. This is not to say that the basin remained closed throughout its entire depositional history, however.

Czechowski (1982) suggested that the paleoenvironment during deposition of the Newark Supergroup strata was more arid than the present climate. His conclusions are based on relative percentage of feldspar and lithic fragments in the Triassic rocks as compared with Quaternary stream sands in the basin. He also showed that sediments within the basin have undergone less than 45 km of transport. Breccia-conglomerate, arkosic conglomerate, arkosic sandstone, and siltstone/shale are the four lithologies found in the basin.

The breccia-conglomerate is brown to reddish-brown rock with angular to subangular clasts ranging from pebble to boulder size. In general, clasts are comprised of metamorphic rocks from the Chopawamsic and Arvonia Formations, and "granitic" gneiss undifferentiated. Clast imbrication indicates that transportation of sediment comprising this unit was from the northwest (Marr, 1981; Czechowski, 1982).

The arkosic conglomerate is medium-grained and light brown to light gray , and has an arkosic sandstone matrix. Clasts are subangular to subrounded ranging from pebble to boulder size, and are predominately metamorphic (Johnson and others, 1985).

The arkosic sandstone is medium-grained, thick-bedded, and brown to light-brown with interlayers of red-brown sandstone, siltstone, and shale (Johnson, and others, 1985). The source of this unit is thought to lie east of the basin (Czechowski, 1982). Siltstone-shale is the youngest sedimentary unit in the basin. These rocks are light-gray and are interbedded with red-brown sandstone, quartz-pebble conglomerate, and dark-gray mudstone and coal. This unit is thought to have been deposited in a lacustrine environment (Czechowski, 1982).

The Mesozoic rocks are distinctive because of their low gravity, magnetic, and intermediate radiometric values (Table 2). These rocks are cross-cut by diabase/granophyre dikes, which have a distinct magnetic signature described below.

Dikes

The diabase dikes are the youngest rocks in the area and are thought to be late Triassic to Jurassic in age (Marr, 1981). The largest exposed dike is shown completely in Figure 3, the outcrop position of other dikes are indicated by letter "d" in this figure. These dikes are medium to fine-grained, and light-gray to dark-gray. Several dikes have been found to contain granophyres (Rogan, 1993). The granophyres are found predominantly in larger and thicker dikes. Compositionally, larger dikes are diabasic along their margins, with

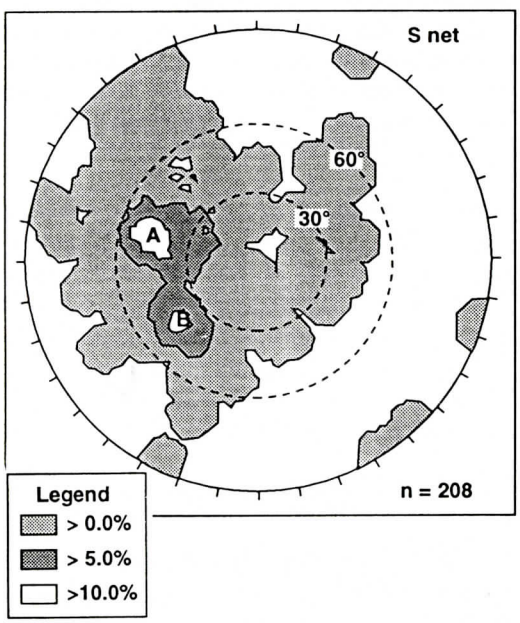

Figure 4: Contour plot of 208 poles to foliation from this study and the geologic map of Marr (1980). Contour plot of poles to foliation plotted as percent of per one percent of total area. The maxima represent foliation planes located at N15^{o}E, 35^{o} SE, and N40^{o}W, 35^{o} NE. Pole maxima are separated by 35 degrees azimuth. The distribution of pole clusters shows that the approximate average foliation plane strikes nearly north-north-east and dips to the south east.

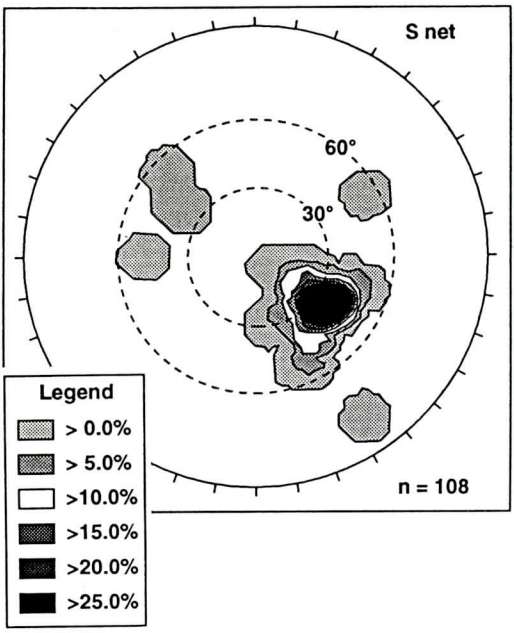

Figure 5: Contour plot of 108 poles to bedding taken in the Farmville Basin. The stereonet projection is a contour plot of the poles to the bedding plotted as percent per one percent of total area, and indicates that bedding in the basin has an average strike of N45^{O}E and dips 30^{O}NW.

increasing granophyre percentages towards their centers. Two sets of dike trends are recognizable in the area. A majority of the dikes trend between N12^{O}W and N25^{O}W, with a second minor set trending between N and N20^{O}E. Dikes in the area cross-cut Triassic rocks and the basin margin, thus they are younger than the Triassic sedimentary rocks.

STRUCTURES

Geological information from publications of Brown (1969) and Marr (1980) as well as geological data collected in this study are presented in Figure 3. This figure also includes the observed direction and dip of foliations, and beddings. Interpretation of geophysical data must be consistent with the known geological data; thus, it is important to understand the structural fabric of the basin prior to any geophysical interpretation. Previous geological studies discuss three phases of folding (Marr, 1980). The cumulative effect of these folding phases is the NE regional trend. The distribution of the poles for the planes of foliation, bedding, and joints observed in the Paleozoic or Triassic rocks are discussed below.

Foliation

Figure 4 is a compilation of 208 foliation measurements from the study area. A program developed by Deker (1988) was used to produce the projections. Two foliation pole maxima are shown on the stereonet, and are separated by 35^{O}. The dominant pole concentration ('A') is in the NW quadrant. The dominant pole is representative of foliation that has an average strike of N15^{O}E and dip of 35^{O} SE, the second dominant pole ('B') is representative of foliation that has an average strike of

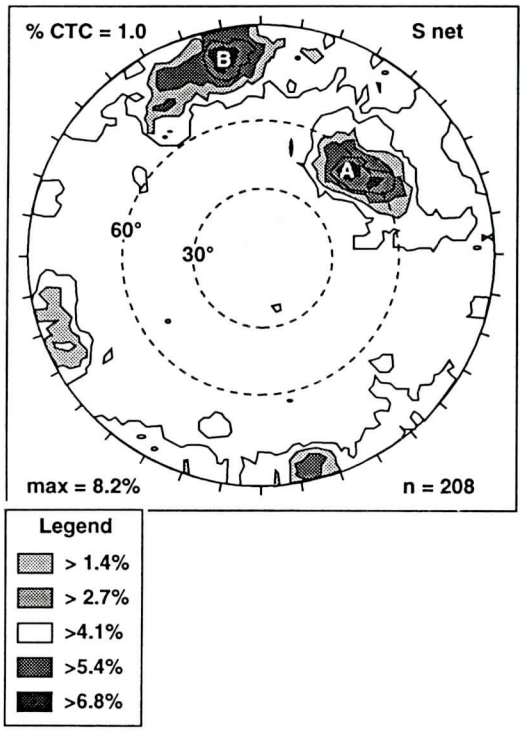

Figure 6: Contour plot of 208 joint poles plotted as percent per one percent of total area. The plot reveals two joint sets at N40^{O}W, 50^{O} SW, and at N70^{O}E, 80^{O} SE.

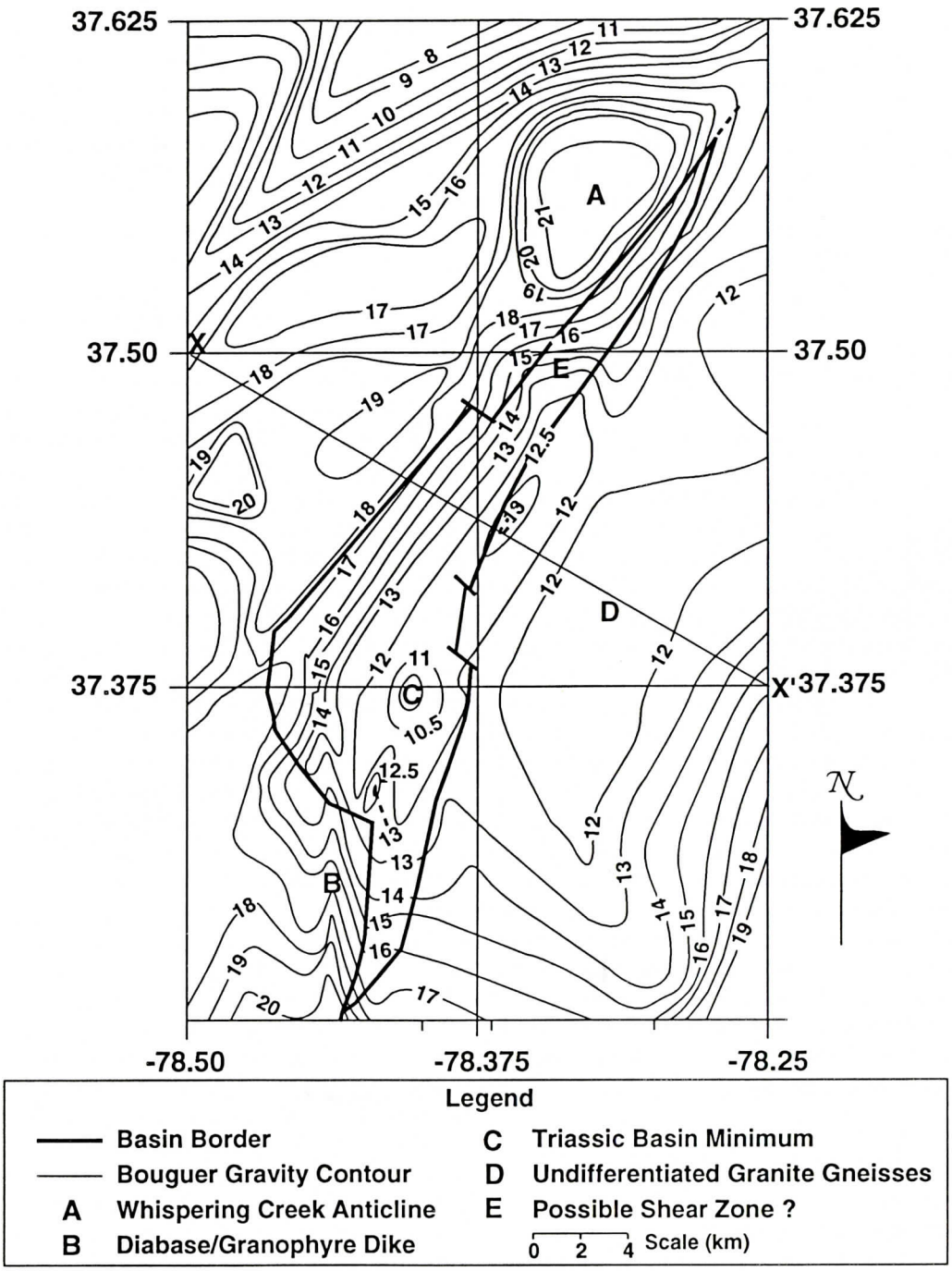

Figure 7: Simple Bouguer gravity anomaly of the Farmville Basin based on over 700 new measurements and the previous work of Johnson and others (1985). Letter A-E on this Figure as well as Figure 8, 9, 10, 11 and 12 are referring to, A: Whispering Creek Anticline; B: Diabase-granophyre dike; C: Deepest part of the basin; D: Granitic-Gneiss Undifferentiated; E: Possible shear zone.

N40°W and dip of 35° NE. The average distribution of foliation shows nearly a north-south orientation and dips toward the east.

Bedding

Poles of bedding within the basin show little variation (Figure 5). Bedding has an average strike of N45°E and dip of 30° NW. Along profile sections, dip variation show a pattern of steep to shallow to steep. This is best documented along the State Road 636 profile (Figure 3).

Joints

Two dominant systematic joint sets are found within the area (Figure 6). The joint set A with poles in the NE quadrant of the stereonet has an average strike of N4O°W and an average dip of 50° SW. The joint set B lies near the perimeter of the net in the NW quadrant. This joint set has an average strike of N70°E and dip of 80° SE. The contour projection indicates that a third less dominant joint set may be present. This joint set has an average strike of N20°W and has a near vertical dip.

The geological information in Figure 3 and the dominant direction of the foliations and joints are consistent with our interpretation of the basin structural boundaries which will be presented later. We assert that the main faults forming the western edge and bottom of the basin moved along weak surfaces indicated either by the foliations or contacts with a dominant NNE-SSW direction, and dip gently at depth toward the east.

GEOPHYSICAL INFORMATION

Several geophysical studies were conducted within the area of study by the Virginia Division of Mineral Resources (VDMR, 1970a, and 1970b). These are the 15-minute quadrangle aeromagnetic map of the Farmville and Dillwyn regions, the 15 minute quadrangle aeroradiometric maps of the same areas (VDMR, 1978a, and 1978b), and a gravity survey of the basin (Johnson and others, 1985). The airborne surveys had flight line spacings of 0.8 kilometer at 152 meters above ground level. The regional gravity map (Johnson and others, 1985) covered approximately five 15-minute quadrangles contains 1202 gravity stations that includes the only published lithologic map of the entire Farmville Basin.

Gravity Data

The Bouguer gravity anomaly map of the Farmville Basin (Figure 7) is prepared from two sets of gravity data. The first contains 700 detailed gravity readings taken along six roads at station spacings of about 61 meters (Figure 2) by Lacoste and Romberg model "G" geodetic gravity-meter which has a reading accuracy of ± 0.01 milligal. Each profile was surveyed and station elevation was determined with an accuracy of a few centimeters James (1991). All readings from this data set either lie within the basin, or within 1.609 km distance from the basin's border. Over 700 additional gravity readings were obtained from data of Johnson and others (1985). These readings lie mostly outside the 1.609 km of the basin's border. Thus, the gravity map is based on over 1400 readings and defines both regional and local anomalies.

Regionally, a general pattern of high gravity anomalies (21 to 19 mgals) is evident on the west side of the basin's border, low anomalies (12 to 13 mgals) occur on the east side of the basin's border, and finally the lowest gravity anomaly (10.5 mgals) occurs within the basin. In addition, a strong NE-SW regional trend is evident on the gravity map which corresponds to the western border fault. Furthermore in a NW-SE direction the regional trend gravity gradient becomes dominant across the basin. Letters A-E, on the map designate some specific gravity anomalies for references which will be discussed later.

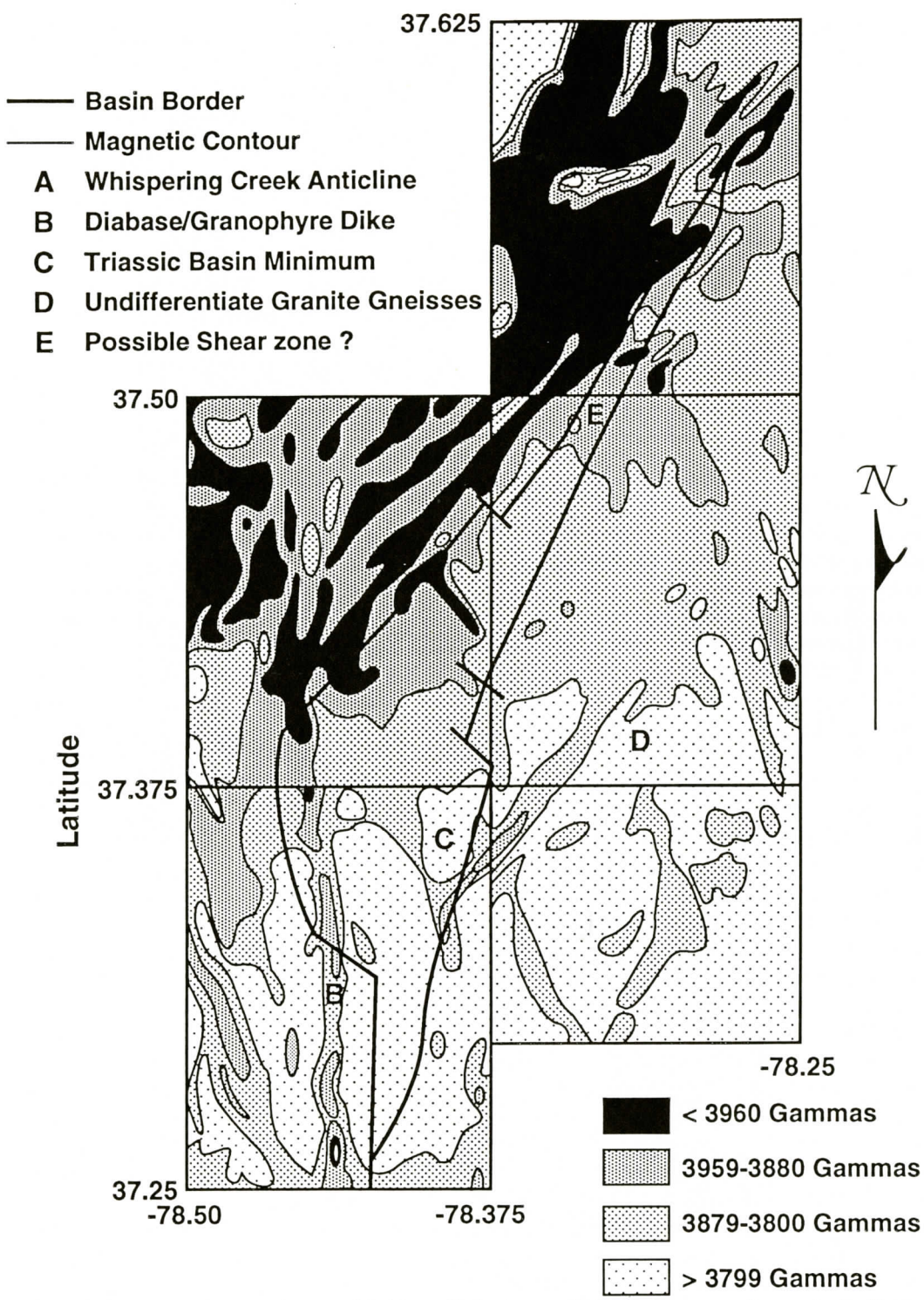

Figure 8: Aeromagnetic anomaly map of the Farmville basin compiled from Aeromagnetic map for the Farmville and Dillwyn 15-minute quadrangle maps. After Virginia Division of Mineral Resources (1970a and 1970b).

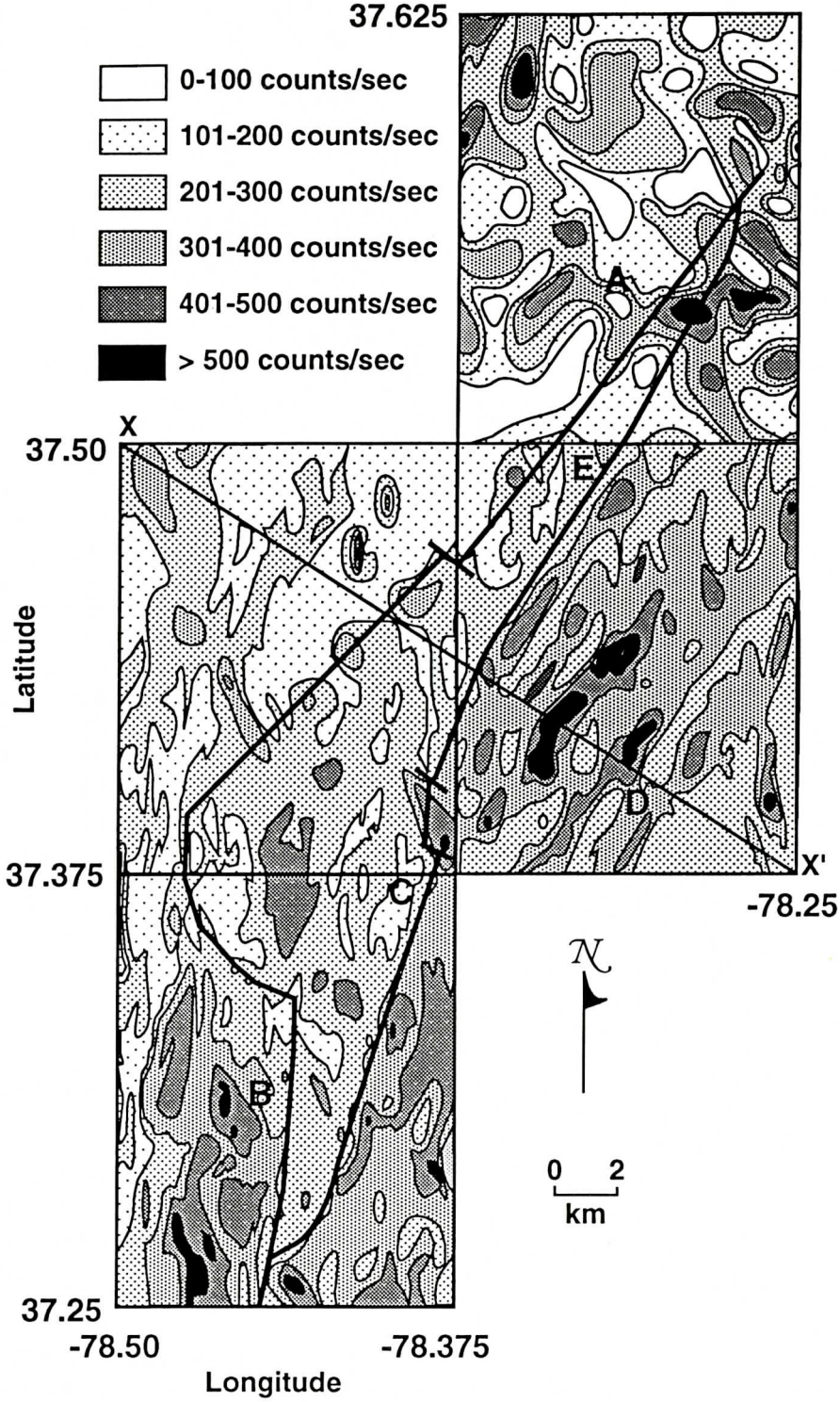

Figure 9: Aeroradiometric map of the Farmville basin compiled from aeroradiometric maps for the Farmville and Dillwyn 15-minute quadrangle maps. After Division of Mineral Resources (1978a and 1978b).

Magnetic Data

The aeromagnetic map (Figure 8) is compiled from VDMR (1970a, and 1970b) publications. Magnetic anomalies in the area decrease in a NW-SE transverse. In addition, the anomalies indicate a strong NE-SW trend corresponding to the western border fault. The narrow linear features with nearly north-south orientation indicate the intrusive diabase dikes; again, several features are indicated by letters A to E for further discussion in the text.

Radiometric Data

VDMR (1978a, 1978b) aeroradiometric 15 minute maps, were used for interpretation of the basin's boundary (Figure 9). Three distinct domains can be identified on the map. The radiometric values across a NW-SE view over the basin indicate that anomalies west of the basin have a range of 100 to 200 count-per-second (cps), while anomalies generally have a range of 300 to 400 cps in the basin, and are higher than 400 cps east of the basin. In contrast to the gravity and magnetic maps which nicely marked the western border of the basin, the radiometric data marked very clearly the eastern border of the basin.

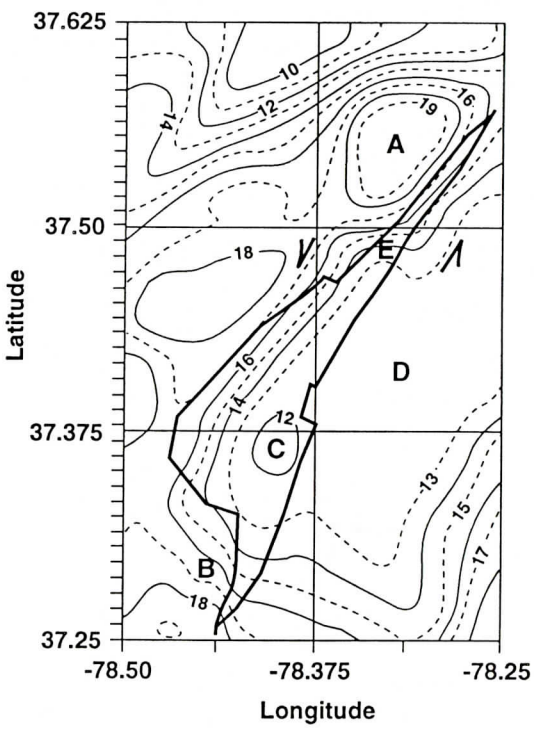

Figure 10: Upward continuation of the Bouguer gravity anomaly field at level of 0.64 km. A comparison of this Figure with Figure 6 indicates that at 0.64 km level two local highs indicated by the 13 mgals contours have been lost; these are very shallow features of the basin.

GEOLOGIC INTERPRETATION

Regional Features

Gravity and magnetic maps are based on potential field measurements which yield a non-unique interpretations. Moreover resolving power and depth of penetration depend on spacing interval between stations and total length of the surveyed cross section respectively. Our station interval is 61 meters , thus we believe that any dike with a width of more than 122 m is probably detected, our depth of penetration varies however, as length of profiles are different, we have modeled to a depth of 3 km for consistency. Both gravity and magnetic measurements, however, are sensitive to the horizontal differences between physical properties and geometries of subsurface structures. Unlike gravity data, however, magnetic values measure mostly near surface features, where rock temperature is less than the Curie temperature (Dobrin and Savit, 1988); at maximum depth of 3 km which was used for modeling, we believe rock temperature is less than the Curie temperature of magnetic minerals contained in the rock. The radiometric survey on the other hand is sensitive to the presence of radioactive elements such as uranium and thorium and radioactive isotope of potassium. The radioactivity of this area is dependent on the concentration of radioactive elements initially present and the changes that the rock has undergone. Metamorphism, weathering, sedimentary diagenesis and erosion are important factors in re-distribution of radioactive ele-

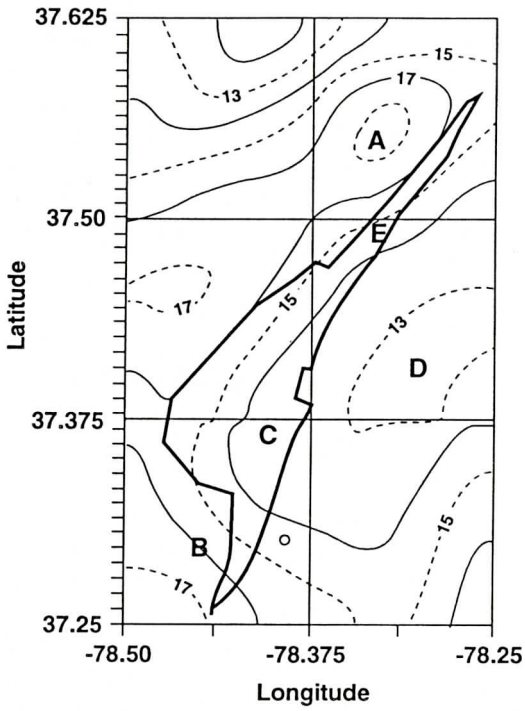

Figure 11: Upward continuation of the Bouguer gravity anomaly field at level of 2.89 km. At this level only the NE-SW trending gravity gradient associated with the western border fault and two closed 17 mgals contour lines outside the basin are observed, but anomaly marked by letter C inside the basin on Figure 7 is lost. Thus basin is relatively shallow.

ments. To find a reasonable subsurface model, geological data as well as geophysical information must be included in modeling processes.

A wealth of information about the regional geology is contained on the gravity map (Fig. 7). Any NW-SE (X-X') profile on the gravity map shows distinct differences in gravity values, leading to the conclusion that structure and densities of lithologies along such a profile vary. This poses the question, whether the variations are a result of shallower local structure or deeper crustal features.

To address this problem, upward continuation of the gravity field was calculated. The details of the method used here are discussed by Tsuboi (1959) Bhattacharyya (1965), and Agarwal (1968). The main idea of upward continuation is filtering out the gravity effect of the shallower structures by their spacial frequency, and preserving selectively the gravity effect of the deeper structure. This is done by recalculating the gravity anomalies at several levels with higher elevations than the ground level at which gravity surveys was performed. The upward continuation was done at 0.64, 2.89 and 8 km levels; the results are shown in Figures 10, 11, and 12, respectively. This resulted in attenuation of anomalies related to the shallower features and isolation of gravity anomalies attributed to the deeper regional structures. At 0.64 km, two local high anomalies are lost: one is within the southern part of the basin indicated by the 13 mgals contour line and, the other one is in the northeastern part of the basin again indicated by the 13 mgals contour line (compare Fig. 7, and 10). However, another local low, indicated by the 10.5 mgals contour line and letter C has been changed only slightly. Furthermore the NE-SW gravity trend associated with the western border fault of the basin is still highly visible. At 2.89 km only the

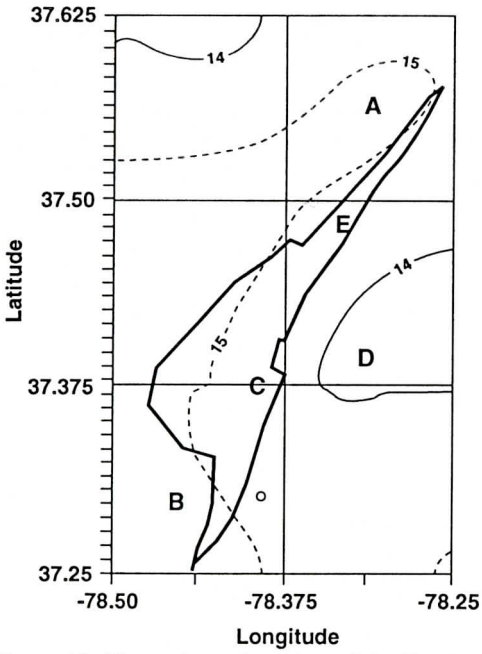

Figure 12: Upward continuation of the Bouguer gravity anomaly field at level of 8 km. At this level barely the NE-SW trend associated with the western border fault is observed, thus this is the most pronounced feature of the basin.

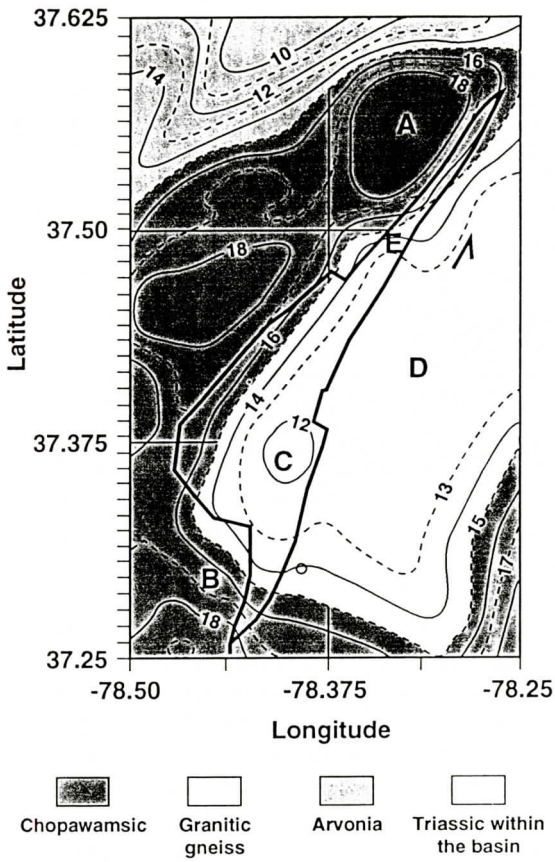

Figure 13: Interpretation of the subsurface basement of the study area using the upward continuation of the gravity field. We have chosen the 15 mgals contour line as an approximate border line between various lithologies, because this was observed at the 8 km level. This map is very close to the map of Marr (1980) and Brown (1969).

NE-SW gravity trend together with two other closed 17 mgals contour lines outside the basin are observed, but the shallower anomaly indicated by the letter C is lost (Figure 11). At 8 km, only the NE-SW trend is barely apparent. the other anomalies are not seen. Thus, qualitative analysis of the upward continuation of gravity field indicates that the basin is indeed very shallow; the most pronounced feature of the basin is its western border fault, and the deepest part of the basin which is associated with the area marked by the letter C.

The magnetic map (Figure 8) like the gravity map, shows the strong NE-SW trend of the magnetic gradient associated with the western border fault. In addition, similar to the gravity anomaly data, the magnetic values generally decrease along NW-SE (X-X') profiles. This again implies that magnetic susceptibilities and geometry of the rocks along the profile are different. This additional information suggests that there are distinct lithologic breaks underneath and outside of the basin. Furthermore, the position of one dike which was observed on the surface on the southwestern side of the basin is marked by a well defined, narrow and elongated anomaly that is oriented nearly N-S. Several other linear anomalies outside of the eastern border of the basin are suspected to be dikes also.

Both gravity and magnetic anomaly maps show a definite change in the density and magnetic susceptibilities of rocks along NW-SE profiles. In addition the aeroradiometric map (Figure 9) indicates that the count rates for decay of the radioactive elements in the rocks across this profile is also different; the count rate varies from mostly 201-300 counts/s within the basin to 300-400 counts/s outside its eastern border.

The observations reported here are supported by the geology. Table 1 shows that there are several distinct lithologies in the study area. The geophysical properties of these rocks are listed in Table 2, and the values are useful in approximating the regional surface geology. For example, using the gravity map (Figure 7) a general set of lithologic boundaries can be drawn. Assuming the 15 mgals contour in the upward continuation map is a lithology break, it is possible to give a preliminary and tentative basement map for this area using the work of Marr (1980) and Brown (1969) as guides. The 15 mgals contour was chosen as the reference contour because it was present on the 8.00 km continuation map (Figure 12), this was interpreted as a regional trend. Figure 13 shows our interpretation using four distinct lithologic groups. These groups from oldest to youngest are: Chopawamsic Formation, "granitic" gneiss, Arvonia Formation, and Triassic rocks.

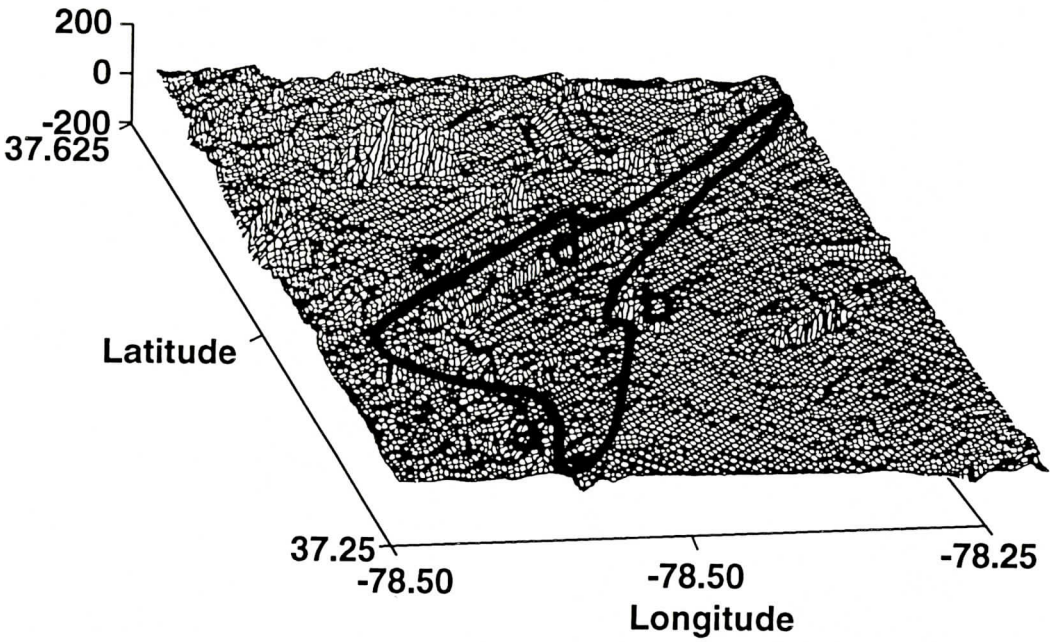

Figure 14: A three dimensional view of the second derivative of Bouguer gravity field over the Farmville Basin. Letters a-d indicate various structures; a: dike; b: probable dike; c: mylonite; and d: probable mylonite.

This map is very close to the detailed map of Marr (1980) and Brown (1969). Folds, foliation, bedding, and joint measurements all have concentrations of poles whose average strike lies within 25 degrees of the NE-SW regional trend. The dominant foliation pole concentration has an average strike of N15^{O}E and dips 80^{O} SE.

Local Features

As discussed before, examination of the gravity and magnetic maps indicate several features labeled A-E. The circular high marked 'A' is in excess of 21 mgals. This high is attributed to the Whispering Creek Anticline (Brown, 1969). A narrow high amplitude feature marked 'B' on the gravity map is a diabase/granophyre dike that exceeds 488 meters in width across U.S. Highway 460E. At location 'C', the gravity values decrease below 10.5 mgals. It is at this point where the deepest portion of the basin is believed to exist. The elliptical gravity low 'D' is typical of batholiths intrusive bodies, Bott and Scott (1964). An unusual gravitational anomaly, marked 'E' may be interpreted as a remanent of a shear zone or a change in the strike of the border fault at depth. This deduction is made from the 'Z' pattern displayed by the gravity contours (Figure 7). If shear zone the 'Z' pattern indicates a left lateral sense of shear motion.

High frequency magnetic values indicate the presence of heterogeneous magnetic sources, perhaps igneous dikes and a basin that is relatively shallow. Linear magnetic features present on the magnetic map (Figure 8) are probably caused by diabase/granophyre dikes. The area marked 'B' and the linear high east of 'C' on the magnetic map are directly related to large dikes. The low marked 'C' on the magnetic map is attributed to the deepest part of the basin.

Two local anomalies are common to both the gravity (Figure 7) and magnetic (Figure 8) maps. The first feature is the gravity and magnetic lows found on the eastern margin of the Farmville Basin, marked 'C'. The second feature common to both maps is a nearly N-S anomaly which aligns with a diabase/granophyre dike marked 'B' on both maps.

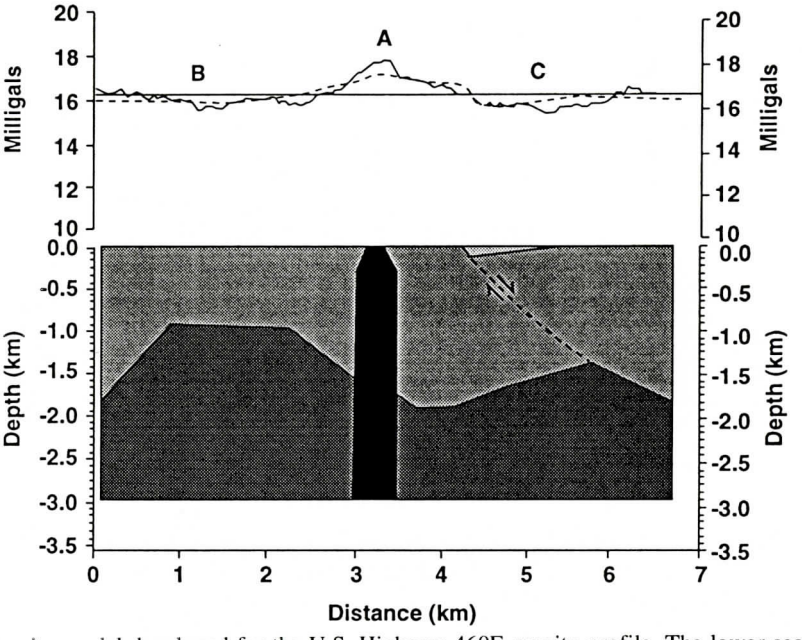

Figure 15: Gravity model developed for the U.S. Highway 460E gravity profile. The lower section is the interpreted geological model; the upper section gives the observed and the calculated Bouguer gravity anomalies. A: diabase-granophyre dike; B: granitic gneiss; C: Triassic basin. Arrows indicate the direction of displacement. Legend for the units in Figure 15-20 are: Triassic rocks: Light density dots; Chopawamsic Formation: Intermediate density dots; Granitic gneiss: High density dots; dikes: Black area. Furthermore in Figure 15-20 solid lines and dash lines give the observed and the calculated anomalies respectively.

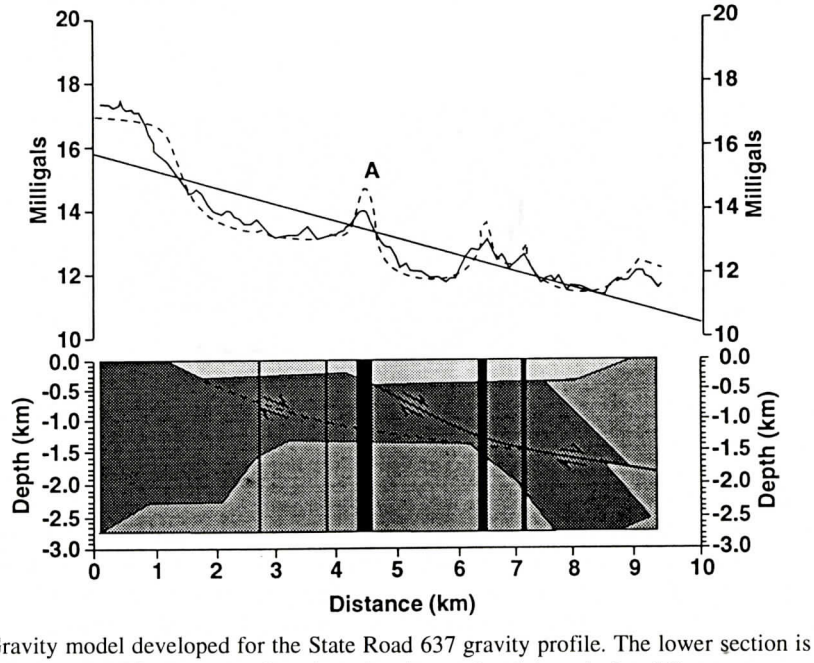

Figure 16: Gravity model developed for the State Road 637 gravity profile. The lower section is the interpreted geological model. The upper section gives the observed and the calculated Bouguer anomalies. A is position of the same diabase-granophyre dike seen on Figure 15.

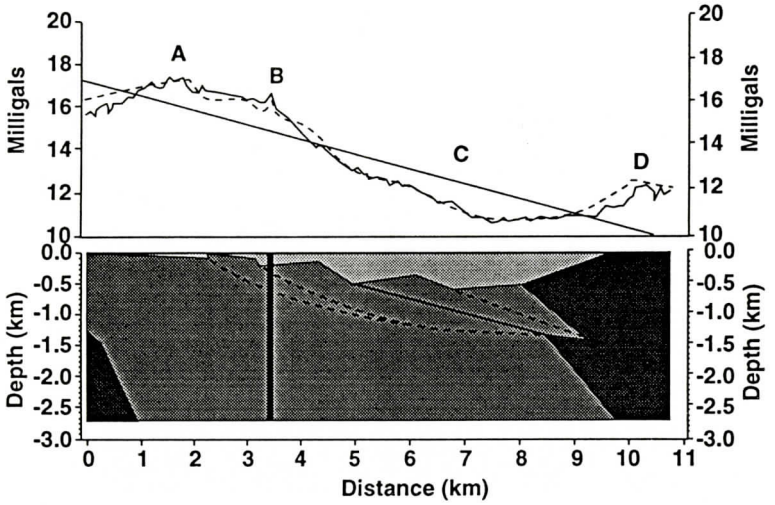

Figure 17: Gravity model developed for the State Road 636 gravity profile. The lower section is the geological model. The upper section gives the observed and the calculated Bouguer anomalies. A: Chopawamsic formation; B: Diabase-granophyre dike; C: Triassic basin; D: Granitic Gneiss.

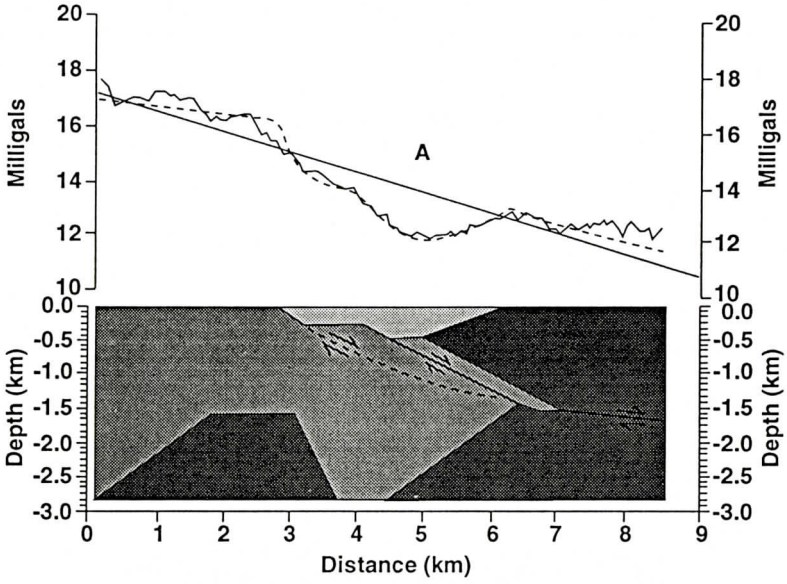

Figure 18: Gravity model developed for the State Road 634 gravity profile. The lower section is the geological model. The upper section gives the observed and the calculated Bouguer anomalies. A: Triassic basin.

It is possible to enhance the shallower structure by examining the first and second derivatives of the potential field data, (Telford and others, 1990). Figure 14 is the second derivative of the gravity field which has several interesting features, labeled by the letters a to d. The linear feature 'a' starts outside the basin and enters its western portion; it is a dike based on field observation. The other linear feature marked 'b' that starts from eastern margin of the basin and moves outward is also believed to be a dike. On the basin margin and inside the basin are linear highs marked 'c' and 'd' respectively. There is field evidence to support that

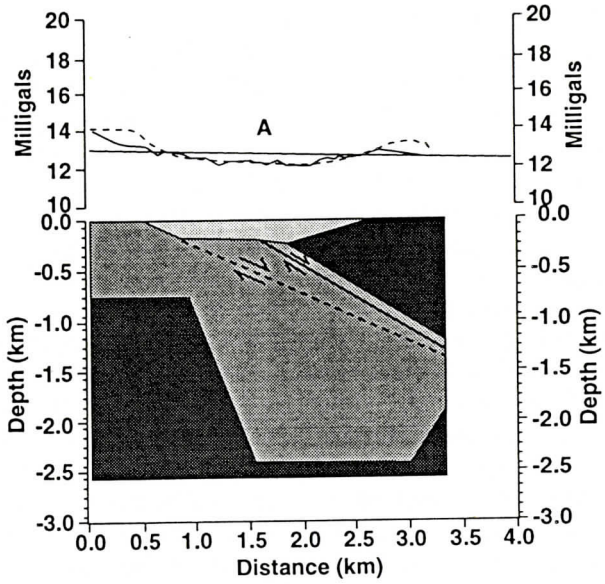

Figure 19: Gravity model developed for the U.S. Highway 60 gravity profile. The lower section gives the geological model. The upper section gives the observed and the calculated anomalies. A: Triassic basin.

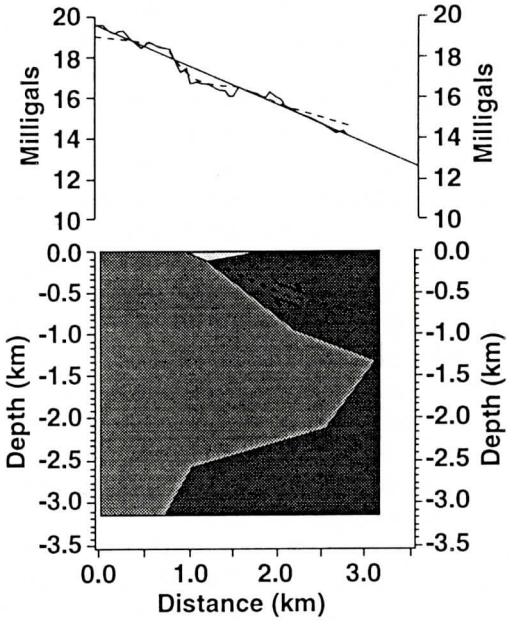

Figure 20: Gravity model developed for the State Road 622 gravity profile. The lower section gives the geological model. The upper section gives the observed and the calculated anomalies.

feature 'c' is due to a mylonite zone, Marr (1980). Inside the basin, the feature 'd' is also believed to be a mylonite zone; however, no field evidence was found to prove or disprove this hypothesis. No diabase outcrop was found in the vicinity of these highs, eliminating the possibility that linear highs in the basin are a result of diking.

INTERPRETATION AND GRAVITY MODELING

In Figure 2 we presented the position of the six detailed gravity profiles which are used for modeling the subsurface structures. Discussion of the models will begin with U.S. Highway 460E and continue north, ending with State Road 622. Field procedures and methods of data reduction are discussed by Nowroozi and Wong (1985). Modeling techniques are similar to those discussed by Talwani and Heirtzler (1964) and Talwani (1965). The lithologies used in the models are described in Table 2. Each modeled profile consist of two sections. The upper section is a plot of the observed and theoretical Bouguer anomalies. The lower section is the geological model that produced the theoretical curve shown on the upper section. The regional gravity gradient is represented by the solid line on the upper graph. The regional gradients are related to the deeper structures. The term "residual" is used to describe the variation of the observed gravity with respect to the regional gradient. In modeling we keep in mind the basin geometry, the positions, the dips, and the strikes of faults and dikes as well as their density contrast with respect to the country rocks.

Models indicate that two sets of faults are present in the study area. Master faults (solid lines on the lower graph on Figures 15-20) are believed to be reactivated Paleozoic faults. The greatest displacement occurred along such faults in the study area. Splay faults (dashed lines on the lower graph) are believed to be Mesozoic in age, and are thought to have formed along existing planes of weakness in the structural grain of the basement rocks. The relative displacement of each fault is shown by the arrows. Faults are drawn so that the models approximate a balanced cross-sections.

U.S. Highway 460E Profile

U.S. Highway 460E crosses the southern portion of the basin. Figure 15 is the gravity model produced for this profile. The profile is 6705 m in length and is modeled to a depth of 3657 m, but a model depth of 2800 m is shown for this profile to keep uniformity between profiles. The anomaly marked on the profile is attributed to a diabase/granophyre dike, as shown in the model. Location of a dike at this point is supported by an outcrop found in field along U.S. 460E (Figure 3), as well as the geomagnetic map (Figure 8) and the second derivative map (Figure 14) which were discussed previously. In outcrop, the dike is at least 305 m in width. Modeling indicates that this width may increase to 488 m in depth. Residual lows, marked 'B' and 'C', occur on both sides of the two mgals high. The residual low 'B' is interpreted to be the result of the "granitic" gneiss undifferentiated lying 305 meters below the surface. Triassic rocks of the basin are responsible for the low marked 'C'. Modeling indicates that the Chopawamsic Formation is present east of the basin. Width and depth of the basin are 1402 m, and 91 m, respectively. The length of the modeled basin is greater than that suggested by Johnson and others (1985). Basin width along this profile is based on the soil map of Prince Edward County (Henery and others, 1949). The western border fault of the basin is defined as a splay fault. This fault dips 35^{o} SE, at the surface, and decreases with depth. A 10^{o} to 15^{o} difference exists between the average dip of foliation and the splay fault. The fault is shown to have normal slip displacement. Palinspastic reconstruction of this profile suggests that 5% extension has occurred.

State Road 637 Profile

State Road 637 is 3.2 km north of U.S. Highway 460E (Figure 16). Observed Bouguer gravity values indicated that there are several residual highs which are interpreted as dikes. Outcrops and float found along the profile support this interpretation. Corresponding dike locations are shown on the model. The largest dike is 274 m in width ('A'), and is the same dike found along profile U.S. 460E. Basin width, along State Road 637, is 7925 m, and

has a depth of 343 m. Rotational listric type faulting (Wernicke and Burchfiel, 1982) is clearly indicated on the model. Both master (solid line) and splay faults (dashed line) are identified in the model, both show normal slip displacement. Splay faults form the western margin of the basin. At the surface the splay fault dips 24^{o} to SE. The master fault is covered by the Triassic rocks. The greatest displacement occurs along the master fault. Ten percent extension is estimated for this profile from the result of palinspastic reconstruction.

State Road 636 Profile

State Road 636 is the longest modeled profile. It is 10896 m long and is modeled to a depth of 2743 m (Figure 17). Two broad residual highs, marked 'A' and 'B' on the profile, represent-high density country rocks occurring along the basins' margin and a 61 m dike, respectively. This dike contains granophyres and is a continuation of the dike present on profile U.S. Highway 460E and State Road 637. The low, marked 'C', is caused by the Triassic rocks. Basin width is 8229 m, and basin depth is 617 m making this the deepest part of the basin. Details on oil and gas potential of the basin are lacking, but Wilkes (1982) states that, in 1917, a local oil company drilled to a depth of 1518 feet, or about 462 m. A show of oil and gas was reported at depth of 938 feet down hole in the Fork Swamp areas of the basin, between U.S. Highway 60 and State Road 634. This company failed in 1921; a second company drilled to 2100 feet, but the occurrence of commercial quantity of oil or gas is doubtful. Unlike basin geometry predicted by existing Mesozoic models, this model shows that the deepest section of the Farmville basin lies near its' eastern margin. This conclusion is supported by the low closures on both gravity and magnetic contour maps in that area. Rotational listric normal slip movement is displayed by both the master and splay faults. A splay fault forms the western margin of the basin, dipping 28^{o} SE on the surface. All faults shallow with depth cross-cutting the foliation. Extension of 15 % was calculated for this model after palinspastic reconstruction.

State Road 634 Profile

Figure 18 is the gravity model of the 8500 m long profile along State Road 634. No sharp high amplitude residuals are present , probably meaning that no near surface large dike crosses the profile; field evidence for dike was not present also. A broad residual low, marked 'A', is caused by the basin. Along this profile the basin is 3554 m in width and 427 m deep. As in previous profiles, the deepest part of the basin lies near its eastern margin. Both splay and master faults are present along this profile. The western margin of the basin is bounded by a splay fault with the master fault lying underneath the basin rocks. All faults are listric, normal slip with the western border fault dipping 28^{o} SE. The palinspastic reconstruction of this model indicates a maximum of 10 % extension along this profile.

U.S. Highway 60 Profile

The gravity profile and model for U.S. Highway 60 is shown in Figure 19. Profile length is 3353 m. Residual highs are found at the NW and SE ends of the basin's border. The highs are attributed to the higher density country rocks that surround the basin. Low area marked A is the anomaly due to the basin's Triassic sediments. Modeling indicates that the basin is a true half graben with listric type fault geometry. The basin is 2591 m in width and 259 m in depth along this area. As in the four previous profiles, a splay fault forms the western margin of the basin. The border fault dips 25^{o} SE, with dip decreasing at depth. Unlike the four previous profiles, modeling suggests that the master fault lies east of the basin. No extension was estimated for this profile because of its particular geometry.

State Road 622 Profile

The northern most of the modeled profiles

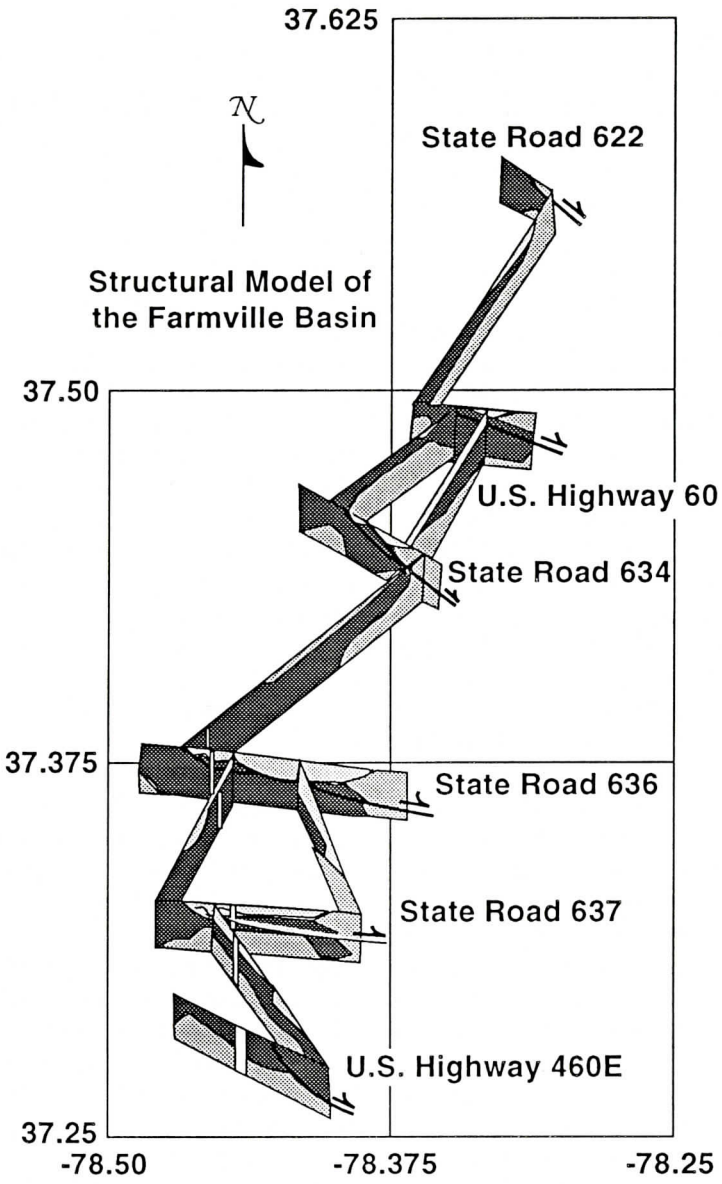

Figure 21: A fence diagram indicating the subsurface relationship of the lithologies in the Farmville Triassic basin.

is along State Road 622 (Figure 20). This profile has a length of 3231 m. The basin is 914 m in width and is 122 m deep at this location. A splay fault forms the basin's western margin, dipping 26^{O} SE. The fault indicates normal displacement, and as the fault shallows with depth it cross-cuts the foliation. The master fault lies east of the profile section. Reconstruction of the profile indicates that this area of the basin has undergone 8 % extension.

In brief, gravity models show the subsurface relationship of the lithologies present in the area. All models indicate that the western margin of the Farmville Basin is bounded by splay faults with the master fault(s) lying beneath or east of the basin, other possibilities

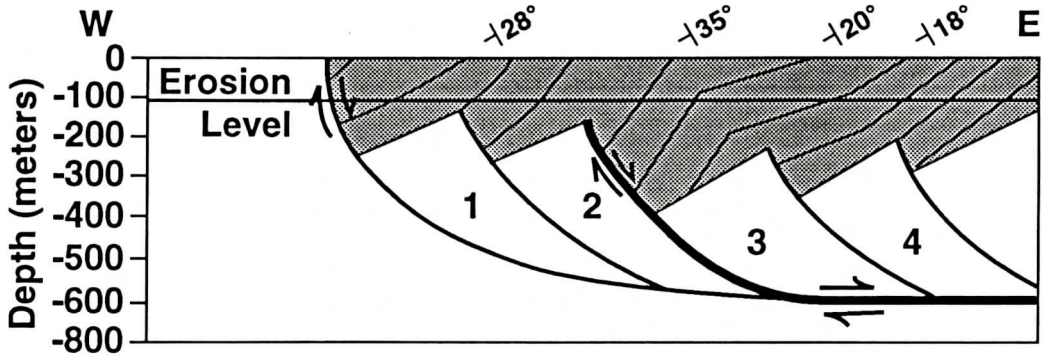

Figure 22: The Farmville Basin is formed as a result of several listric splay faults which shallow with depth and eventually join the master fault at depth. Light solid lines: dip of Triassic beds; dotted area: Triassic rocks; heavy line: master fault; Intermediate solid line: splay faults; 1,2,3, and 4: fault blocks. Approximate positions of observed dip on the surface are indicated. This model is similar to the model developed for State Road 636 gravity profile. Vertical exaggeration is about 32.5 percent.

were considered during the modeling process but the fits were not as good and are not reported here. Along U.S. Highway 460E and State Road 622 the master fault lies to the east of the profiles. Modeling further indicates that the basin's geometry is consistent with a depression formed by several normal, listric, rotational faults. We present the approximate average extension of the profiles as 9 %. The total extension does not include extension caused by dilation as a result of dike emplacement. Extension as noted only measures fault slip or horizontal heave.

STRUCTURAL AND KINEMATIC MODEL

A fence diagram compiled from these profiles (Figure 21) illustrates the three-dimensional geometry of the basin and lithologic relationships within the basin. The profiles indicate that the "Granitic" Gneiss Undifferentiated varies in depth and form across the basin, and generally lies on the eastern side of the basin, and rocks of the Chopawamsic Formation generally lie west of the basin's margin, at the surface. The contact between this unit and Chopawamsic Formation is not exposed at the surface, however. This contact is covered by the Carnian aged rocks of the Farmville Basin, which in turn are cut by younger dikes. The structural model indicates that the Farmville Basin's geometry is controlled by a series of down faulted blocks. Using the classification of Wernicke and Burchfiel (1982), this basin is formed by listric normal faults with a rotational component of motions.

The kinematic model for the Farmville Basin attempts to explain the evolution of the basin, and how various structures interacted during its formation. Basin geometry reflect stresses inherited from the Alleghenian orogeny in the late Paleozoic, and changes in stress pattern in Triassic and Jurassic time.

The Alleghenian orogeny occurred during the Middle Carboniferous to Late Permian (Lefort and Van der Voo, 1981) due to collision between North America and Africa. A majority of the regional structural trends found in the study area, are thought to be a result from this orogeny. These are the NE-SW orientation of folds, foliations, and master joints which were formed as a result of NW-SE compression, P1, during the Alleghenian orogeny. A majority of the folds plunge to the SE and are classified as tight isoclinal (Fleuty, 1964). In general, foliation dips to the SE between 35^{o} and 45^{o}. Crustal cooling during post-Alleghenian time is believed to be responsible for the NW-SE joints. This joint set is related to extension or release fracturing during cooling. Features

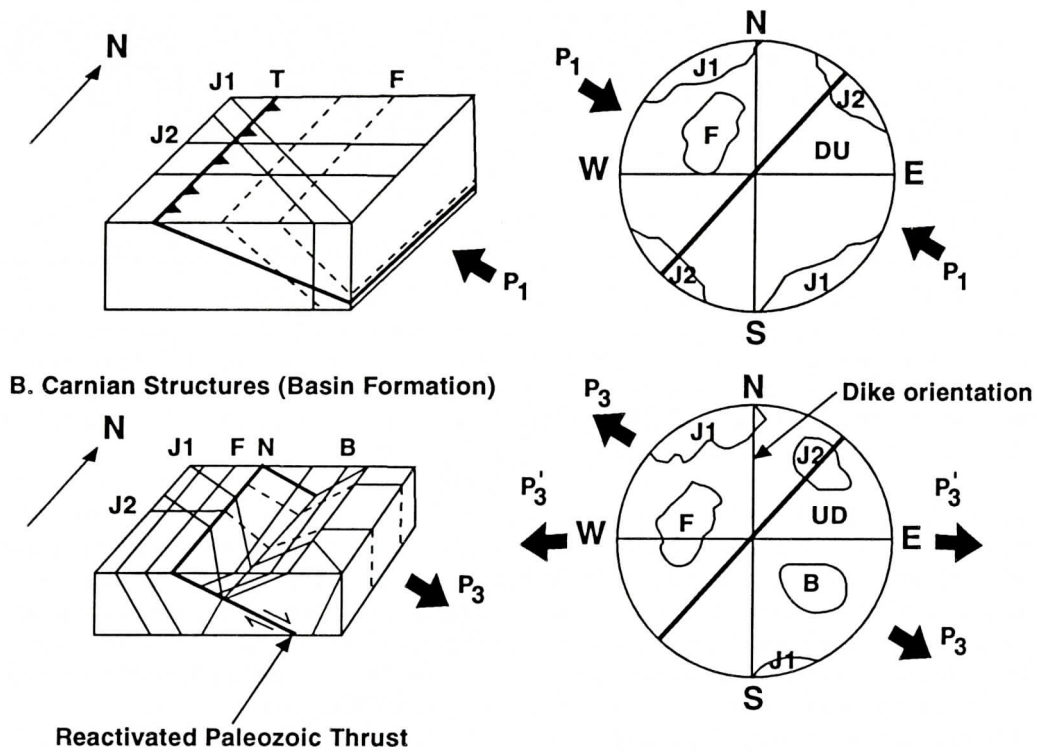

Figure 23: Kinematic model for evolution of the Farmville Basin. The simplified block diagram illustrates the major structural features together with the associated stereonet projections. P1: compressional axis; P3: tensional axis, P'3: tensional axis after rotation; T: thrust fault, N: reactivated thrust fault; F: foliation; J1: NE-SW release fractures; J2: E-W extension joints; B: bedding.

formed during the Alleghenian and post-Alleghenian were the primary structures determining the geometry of the Farmville Basin.

Basin Formation

Manspeizer (1981, 1988) suggested that the breakup of Pangaea began during the late Permian to middle Triassic, with the onset of continental uplift which caused tensional stresses, resulting in graben type structures on both American and African continents. Dooley and Smith (1982) cited geological evidences to support the conclusions of Manspeizer (1981,1988). Van der Voo and others (1976) concluded that a counter-clockwise rotation of Africa relative to North America occurred during the Triassic. Venkatakrishnan and Lutz (1989) presented a kinematic model of the Richmond basin based on two stages of stress orientation. The first stage started in early Triassic with NE-SW-directed compression, P1, when the western margin Hylas fault zone was reactivated as an oblique normal-slip, right-lateral brittle shear zone. The second stage of the basin's development was produced probably by reorientation of the stress field when the P1 axis was directed NNW-SSE.

Field evidence, basin shape and geophysical modeling suggests that the Farmville Basin was formed by several listric faults with rotation (Figure 22). Marr (1980), however, assumed a high-angle normal fault for the western border of the basin marked by a fine-grained siliceous mylonite zone.

Pavlides (1980) detected a linear geophysical boundary of considerable regional extent on small-scale aeromagnetic map and desig-

nated it as Spotsylvania lineament further northeast in Virginia. The western boundary fault of the Farmville Basin has same strike as the Spotsylvania lineament and lies along its continuation, thus it may be part of the NE-SW trending Spotsylvania lineaments. Furthermore, the western boundary fault of the Farmville Basin has nearly the same orientation as the Hylas fault which forms the western border of the Richmond and Taylorsville Basins, Nowroozi and Wong (1989). Our model of the basin's evolution is similar to that of Venkatakrishnan and Lutz (1989). The NE-SW direction of the main fault during the Alleghenian orogeny places the maximum compressional axis, P1, in about E15^{o}S direction. This implies that the P3 axis, maximum tensional stress axis, was nearly perpendicular to the NE-SW strike of the foliation, and less than 30^{o} from being parallel with the NW-SE joint set. As extension continued through the Carnian, reactivation of the NE-SW fabric occurred forming listric faults. During this period the maximum tensional axis, P3, was about E15^{o}S direction (Figure 23). If this model is accepted then it is suggested that the basin oversteps the western marginal fault (see also Wernicke and Burchfiel, 1982).

The geophysical models also support the above interpretation. After its formation, the basin was filled with Triassic sediments, breccia, conglomerate, sandstone, siltstone, shale, mudstone, and coal beds. Later on several diabase dikes have been injected into the sediments, thus dikes postdate the sedimentary rocks and are considered to be late Triassic or early Jurassic (Wilkes, 1986). The changing direction of the tensional principal stress system, P'3 in Figure 23, appears to have caused the emplacement of dikes that trend from NNW-SSE to NE-SW. The dikes were part of a major igneous event that occurred along eastern North America, Europe, Africa, and South America during the Jurassic (Dooley and Smith, 1982). Dikes striking in a NE-SW direction are nearly parallel to the strike of regional foliation. This may indicate that foliation was the structural feature responsible for this group. The NE-SW oriented dikes were found to have a high concentration of granophyre (Rogan, 1993). This may lead to the conclusion that two dike groups were emplaced at different times. Granophyres found in the NE-SW dike group indicated that the parent magma of this dike group was chemically mature compared to the parent magma of the NNW-SSE dike group. This implies that the NE-SW dike group was probably emplaced before the NNW-SSE dike group, and lends support to the two phases igneous event suggested by Smith and Noltimier (1979). They claim an igneous event occurred at 190 million years and a second igneous event occurred at 170-175 million years before present. Further field and laboratory analysis is needed however to confirm the proposed two phase igneous events.

Since formation of dikes, the history of stress regime is vague, we assert that from then to present time regional stresses in the study area are probably attributed to the opening of the Atlantic Ocean and to isostatic rebound. This conclusion is supported by the lack of structural features cross-cutting the dikes in the area. To test this reasoning James (1991) conducted a rectified stream analysis to determine structural trends. His results indicate that there are three significant trends within the study area, including a N-S, a NE-SW, and a NW-SE trend. The trends approximate the pre-Jurassic NE-SW foliation, N-S dikes, and NW-SE joint set.

DISCUSSION

Our synergistic analysis of multisensor geophysical observations reveals a general subsurface picture of the Farmville Basin. We concluded that the basin is formed by the east-facing listric normal faults with some degree of rotation according to the Wernicke and Burchfiel (1982) classification. Furthermore, our analysis has shown that the basin shape, structure, and intrusive history have been affected by preexisting structures and variation of stress system with time. There are several other mod-

els that attempt to explain the formation of the Newark Supergroup in the literature (Lindholm, 1978; Swanson, 1982; and Ratcliffe and Burton, 1985).

There is no consensus of opinion about the mechanism of rift formation in general and the mechanism for formation of the Farmville basin in particular. Many hypotheses have been put forward for the underlying mechanism of lithospheric extension for formation of a rift basin. Sengor and Burke (1978) and Allen and Allen (1990) summarized them into two general classes of active and passive rifting. In active rifting, the crustal deformation is caused by magmatic intrusion into the base of the lithosphere, while in passive rifting, tensional stresses within the continental lithosphere are the cause of extension and subsequent failing of the upper crust and intrusion of hot mantle rock into the failed zone. In passive rifting, extension is due to a pure shear deformation and no rotations of the faulted block have occurred. Deformation may be due to a uniform extension, McKenzie (1978), uniform extension with induced mantle convection, Buck (1986), or discontinuous and non-uniform extension, Rowley and Sahagian (1986). In passive rifting, extension is due to a simple shear deformation and there is rotation in the faulted blocks, Wernicke (1985) and Coward (1986). The possibility that the mechanism depends on time history of deformation and regional tectonic elements is high. As an example, Green and others (1991) used a tomographic image of the seismic structure beneath the Kenya rift and suggested that a narrow wedge of asthenosphere beneath the rift axis is a result of extension by pure shear deformation. However, Effimoff and Pinezich (1986) have reported listric normal fault with large displacement in the Basin and Range province using reflection seismic data. In addition, based on gravity modeling, Okaya and Thompson (1986) suggested that a simple shear deformation and intrusion may be the preferred mechanism for basin formation in areas where intrusions do not have an expected high gravity anomaly. Our results indicate listric faulting with displacement, whether original extension was caused by horizontal tectonic forces in the lithosphere or was caused by the intrusion of hot mantle magma from subsurface in not clear. Although, after formation of the basin, clearly the sediments were cut by basaltic dikes which originated from deeper region.

We compare our model to those presented by the other workers. Lindholm (1978) stated that the geometry of Triassic basins and their location depended on the Paleozoic foliation, and its orientation to P1 axis, during the breakup of Pangaea. We consider foliation as well as other structural features in modeling of the Farmville Basin's geometry. Swanson (1986) similarly asserted that the primary factor controlling the basin's geometry and location were Paleozoic mylonite zones. The model proposed by Ratcliffe and Burton (1985) has some similarity with our model. Both models assume that the geometry of the basin is a direct result of the Paleozoic structures. Ratcliffe and Burton propose reactivation of concave and convex Paleozoic thrust systems as a primary controlling factor for formation of the basin. However our geophysical modeling does not support a duplex form. Strongest similarity between their model and the model presented in this study is that the geometry of the Farmville Basin is a direct result of Paleozoic structures. This study concludes that foliation, joints, and Alleghenian thrusts are the structural features most strongly controlling the geometry of the Farmville Basin. In contrast, the duplex reactivation model of Ratcliffe and Burton (1985) proposes reactivation of concave and convex Paleozoic thrust systems as the primary factor controlling the basin's geometry. We have concluded that the geometry of the Farmville Basin is of rotational listric type as defined by Wernicke and Burchfiel (1982) and convex and concave fault geometry does not appear to be present. In other words, the basin is comprised of a series of block faults joining a master decollement at depth. The fault with maximum displacement in the Farmville Basin is believed to lie underneath the basin as opposed to the western margin of the basin, as required by the duplex

reactivation model. Ratcliffe and Burton (1985) suggested that the deepest part of a basin occurs near the west border fault. The results of this study clearly show that the deepest part of the Farmville Basin lies farther to the east of the west border thrust closer to the eastern part of the basin.

CONCLUSIONS

Geological and geophysical data show that the Farmville basin is a relatively narrow east-facing half graben structure with a shallow depth of 617 m. The basins trough is formed by several listric normal faults with rotational movements. The half graben was formed during NW-SE directional Mesozoic extension. However, unlike the generally accepted and existing models suggesting that basin formation nucleates on one common marginal border fault, our model shows that the faults display maximum down-dip movement and hence controlling the deepest part of the basin may indeed lie within the central part of the basin. In other words, the Newark Group of Triassic basins need not all be nucleated on a western, down-to-the-east marginal fault. The geophysical models also clearly displayed the staircase geometry of reactivated Paleozoic listric faults. However, amounts of down-dip (to the east) movement varied. The deepest part of the Farmville basin is near the eastern margin of the basin.

The area is dominated by a NE-SW regional trend which is present in the basement, as well as the local in lithologies. As a result, this trend can be identified on all geophysical and geological maps.

There are four lithologic units in the area affecting the basin's geophysical expression. These are the Chopawamsic Formation, "Granitic" Gneiss Undifferentiated, Triassic rocks, and diabase/granophyre dikes which are in shallow contact with the Triassic rocks. It is the unique physical properties of these lithologies that are detected and observed by the local anomalies found on the geophysical maps. These anomalies support the hypothesis that the Farmville Basin covers the lithologic contact between the Chopawamsic Formation and the "Granitic" Gneiss. If this is the case, then the lithologic contact is a possible plane of weakness along which faults could form. This interpretation is consistent with our gravity modeling.

All models indicate that the Farmville Basin is bounded by several splay faults with the master fault(s) lying beneath or east of the basin. Along U.S. Highway 60 and State Road 622 the master fault lies to the east of the profiles. Modeling further indicates that the basin's geometry is due to normal, listric, rotational-type faulting as described by Wernicke and Burchfiel (1982). Furthermore, extension due to faulting is about nine percent based on modeling of gravity profiles.

ACKNOWLEDGMENT

We are thankful to Stanley Johnson, Division of Mineral Resources and Ramish Venkatakrishnan for their interest in this work. Dr. Frank Dudas, Department of Geological Sciences, Old Dominion University, read the paper and made valuable editorial suggestions, we thank him for his effort. We have used a set of programs for maintaining and analyzing geological structural data by E. W. Deker to produce Figure 4, 5 and 6. We thank him for allowing us to use his programs.

REFERENCES

Agarwal R.G., 1968. Double Harmonic Analysis for Upward and Downward Continuation: Unpublished Dissertation, Department of Physics, Edmonton, Alberta.

Allen, P.A. and Allen, J.R., 1990. Basin Analysis Principles and Applications. BlackwellScientific Publications: Oxford, London, 451.

Benson, R.N., 1984. Structure contour map of pre-Mesozoic basement, landward of BaltimoreCanyon trough. Delaware Geological Survey, Misc. Map Ser. No. 2, scale 1:500,000, with discussion.

Bhattacharyya, B.K., 1965. Two-Dimensional Harmonic Analysis As a Tool For Magnetic Interpre-

tation: Geophysics, v. 20, p. 829-857.

Bott, M.H.P. and Scott, P., 1964. Recent geophysical studies in southwest England. *In* present view of some aspects of the geology of Cornwall and Devon, p. 25-44, edited by Hosking, K. F. G. and Shrimpton, Geophysical Journal, Royal Geological Society of Cornwall.

Brown, W.R., 1969. Geology of the Dillwyn quadrangle, Virginia: Virginia Division of Mineral Resources. Report of Investigation 10, 77 p.

Buck, W.R., 1986. Small-scale convection induced by passive rifting: the cause of rift shoulders. Earth and Planetary Science Letters, 77, 362-372.

Conley, J.F. and Johnson, S.S., 1975. Road log of the geology from Madison to Cumberland counties in the Piedmont, central Virginia: Virginia Minerals, v. 21, No. 4, P. 29-38.

Cornet, B., 1977. The palynostratigraphy and age of the Newark Supergroup: University Park, Penn. State University, Unpublished Ph.D. Dissertation, p. 501.

Coward, M.P., 1986. Heterogeneous stretching, simple shear and basin development. Earth and Planetary Science Letters, 80, 325-336.

Czechowski, D.A., 1982. Petrologic Comparison of Holocene Stream Sands and Triassic Sandstones in The Central Piedmont of Virginia: Evidence For Triassic Paleoclimate: Unpublished Masters Thesis, Southern Illinois University., 96p.

Dobrin, Milton B., and Savit, Carl H., 1988, Introduction to geophysical prospecting, 4th ed.: New York, McGraw-Hill, 867 p.

Dooley, R.E., and Smith, W.A., 1982. Age and magnetism of diabase dikes and tilting of the Piedmont: Tectonophysics, 90, p. 283-307.

Effimoff, I., and Pinezich, A.R., 1986. Tertiary structural development of selected basins: Basin and Range Province, Northern Nevada, Geological Society of America, Special Paper 208, 31-42.

Espenshade, G. H., and Potter, D. B., 1960. Kyanite, sillimanite, and andalusite deposits of the south - eastern states: U.S. Geological Survey Professional Paper 336, 121 p.

Fleuty, M. J., 1964. The description of folds: Proceeding of American Geological Institute. v. 75, Part 4, p. 461-489.

Goodwin, B. K., Weems, R. E., Wilkes, G. P., Froelich, A. J., and Smoot, J.P., 1985, Guidebook to the geology of the Richmond and Taylorsville basin, east-central Virginia. Eastern Section American Association of Petroleum Geologists. Meeting, Field Trip Number 4, 60 p.

Goodwin, B.K., Ramsey, K.W., and Wilkes, G.P., 1986, Guidebook to the geology of the Richmond, Farmville, Briery Creek and Roanoke Creek Basins, Virginia. 18th annual meeting of the Virginia Geological Field Conference, p 75.

Green, W.V., Achauer, U., and Meyer, R., 1991. A three-dimensional seismic image of the crust and upper mantle beneath the Kenya rift. Nature, 354, 199-203.

Henery, E.F., Welch, W.J., Fussell, K.E., Bailey, H.H., and Smith, G.K., 1958. Soil survey of Prince Edward County Virginia: United States Dept. of Agriculture, Series 1949, No. 4.

Higgins, M.W., Sinha, A.K., Zartman, R.E., and Kirk, W.S., 1977. U-Pb zircon dates from Central Appalachian Piedmont: A possible case of inherited radiogenic lead: Geological Society America Bulletin, v. 88, p. 124-132.

James, G. James Jr., 1991, A geophysical and geological study of the Farmville Triassic Basin, Department of Geological Sciences, Old Dominion University.

Johnson, S.S., 1981. Regional geophysics, *in* Geologic investigations in the Willis Mountain and Andersonville quadrangles: Virginia Division of Mineral Resources Publication 29, p. 9-16.

Johnson, S.S., Wilkes, G.P., and Zeigler, T.L., 1985. Simple Bouguer gravity anomaly map of the Farmville, Briery Creek, Roanoke Creek, Randolph, and Scottsburg basins and vicinity, Virginia: Virginia Division of Mineral Resources, Publication 47, one sheet.

Jonas, A.I., 1932. Geology of the kyanite belt of Virginia, *in* Kyanite in Virginia: Virginia Geological Survey Bulletin. 38, p. 1-38.

Lefort, J.P., and R. Van der Voo, 1981. A kinetic model for the collision and complete suturing between Gondwana and Laurasia in the Carboniferous: Journal of Geology, v. 84, p. 537-550.

Lindholm, R.C., 1978. Triassic-Jurassic faulting in eastern North America-A model based on pre-Triassic structures: Geology, v. 6, p. 365-368.

Lacoste and Romberg, 1980. Model G Instruction Manual: Lacoste and Romberg Inc.

Manspeizer, W., 1981, Early Mesozoic Basins of the Central Atlantic Passive Margins, *in* Geology of Passive Continental Margins, American Association of Petroleum Geologists Eastern Sectional Meeting, Education Course Note Series #19, p. 4:1-4:60.

Manspeizer, W., 1988, Triassic-Jurassic rifting and opening of the Atlantic: An overview *in* Manspeizer, W. (ed.), Triassic-Jurassic Rifting,

Continental Breakup and the Origin of the Atlantic Ocean and Passive Margins. Part A. Elsevier, New York, 41-79.

Marr, J.D., Jr., 1980. The geology of the Willis Mountain quadrangle, Virginia: Virginia Division of Mineral Resources Publication 25, text and 1:24,000 scale map.

Marr, J.D., Jr., 1981. Stratigraphy and structure (Triassic System by M.B. McCollum), *in* Geologic investigations in the Willis Mountain and Andersonville quadrangles, Virginia: Virginia Division of Mineral Resources Publication 29, p. 3-8.

McKenzie, D.P., 1978. Some remarks on the development of sedimentary basins. Earth and Planetary Science Letters., v. 40, p. 25-32.

Mose, D.G., and Nagel, M.S., 1983. Plutonic Events in the Piedmont of Virginia: Southeastern Geology, v. 23, p. 25-39.

Mose, D.G., 1980. Rb-Sr Whole-Rock Studies: Virginia Piedmont II: Year Book, Carnegie Institution of Washington, p. 483-485.

Nowroozi A. A., and Wong, A., 1989. Interpretation of gravity and magnetic anomalies of the Richmond Triassic basin. Virginia Division of Mineral resources, Publication 88. Department of Mines, Minerals and Energy. Charlottesville, Virginia, P. 41-60.

Okaya, D., and Thompson, J., 1986. Involvement of deep crust in extension of Basin and Range province. Geological Society of America, Special Paper 208, 15-22.

Pavlides, L., 1980. Revised nomenclature and stratigraphic relationships of the FredericksburgComplex and Quantico Formation of Virginia Piedmont: U.S. Geological Survey Professional Paper 1146, p.29.

Ratcliffe, N.M., and Burton, W.S., 1985. Fault reactivation models for origin of the Newark basin and studies related to Eastern U.S. seismicity: U.S. Geological Survey Circular 946, p. 36-44.

Robbins, E.I., 1985. Palynostratigraphy of coal-bearing sequences in early Mesozoic Basins of the eastern United States: U.S. Geological Survey Circular 946, p. 27-28.

Rogan, P., 1993. Petrology of a Large, Granophyric-rich Mesozoic Diabase Dike near Farmville, Virginia. Department of Geological Sciences. Old Dominion University.

Rodgers, W.B., 1840. Report of the progress of the geological survey of the state of Virginia for the year 1839. Richmond, 1840. p. 1-161, pls. 1-2. (Reprinted in an annual reports and other papers on the geology of the Virginians, by the late William Barton Rogers. New York, 1889, p. 285-410, pl. p. 276, and p l.1).

Rowley, D.B. and Sahagian, D., 1986. Depth-dependent stretching: a different approach. Geology 14, 32-35.

Russell, I.C., 1892. Correlation papers-the Newark System: U.S. Geological Survey Bulletin 85, p. 344.

Sengor, A.M.C. and Burke, K. and Dewey, J.F., 1978. Rifts at high angles to orogenic belts: tests for their origin and the Upper Rhine Graben as an example. American Journal of Science, 278, 24-40.

Smith, T.,E., and Noltimier, H., C., 1979. Paleomagnetism of the Newark trend igneous rocks of the central Appalachians and the opening of the central Atlantic ocean. American Journal of Science, v. 279, 778-804.

Smoot, J.P., 1985. The closed-basin hypothesis and it's use in facies analysis of the Newark Supergroup: U.S. Geological Survey Circular 946, p. 4-9.

Southwick, D.L., Reed, J.C., Jr., and Mixon, R.B., 1971. The Chopawamsic Formation: A new stratigraphic unit in the Piedmont of northern Virginia: U.S. Geological Survey Bulletin 1324-D, 11 p.

Swanson, M.T., 1986. Preexisting fault control for Mesozoic basin formation in eastern North America: Geology, v. 14, No. 5, p. 36-38.

Telford, W. M., Geldart, L. P., Sheriff, R. E., and Keys, D., 1990, Applied Geophysics, Cambridge University Press, New York, p. 770.

Tilton, G.R., 1970. Zircon age measurements in the Maryland Piedmont with special reference to Baltimore Gneiss problems; *in* Fisher, G.W., eds. Studies of Appalachian Geology-central and southern: New York, Interscience, p. 429-434.

Talwani, M., Heirtzler, J.R., 1964. Computation of magnetic anomalies caused by two-dimensional structures of arbitrary shape, *in* Computers in the Mineral Industries, Part 1: Stanford University Publications, Geological Sciences v. 9, No. 1, p. 464-480.

Talwani, M., 1965. Computation with the help of a digital computer of magnetic anomalies caused by bodies of arbitrary shape: Geophysics, v. 30, p. 797.

Tsuboi, C., 1959. Applications of Double Fourier Series to Computing Gravity anomalies and other Gravimetrical Quantities at higher elevations from Surface Anomalies: Report No. 2 Institute Geodesy, Photogrammetry, and Cartog-

raphy, Ohio St. University.

Van der voo, R., Mauk, F.J., and French, R.B., 1976. Permian-Triassic continental configurations and the origin of the Gulf of Mexico. Geology, 4, 177-180

Venkatakrishnan, R., and Lutz, R., 1989. Chapter 13: A Kinematic Model For The Richmond Triassic Basin, Virginia, *in* Triassic-Jurassic Rifting, Manspeizer, W., (ed.). Elsevier New York, 445-462.

Virginia Division of Mineral Resources, 1970a. Aeromagnetic contour map of Farmville Quadrangle (15-minute map; scale 1:62,500): Open file report, Virginia Division Of Mineral Resources.

Virginia Division Of Mineral Resources, 1970b. Aeromagnetic contour map of the Dillwyn quadrangle (15-minute map; scale 1:62,500): Open file report, Virginia Division of Mineral Resources.

Virginia Division of Mineral Resources, 1978a. Aeroradiometric contour map of Farmville quadrangle (15-minute map; scale 1:62,500): Open file report, Virginia Division Of Mineral Resources.

Virginia Division Of Mineral Resources, 1978b. Aeroradiometric contour map of the Dillwyn quadrangle (15-minute map; scale 1:62,500): Open file report, Virginia Division Of Mineral Resources.

Weems, R.E., 1980. Geology of the Taylorsville basin, Hanover County Virginia. In: Contribution to Virginia Geology - IV. Virginia Division of Mineral Resources, Publication 27: 23-38.

Wernicke, B., 1985. Uniform-sense normal simple shear of the continental lithosphere. Canadian Journal of Earth Sciences, 22, 108-125.

Wernicke, B., and Burchfiel, B.C., 1982. Modes of extensional tectonics: Journal of StructuralGeology, No. 4, p. 105-115.

Wilkes, G.P., and Lasch, D.K., 1979. The Farmville Triassic Basin: an integratedgeological and geophysical study: Virginia Journal of Science, v. 30, No. 2.

Wilkes, G.P., 1982. Geology and mineral resources of the Farmville Triassic basin, Virginia,Virginia Minerals, v 28, no. 3,25-32.

Wilkes, G.P., 1986. The Farmville Basin and the Briery Basin. in: Goodwin, B. K., Ramsey, K. W., and Wilkes, G.P. (ed.): Guidebook to the geology of the Richmond, Farmville, Briery Creek and Roanoke Creel Basins, Virginia 18 Annual Meeting Virginia Geological Field Conference, 26-74.

SOUTHEASTERN GEOLOGY
V. 34, No. 3, September 1994, p. 129-137

SEDIMENTOLOGY AND ALKALINE GEOCHEMISTRY OF RIFT LAKE MANYARA, NORTHERN TANZANIA, EAST AFRICA: AN ANALOGUE TO LACUSTRINE FILL IN SOME EARLY MESOZOIC LAKES OF SOUTH EAST USA

SAIDI A. HASSANI

8100 Majestic Ct.
Anchorage, Alaska 99504

CHRISTOPHER G. ST. C. KENDALL

Department of Geological Sciences
University of South Carolina
Columbia, S.C. 29208, U.S.A.

ABSTRACT

The Lake Manyara rift basin is an asymmetric half-graben formed in Precambrian basement rocks. It is filled by Neogene to Recent clastic sediments which include carbonates, evaporites, microbial material (organic matter), and undifferentiated basaltic lavas. Ash-derived clays are also part of the fill and include analcime, zeolites, phillipsite, erionite, and chabazite. Hot-spring water rich in sodium and calcium leached from volcanoclastic materials enrich the lake waters in sodium bicarbonate and calcium carbonate. The pH ranges from 9.2 to 11.0 and alkalinity ranges from 2000 to 3000 meq/L. An electron microprobe study of oolitic limestone grains shows higher levels of strontium and magnesium and depletions of iron and manganese relative to the calcite cement of other eastern branch rift lakes. A phosphatic (Plio-Pleistocene) lake-bed limestone unit is related to the accumulation of bird droppings on and around " roosting " islands set in a nutrient-rich saline lake.

Lake Manyara and its environments are useful modern analogue for several Triassic and Jurassic lake sequences in the Newark rift system. The clastic and chemical sedimentary fill of many of the Triassic and Jurassic lakes includes sodium rich clays, phosphates, carbonates, and evaporites. The setting and sedimentary facies of the modern lake and its valley should help interpret the sequences that fill the ancient rift, characterizing and enhancing the search for economic deposits in the subsurface.

INTRODUCTION

Most evaporite deposits are marine in origin, but lacustrine evaporite sequences are also common in certain rift valleys. In the East African Rift System, the chemistry of the lakes in the Central and Gregory rift valleys is influenced by both volcanoclastic and hydrothermal sources. In this rift, Lake Manyara is one of a series of strictly evaporitic lakes in this latter rift system. Lake Manyara is a remnant of a once much larger lake which included Lakes Natron and Eyasi and was 300 m deeper than the present lake. In fact, in the past 48,200 years or so, Lake Manyara has shrunk to one-fourth its original size (Holdship 1976). Lake Manyara lies 960 m above mean sea level, and is located between lat. 3° 20' and 3° 40' S, and long. 35° 45' E (Fig. 1); it is 40 km long and 12 km wide, covering approximately 570 km^2 in area. Its maximum depth was less than 3 m in 1989. An older shoreline, almost 100 m above the present lake shoreline, surrounds the present lake. A series of terraces mark the former higher lake levels.

The climate of the region is hot and dry, a factor that affects the salinity of all the lakes in the Central rift valley. The mean annual tem-

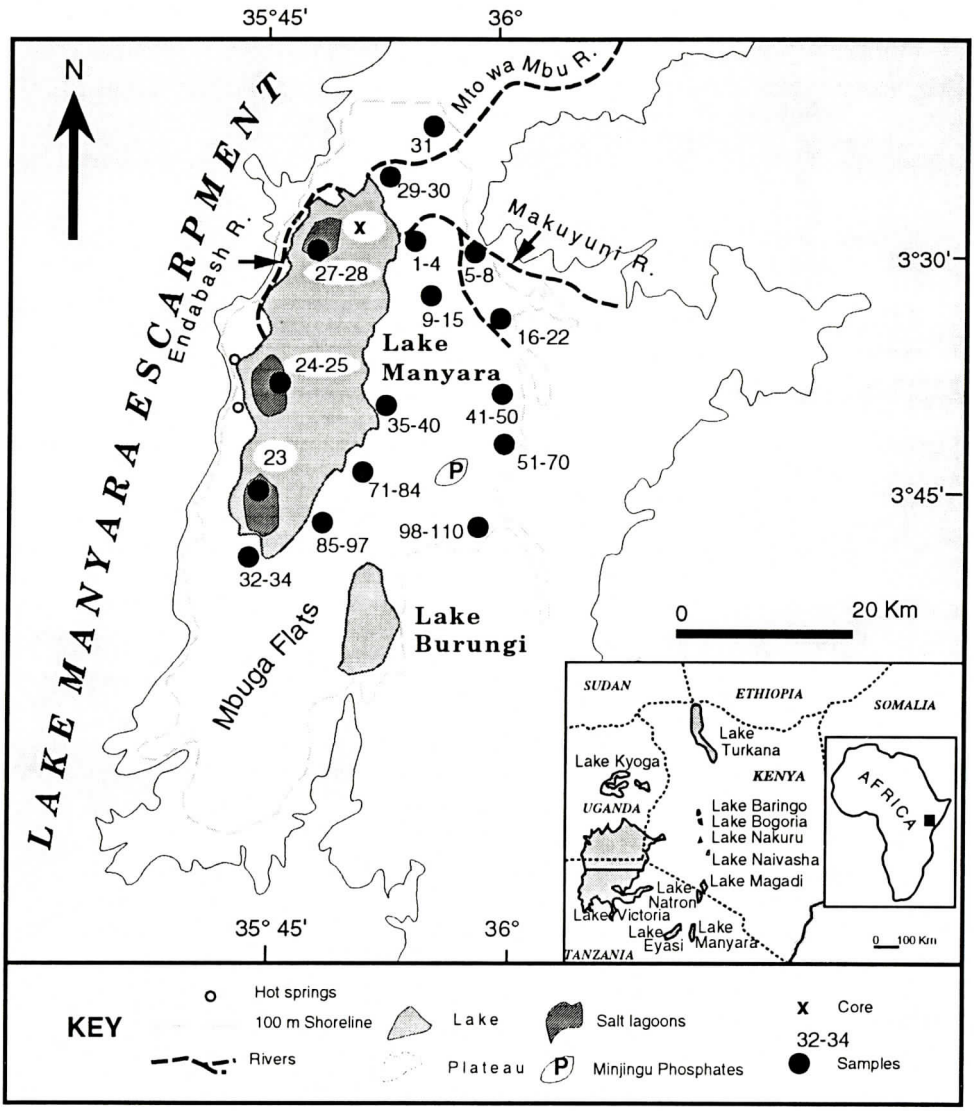

Figure 1. Map showing the location of Lake Manyara and the locations of samples collected for this study.

perature is 30°C, while lake temperatures vary between 40° and 42°C (Greenway and Vesey-Fitzgerald, 1969; and this paper). Measured hot springs range between 72°C and 87°C (Table 1). The average rainfall is 760mm, most of which falls between March and May (Williams, 1954). During the rainy season Lake Manyara is brackish. In contrast, during the dry season (September - November), it nearly dries out and is locally covered by a sodium carbonate salt crust (L. Manyara park warden, personal communication, 1989). In the dry season, saline pools remain at the northern and southern ends of the lake, and the largest pool remains in a subbasin along its northwestern shore (Fig. 1).

Methods Of Study

The field work for this study began shortly after the rainy season in July of 1989. This paper reports on sections measured, and rocks

Table 1. Lake Manyara hydrogeochemistry

Lake Manyara surface water analysed for dissolved solids (6-7, 1989)												
Location	**T°C**	**Na**	**K**	**Ca**	**Mg**	**Cl**	**SO_4**	**PO_4**	**CO_3**	**HCO_3**	**SiO_2**	**pH**
Surface Lake Water	30.0	(mg/l) 2500 - 21,500	(mg/l) 12 - 137	(mg/l) 1.4 - 10	(mg/l) 1 - 30	(mg/l) 1170 - 8670	(mg/l) 230 - 2280	(mg/l) 0.02 - 0.2	(mg/l) 1612	(mg/l) 3002	(mg/l) 16.3 - 19	10
Chemical Analysis for Lake Manyara surace water, hot springs and rivers (6-7, 1989)												
Location	**T°C**	**$CaSO_4$**	**NaCl**	**Na_2SO4**	**Na_2CO_3**	**K_2CO_3**	**$CaCO_3$**	**$MgCO_3$**	**Organic & K_2SO_4**	**K_2SO_4**	**Na_2PO_4**	**Na_2S**
Small hot spring	72.2	7.2	388.9	44.4	1500	12.5	8.0	15.0	-	-	-	-
Big hot spring	87.0	7.3	620	45.1	1505.2	15.3	10	30	116.4			
Lake Water	30.0	-	4800	530	12040	-	-	-	-	240	120	Trace
Makuyuni River	32.7	7.3	13.2	4.6	38.5	-	-	43.7	51.8	-	-	-
Mto wa Mbu River	29.6	26.2	42.9	249.9	72.3	13.7	358.0	63.9	-	-	-	-
Chemical analysis of the Lake Manyara soda crust sediments (6-7, 1989												
Location	**T°C**	**NaCl**	**Na_2SO_4**	**Na_2CO_3**	**Na_2PO_4**	**clay & sand**	**Total**					
North Salt Lagoon	30.5	59.5	22.7	13.1	0.40	-	95.7					
South Salt Lagoon	31.3	5.38	20.46	48.63	0.34	25.19	100.00					

and sediment sampled for the purpose of providing information from an important alkaline lake system. Water samples were analysed from the lake surface, rivers, and hot springs.

Laboratory Analyses

a. Carbonate/Evaporate Petrographic Analyses.

A total of eighty six samples were impregnated with epoxy mixed with a blue dye. These were then sectioned and stained with alizarine Red S and potassium ferricyanide to differentiate between calcite and aragonite grains (Dickson, 1965). The dominant lithologies and sedimentary textures rock constituent grains, cements and porosity were described using the classification of Folk (1962).

b. Electron Microprobe Analyses.

Analyses were conducted on the rock samples to determine the chemical composition of carbonate/evaporate minerals and their associated trace elements.

c. Wet Chemical Analyses.

Water samples were collected from both the lake surface and hot springs. Temperature and salinity were recorded. Total dissolved solids in water samples from selected hot springs and the lake surface and their original temperature were recorded (Table 1).

Geologic Setting Of the Study Area

Most of the Lake Manyara area is underlain by Precambrian gneisses and quartzites which also crop out as isolated inselbergs. Pleistocene to Recent alluvial fans, formed of gravels and conglomerates eroded from the uplifted western margin escarpment fringe the western margin of the rift basin.

At the foot of this western escarpment, hot springs issue from beneath large boulders and coalesce to form streams, salt marshes and salt lagoons (Fig. 2). Hot spring outlets are flanked

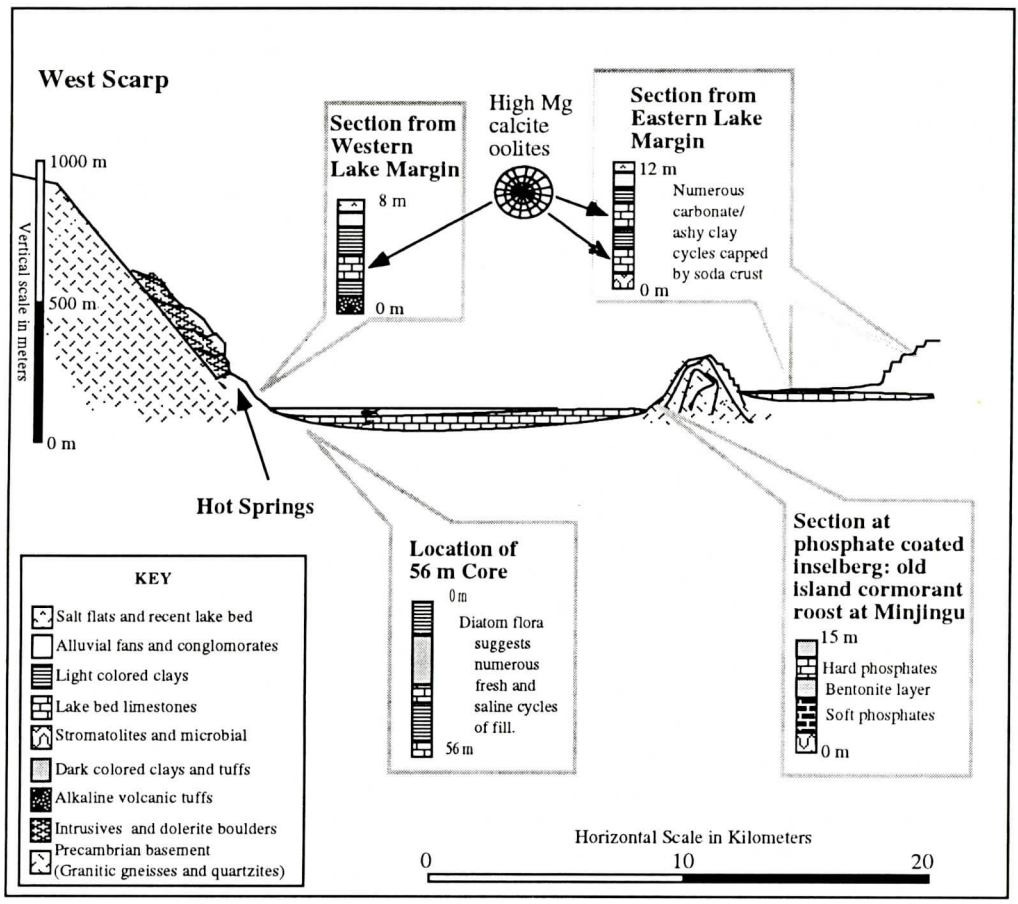

Figure 2. Schematic cross section of Lake Manyara showing the major sedimentary character of valley fill.

by soda deposits and mats of red algae and cyanobacteria (blue-green algae). From the northwest, several perennial streams flow into the lake (Fig. 1), forming fresh-water marshes.

Volcanoes are common in the rift valley near Lake Manyara. To the south is Kwaraha Volcano, while to the north lie the extinct volcano Lossiminguri and the active carbonatitic volcano Oldoinyo Lengai.

PLIOCENE TO HOLOCENE STRATIGRAPHY AND LAKE MANYARA SEDIMENTOLOGY

During the Pliocene to Recent, Lake Manyara was filled with clastic sediment transported to the basin by local drainage. The shores of the lake over this time interval often extended well beyond and above their present level. The current lake is enveloped by five successive shorelines which are now represented by terraces. These are best developed in the Minjingu area, where the oldest shoreline is as much as 100m above the present lake level (Fig. 2). The diatom flora of the lake sediments indicate that at times Lake Manyara was transformed into a fresh-water lake, that was 100-fold less saline than the present lake (Beadle, 1974; Holdship, 1976). The present lake bottom is characterized by alternating assemblages of clay mineral, silts, and organic layers formed of cyanobacterial remains. A 56m core collected by Holdship (1976) did not reach basement but penetrated interbedded marl limestone and clay-rich layers, some of which

are as much as 4m in thickness (Fig. 2). Associated clay minerals in the clay - rich layers are dominated by smectite; illite and authigenic silicate minerals including analcime, zeolites, phillipsite, erionite, and chabazite. Beds of Pliocene-Upper Pleistocene limestones (Min. Res. Div., 1965) a few centimeters to a maximum of 3m thick, crop out along the eastern and western lake margins. Extensive oolites, pisolites, and massive algal limestones which formed during former lake highstand are well exposed along the Makuyuni River (Samples 1 - 8) and along the present lake shoreline (Samples 16 - 22, 41 - 98). These calcareous components form the oldest lake bed sequence. Along the eastern lake margin at Minjingu (Fig. 2), this oolitic limestone also contains phosphatic layers. The phosphate occurs on and around old islands all of which now stand about 92 m above the present lake level. These islands have cores of Proterozoic quartz and gneiss. The upper, dehydrated phosphate layers are hard, whereas the lower portions, just above the present lake bed, are soft and extensively bioturbated. They commonly contain slump structures. Bones of the fish *Tilapia*, and of the cormorants which ate them, have been identified in outcrop and thin sections. The lake waters have elevated concentrations of both phosphate and uranium leached from local carbonatites by the inflowing waters. Aswathanarayana (1988) reported 1.5 % phosphorus, 3 ppm uranium, and 0.9 % fluorine in lake water. Such an elevated nutrient level undoubtedly affected the whole food chain through time causing fish populations and influencing a concomitant increase in guano accumulation.

The uppermost lake bed sequences of the old shoreline to the east (Fig. 2) contain lenses of evaporite materials, including trona, magadiite, and kenyaiite. Stromatolites and cauliflower cherts are also present in these lenses. Crystal shapes suggest that the cherts have replaced earlier gypsum and anhydrite.

HYDROGEOCHEMICAL STUDY OF LAKE MANYARA

The Manyara hot-spring and lake waters contain large quantities of carbonate and sodium (Harris, 1948; Holdship, 1976; Singer and Stoffers, 1980; and Table 1), whose concentrations in lake waters increase during the dry season and decrease during the rainy season. The pH ranges from 9.2 to 11.0, responding to increases in concentrations of CO_3^{-2} and Na^+ during the dry season.

Our chemical analyses from Lake Manyara and studies from other East African lakes suggest that dissolved Mg^{+2}, Ca^{+2}, F^-, SO_4^{-2}, and PO_4^{-2} (Table 1) have been derived from hot springs and leached from sodium-rich younger volcanic rocks (Williams, 1954; Eugster, 1970; Mushi, 1975; Jones et al 1977 and this paper). Guest (1954) and Dowson et al. (1990) also reported high NaO/K_2O ratios in samples of volcanic debris collected north of Lake Manyara. Here, volcanoes have extruded alkaline and carbonatite-rich fluids which are remarkably high in Cl^- and F^- volatiles (Dowson et al.,1990). The basement lithologies also include basic intrusive rocks and volcanics that undoubtedly contribute to the increased level of dissolved constituents, especially where they were leached by corrosive fluids of volcanic origin.

The precipitation of trona and halite in Lake Manyara during the dry season is directly related to the abundant supply of Na^+ and CO_3^{2-} in an alkali-and carbonate-rich setting. Microprobe analyses of salt crusts and older limestones reveal that sodium bicarbonate occurs in combination with sodium carbonate as trona ($NaHCO_3$. $NaHCO_3$. $2H_2O$). This mineral exhibits both the compact and radiating forms. Halite is the second most common evaporite mineral in the lake. It occurs as cubic crystals filling polygonal fractures in and above the trona deposits. The presence of algal and bacterial pigments and the breakdown of organic material by anaerobic bacteria and result in a pink color and characteristic H_2S odor along the lake margins.

Oolites from shoal areas along the eastern margin of Lake Manyara (Fig. 3) are remarkably similar to mixed concentric bands of aragonite and radial calcite oolites of Great Salt

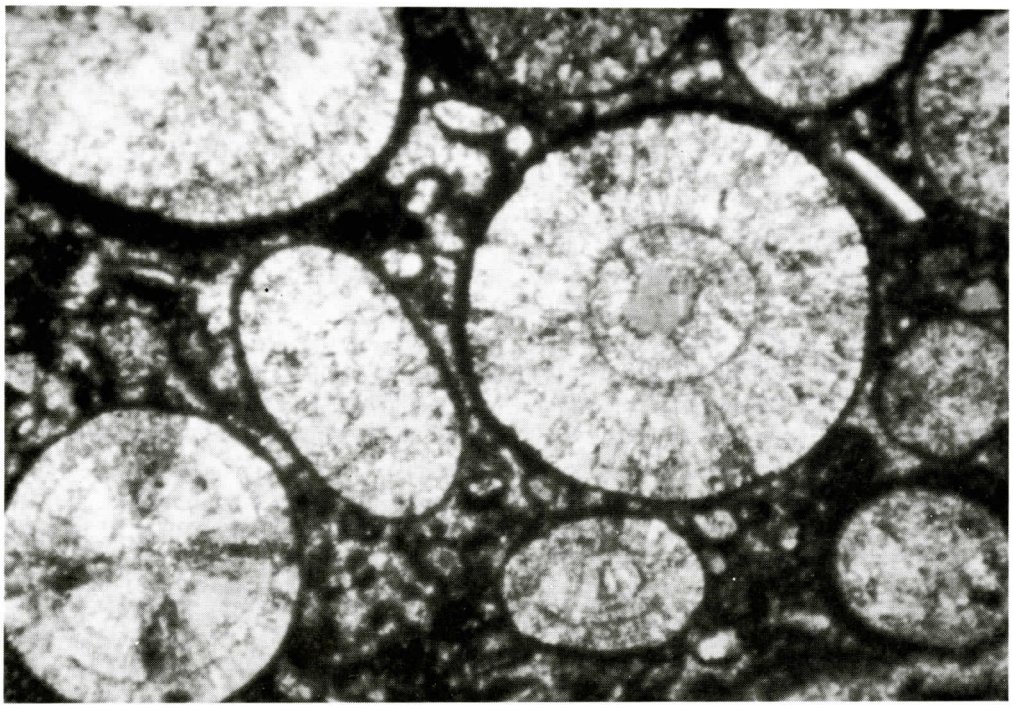

Figure 3. Photomicrograph of Lake Manyara oolites having high-Mg calcite and concentric and radial fabrics.

Lake (Eardley 1938; Halley 1977). Electron microprobe analysis reveals that the youngest oolitic limestone grains of Lake Manyara are enriched with respect to Sr and Mg and depleted with respect to Fe and Mn relative to calcite cement (Table 2). High peaks of Fe and Mn are measured hot spring samples (Table 2); the high values may explain the depletion in the oolite grains.

SIMILARITIES TO THE TRIASSIC LAKES OF SOUTHEASTERN USA

In the southeastern United States, Triassic and Jurassic rocks are characterized by a mixed fluvial and lacustrine rift setting that is related to the initial rifting of Pangea (Van Houten, 1964, 1965; Thayer 1970a &b). Clastic fill predominates, exhibiting a strong cyclic character which is thought to be related to cyclic changes in lacustrine deposition (Van Houten, 1964, 1965; Thayer 1970a &b; Olsen 1989). In the Triassic Lockatong Formation of New Jersey, many of the sedimentary cycles consists of alternations of clastic and chemical sediments (Van Houten, 1964). Periods of exposure would have resulted in the development of lake mud flats not unlike those seen in and around Lake Manyara. A similar comparison can be made with the Dan River Danville Basin which formed in a Triassic rift basin in the Carolina Piedmont (Robbins, 1981). This basin was largely filled by mudrocks and silts which interfinger at the basin margin with fluvial sands and conglomerates (Thayer 1970a &b). The mudrocks and silt are largely lacustrine in origin (Thayer 1970b and Robbins 1982). These lacustrine beds contain sodium rich riebekite (Robbins, 1982) that may have once been clays containing analcime, illite, gibbsite, zeolites. Thayer (1970b) noted the presence of both calcite and dolomite. Local beds, as in many of the Triassic - Jurassic rift basins, in the

Table 2. Electron microprobe analysis of trace elements in oolites, cements, and other sedimentary materials from Lake Manyara.

Trace elements from microprobe analysis (wt %)							
Samples	**Mg**	**Sr**	**Ca**	**Fe**	**Mn**	**O**	**Total %**
No. 76 Oncolite	0.47	0.00	33.41	1.07	0.27	14.04	49.26
No. 76 Cement	0. 09	0.01	39.55	0.03	0.00	15.86	55.53
No. 16 Gastropod shell	0.00	0.43	35.55	0.02	0.00	14.28	50.29
No. 16 Oolite	7.79	0.00	14.10	5.60	0.10	12.39	39.99
No. 70 Oolite	0.97	0.06	24.65	1.59	0.03	10.95	38.26
No. 70 Cement	0.00	0.00	0.03	0.00	0.00	0.04	0.14
No. 24 Hot spring ooid	6.25	0.00	6.31	14.21	0.14	10.74	37.64
No. 24 Cement	0.00	0.00	4.11	0.04	0.00	1.65	5.81
No. 49 Mineral grain	0.00	0.00	0.01	0.00	0.00	0.01	0.03
No. 17 Tuff	0.20	0.88	27.57	0.01	0.01	11.31	39.99
No. 7 Cement	7.22	0.00	0.17	4.64	0.02	6.16	18.21
No. 29 Oncolite	0.80	0.47	42.95	0.13	0.27	17.87	62.50
No. 29 Cement	0.92	0.34	33.26	0.73	0.05	14.18	49.51
No. 75 Ooid	0.55	0.57	42.04	0.27	0.15	17.37	60.97

Deep River basin of North Carolina contain phosphatic material rich in fish bones (Porter and Robbins, 1981; Robbins and Textoris, 1986). The Dan River Danville Basin is also characterized by the presence of volcanic dikes (Thayer 1970b).

Many authors have made good comparisons between the East Africa and the Newark lakes. Detailed analysis of sedimentary structures and geochemical data from Lake Manyara may be of particular use in helping to interpret the economic potential of lacustrine sequences in this ancient rift. The similarity of the geological setting expressed by the sedimentary rocks, structural style, and vulcanism suggest that both sodium carbonate minerals and phosphates may be commoner than previously recognized in the Triassic sedimentary sequences buried in the coastal Piedmont of southeastern United States.

CONCLUSIONS

Lake Manyara is a lake that stores and precipitates flora, halite and phosphates. It is surrounded by volcanic rocks that have had a significant influence on the hydrogeochemistry of the lake. Sodium carbonates are supplied by anhydrous carbonatite lavas and tuffs in the vicinity of Lake Manyara. Sodium salts are emitted by the main source for soda deposits and carbonate in the lake. Carbonatite volcanism supplied much of the high magnesium content of the sediments in the lake. Phosphate in the older Plio-Pleistocene lake-bed limestones is unique to Lake Manyara with respect to other East African lakes. Its presence is probably related to the chemistry of leachable P-rich carbonatitic lavas which, in turn affected nutrients and fish productivity when the lake was larger. In turn, this affected the concentration of guano around inselberg islands which acted as roosting sites for birds such as cormorants.

The sedimentary fill and setting of Lake Manyara are useful analogues for Triassic and Jurassic rift valley fill in the southeastern United States. Because of the similarities, it may be possible to predict that sodium carbonates and phosphates may be present in the deeper unexplored parts of these ancient rift basins.

High magnesium oolites are enriched in Strontium but depleted in ion and manganese. This depletion may be to an association with the adjacent hot spring waters.

ACKNOWLEDGMENTS

We thank Eleanora Robbins for helping make the initial contacts with scientists working in East Africa and for her vigorous editorial review; Douglas Shearman, who supervised field work; and Clark Alexander, John Carpenter, Arthur Cohen, Robert Dill, Donna Hassani, Tom Johnson and Ann Watkins who provided comments and reviewed this manuscript.

REFERENCES CITED

Aswathanarayana, U., 1988, Natural environment in the Minjingu area, Northern Tanzania, *in* Norwegian Academy of Science Letters from Jul Lag (Ed). p. 79-85.

Beadle, L. C., 1974, The inland waters of tropical Africa: Longman, London, 365 p.

Dickson, J. A. D., 1965, A modified staining technique for carbonates in thin section: Nature, v. 205, p. 587.

Dowson, J. B., Pickerton, H., Norton, G. E., and Pyle, D. M, 1990, Physicochemical properties of alkali carbonatite lavas: Data from the 1988 eruption of Oldoinyo Lengai, Tanzania: Geology, v. 18, p. 260 - 263.

Eugster, H. P., 1970, Lake Magadi, Kenya, and its precursors: Developments in Sedimentology 28: Hypersaline Brines and Evaporitic environments. Elsevier, Nissenbaum (Ed.)., p. 195 - 232.

Eardley, A. J., 1938, Sediments of Great Salt Lake, Utah: American Association of Petroleum Geologists Bulletin, v. 22, p. 1305-1411.

Folk, R. L., 1962, Spectral subdivision of limestone types: American Association of Petroleum Geologists Memoir 1, p. 622 - 84.

Greenway, P. J., and Vesy-Fitzgerald, D. F., 1969, The vegetation of Lake Manyara National Park: Journal of Ecology, v. 57, p. 127 - 149.

Gregory, J. W., 1921, The rift valleys and geology of East Africa: Seely, Service and Co. Ltd., London.

Halley, R.,B., 1977, Ooid fabric and fracture in the Great Salt Lake and the geologic record: Journal of Sedimentary Petrology, v. 47, p. 1099-1120.

Harris, J. H., 1948, Lake Manyara: Geological Survey Dept. Tanganyika. Unpublished Report. 11 p.

Holdship, S. A., 1976, The paleolimnology of Lake Manyara, Tanzania : A diatom analysis of a 56 meter sediment core: Unpublished PhD. dissertation, Duke University, 121 p.

Jones, B. F., Eugster, H. P., and Rettig, S. L., 1977, Hydrochemistry of the lake Magadi basin, Kenya: Geochimica et Cosmochimica Acta, v. 41, p. 53 - 73.

Kinsman, D. J. J., 1969, Interpretation of Sr^{2+} concentrations in carbonate minerals and rocks: Journal of Sedimentary Petrology, v. 39, p. 486 - 508.

Mineral Resources Division, Dodoma, Tanzania, 1965, Mbulu Quarter Degree Sheet 69.

Mushi, J. M., 1975, Mineralogy, sedimentology and geochemistry of the Lake Natron Area: Geology and Mines Division, Tanzania Unpublished Report, 28 p.

Olsen, P. E. and Gore, P. J. W., 1989, Tectonic, depostional, and paleoecological history of the Early Mesozoic rift basins, Eastern North America: 28th International Geologocial Congress, Field Trip Guidebook T351, 106 p.

Porter, K. G., and Robbins, I. E., 1981, Zooplankton fecal pellets link fossil fuel and phosphate deposits: Science, v. 212, p. 931 - 933.

Robbins, E. I., 1981, A Preliminary account of the Newark rift system. Lunar and Planet: Institute Conference on Proceeding of Planet Rifting, St. Helena, California, Dec. 2 -6, p. 107 - 109.

Robbins, E. I., 1982, "Fossil Lake Danville": The Paleoecology of Late Triassic ecosystem on the North Carolina - Virginia border: Unpublished PhD. dissertation, The Pennsylvania State University, 400 p.

Robbins, I. E., and Textoris, D. A., 1986, Fossil fuel potential of the Deep River Basin, North Carolina: SEPM Field guide books, Southeastern United States 3rd Ann. Midyear Meeting. Raleigh, North Carolina, p. 75 - 115.

Singer, A., and Stoffers, P., 1980, Clay mineral

diagenesis in two East African lake sediments: Clay Minerals, v, 15, p. 291 - 307.

Thayer, P. A., 1970a, Geology of Davie County Triassic Basin, North Carolina: Southeastern Geology, v, 11. no. 3, p. 187 - 198.

Thayer, P. A., 1970b, Stratigraphy and geology of Dan River Triassic Basin, North Carolina: Southeastern Geology, v. 12. no. 1, p. 1 - 32.

Van Houten, F. B., 1964, Cyclic lacustrine sedimentation, Upper Triassic Lockatong Formation, Central New Jersey and adjacent Pennsylvania: Kansas Geology Survery Bulletin, v. 169, p. 497 - 531.

Van Houten, F. B.. 1965. Crystal casts in Upper Triassic Lockatong and Brunswick Formations: Sedimentology, v. 4, p. 301 - 313.

Williams, W. R., 1954, Some note on the geology of the rift valley in the Lake Manyara Area, Northern Province: Geological Survey of Tanganyika. Unpublished Report, 8 p.

SOUTHEASTERN GEOLOGY
V. 34, No. 3, September 1994, p. 139-161

TEXTURAL FACTORS AFFECTING PERMEABILITY AT THE MWD WELL FIELD, SAVANNAH RIVER SITE, AIKEN, SOUTH CAROLINA

William P. Kegley
SAIC Corporation, P. O. Box 2502, Oak Ridge, TN 37831

W. C. Fallaw
Department of Geology, Furman University, Greenville, SC 29613

David S. Snipes
Department of Earth Sciences, Clemson University, Clemson, SC 29634

Sally M. Benson
Earth Sciences Division, Lawrence Berkeley Laboratory, Berkeley, CA 94720

Van Price, Jr.
Westinghouse Savannah River Company, Aiken, SC 29801

ABSTRACT

Analysis of texture and permeability of Eocene and Miocene(?) units in the MWD area at the Savannah River Site indicates that lithostratigraphic units also are distinct permeability units. Permeability distribution, as determined by thousands of minipermeameter measurements, is primarily controlled by mud (silt and clay) content of the sediment; units with low mud content have higher permeability than units with high mud content. Permeability distribution is also more variable for units with varying mud content compared to units with uniform mud content. In general, permeability increases as mean grain size increases, and permeability decreases as sorting becomes poorer. Graphs of permeability values show a remarkable similarity to gamma ray logs. Statistical analyses support the qualitative findings regarding lithologic control of permeability distribution.

INTRODUCTION

Location and Description of Study Area

The U. S. Department of Energy's Savannah River Site (SRS) encompasses approximately 800 km^2 in Aiken, Barnwell, and Allendale counties, South Carolina (Figure 1). The SRS is underlain by a southeasterly thickening wedge of consolidated to unconsolidated Upper Cretaceous and Tertiary sands, muds (silts and clays), and gravels. Interbedded limestone and calcareous sand occur sporadically. In general the Tertiary section is in a transition zone between updip fluvial and deltaic clastic units and downdip marine clastic and carbonate sediments. This investigation focuses on the Eocene and Miocene(?) sediments.

The Coastal Plain section is approximately 240 m thick at the northwestern boundary of the SRS and 530 m thick at the southeastern boundary (Snipes and others, 1993). In the northwestern part of the SRS the sediments are underlain by Paleozoic crystalline rocks, and in the southeastern part they are underlain by Triassic red beds (Marine and Siple, 1974).

The study area is in the north-central portion of the SRS about 40 km southeast of the Fall Line and encompasses about 3 km^2. Sixty three monitoring wells are in the area of study (Figure 2). Many of the locations in Figure 2 are "clusters" with wells screened at different stratigraphic horizons. The focus of this study is the Mixed Waste Disposal (MWD) Well Field at the southern end of the study area. Fifteen monitoring wells have been installed at

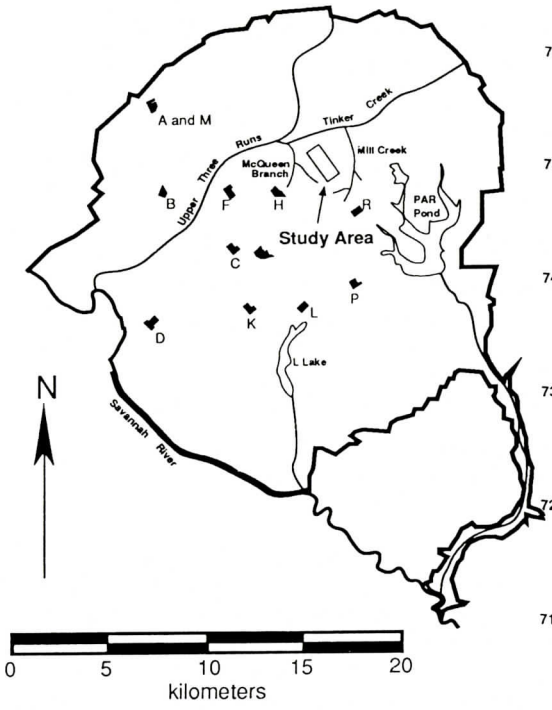

Figure 1.-Location of study area within the Savannah River Site.

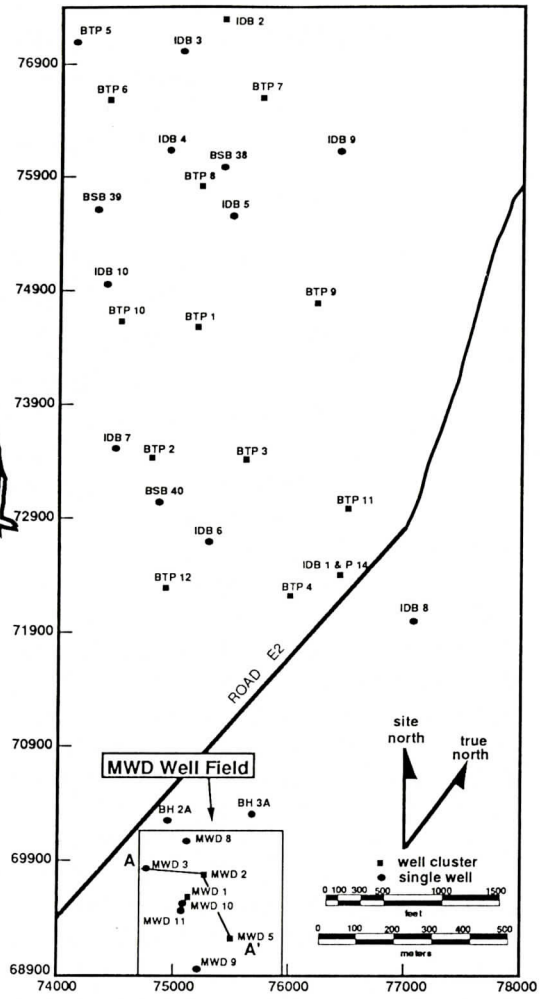

Figure 2.-Wells in the study area. SRS plant coordinates are shown in feet.

eight locations here. Wells MWD 1A, 2A, 3A, and 5A were continuously cored to a depth of about 90 m. The 48 wells located to the north of the MWD Well Field were studied in order to establish additional control.

Methods of Investigation

The stratigraphic framework and lithologic character of the Tertiary units were determined by evaluation of lithologic and geophysical logs. Lithologic logs were prepared from unpublished core descriptions made by M. K. Harris of the Westinghouse Savannah River Company and by visual inspection of core by the authors. Size distribution characteristics of the stratigraphic units were determined by 144 sieve analyses of MWD Well Field cores. The permeability distribution was determined by taking 4,200 permeability measurements with a minipermeameter.

Influence of Texture on Permeability

Texture is the fundamental building block of a lithofacies. Because texture determines the tortuosity of fluid flow and pore throat diameter, it controls permeability. Grain size, sorting, and packing have a major influence on permeability, and sphericity and roundness influence permeability to a lesser extent (Fraser, 1935; Beard and Weyl, 1973). In general, permeability increases with increasing grain size and improved sorting values (Krumbein and Monk, 1943). This is because tortuosity increases and

pore throat diameters decrease as the grain size gets finer and sorting becomes poorer. It is difficult to determine quantitatively the influence of packing on permeability (Beard and Weyl, 1973).

Previous Investigations

There have been some detailed analyses of relationships between permeability, texture, and depositional environments. Pryor (1973) determined porosity, permeability, and textural parameters for 992 oriented, undisturbed sand samples from Holocene river bar, beach, and dune environments. Results from Pryor (1973) indicate that the largest variation in permeability of the three environments studied was in river point bars, ranging from 4 millidarcies to 500 darcies with an average of 93 darcies. Beach sands had the second largest permeability distribution with a range of 3.6 to 166 darcies and an average of 68 darcies. Dune sands had the least variation in permeability with a range of 5 to 104 darcies and an average of 54 darcies. Of these three environments, point bars are the most heterogeneous and have the widest variation in texture; dune deposits are the least heterogeneous and contain the least variation in texture (Reineck and Singh, 1980).

Weber and others (1972) examined permeability distribution in unconsolidated Holocene channel-fill sands. They found that higher permeability values occur near the center of the channel-fill and gradually decrease toward the bank. They also found that permeability anisotropy in cross-beds is small.

Chandler and others (1989) and Goggin (1988) characterized permeability distribution in Jurassic eolian sandstone. They found a close correlation between strata type and permeability, that average permeability of each lithology is significantly different from that of other types, that permeability within each lithology is essentially log-normally distributed, and that permeability distribution closely follows geologic features which reflect specific depositional processes.

Dreyer and others (1990) made detailed permeability measurements of outcrops of Triassic ribbon-like distributary sand bodies. They documented a close connection between depositional facies and permeability, and delineated five site-specific permeability classes corresponding to different depositional environments. Through statistical evaluation, they showed that permeability distribution was significantly different for each permeability class.

Tyler and others (1991) characterized the permeability distribution in surface exposures of a wave-dominated deltaic sandstone. They found that permeability distribution corresponds closely to lithology, and that permeability distribution waslog-normal within each stratification type.

STRATIGRAPHIC UNITS

Introduction

In the MWD area and vicinity, the Coastal Plain section is about 270 m thick (Snipes and others, 1993). Figure 3 is a composite strati-

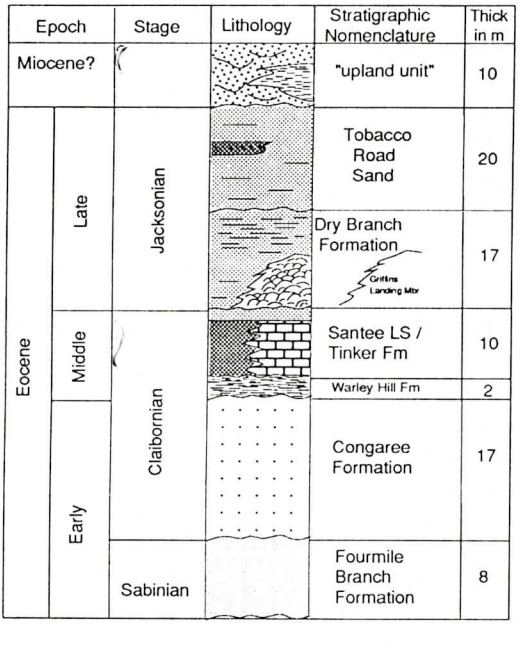

Figure 3.-Stratigraphic column for Eocene and Miocene(?) section at the MWD Well Field.

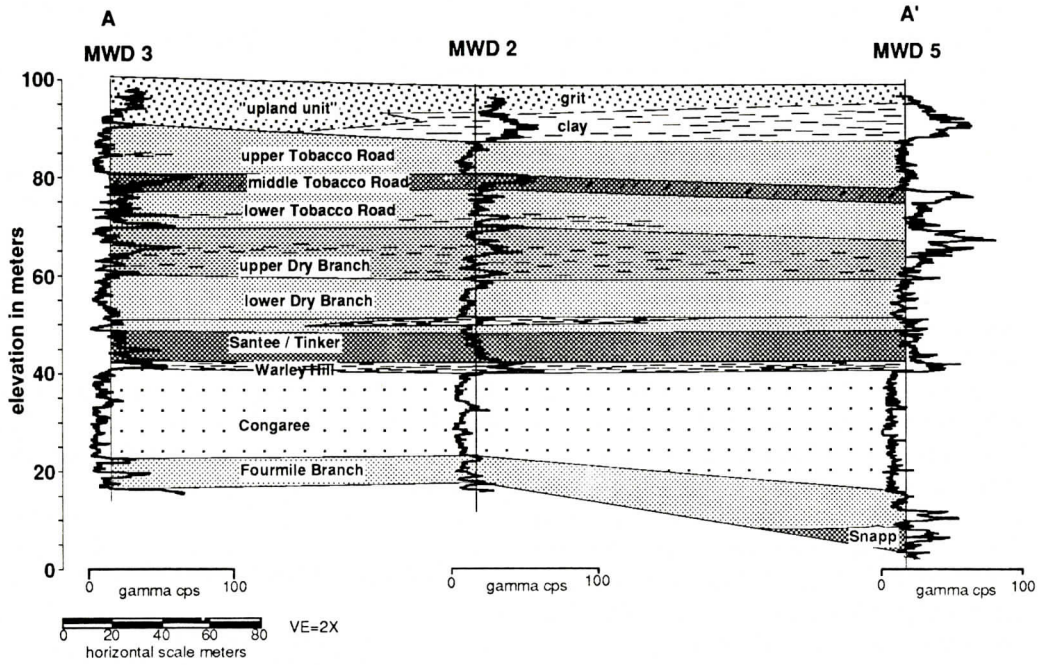

Figure 4.-Stratigraphic cross-section of the MWD Well Field.

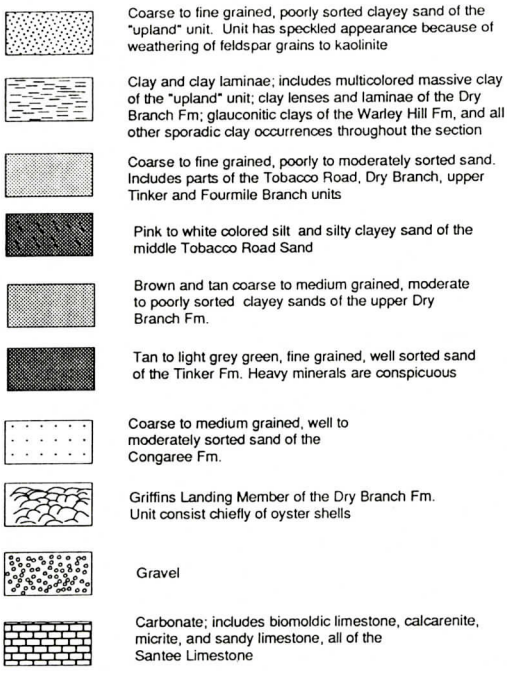

Figure 5.-Lithologic symbols used in stratigraphic column and cross-sections.

graphic column for the units studied, based on core descriptions from the MWD wells, well P 14, and well IDB 2. Figure 4 is a stratigraphic cross-section through the MWD Well Field. Lithologic symbols in the stratigraphic column and cross section are explained in Figure 5.

Fourmile Branch Formation

Prowell and others (1985) assigned an early Eocene age to sands, silts, and clays at SRS, and Fallaw and Price (1992; in preparation) named these sediments the Fourmile Branch Formation. In the MWD area the formation is composed of loose, fine to coarse grained, poorly sorted sands. Muscovite, glauconite, iron sulfide, and mud laminae are present in places. Silicified sand was encountered near the top of the formation in wells MWD 1A, MWD 5A, and BTP 10C. Average thickness of the unit is 8 m, but thickness varies considerably from well to well. The sediments are generally dark to light gray. The Fourmile Branch is more poorly sorted and has a slightly higher mud content than the overlying Congaree For-

mation. The distinction between the Congaree and Fourmile Branch, however, is vague in many areas because the two units are often lithologically similar. Sediments and dinoflagellates suggest a shallow marine environment in the MWD area.

Congaree Formation

The term "Congaree Phase" was used by Sloan (1908) for exposures of clay and sand in the updip Coastal Plain. Siple (1967) described sands of the Congaree Formation, as defined by Cooke and MacNeil (1952), at the SRS. Sands of the Congaree and Fourmile Branch constitute the principal Tertiary aquifer in the area. Previous investigations (Siple, 1967; McClelland, 1987; Dennehy and others, 1989; Logan and Euler, 1989; Robertson, 1990) included in the Congaree Formation sands and muds now assigned to the Fourmile Branch. At the SRS the Congaree is almost entirely quartz sand with very little interstitial mud (Robertson, 1990). It consists of orange to light gray, well to moderately sorted, coarse to medium grained unconsolidated sand. Mud laminae are uncommon in the cores from the MWD Well Field. Average thickness of the formation is 17 m in the study area. The texture of the Congaree sediments indicates deposition in high energy, neritic and littoral environments.

Warley Hill Formation

The term "Warley Hill Phase" was used by Sloan (1908) for glauconitic "marls" and sands between his Congaree and Santee phases. Siple (1967) referred to spotty and discontinuous exposures of Warley Hill Formation at the SRS and reported "glauconitic sand similar to that generally associated with the Warley Hill" from well cuttings. In the MWD Well Field the Warley Hill is represented by a pronounced gamma ray spike approximately 55 to 58 m below ground surface (Figure 4). The formation consists of green and dark orange muds, sandy muds, and muddy sands, with glauconite common in muddy portions of the unit. Average thickness of the unit is 2 m in the MWD Well Field, but thickness varies considerably over the study area. The formation is an aquitard. At the MWD Well Field the Warley Hill corresponds to the entire "green clay interval", but elsewhere at the SRS the "green clay interval" may include portions of the underlying and overlying formations (Snipes and others, 1992). Sediments and fossils indicate shallow marine and lagoonal environments of deposition for the formation.

Santee Limestone and Tinker Formation

At the SRS middle Eocene calcareous sediments and age-equivalent siliciclastics have been referred to as the "McBean Formation" by most previous workers (e.g., Siple, 1967; Dennehy and others, 1989; Logan and Euler, 1989). Fallaw and Price (1992; in preparation) propose assigning the carbonates to the Santee Limestone and the clastics to their newly named Tinker Formation.

At the MWD Well Field the Santee and Tinker are interfingering and intergradational. The calcareous facies is composed of fine grained quartz sand supported in a micrite and calcarenite matrix. Shell fragments are common. Some parts of the carbonate facies consist of indurated biomoldic limestone. The siliciclastic facies is composed of a well-sorted, fine grained quartz sand and poorly sorted coarse to medium grained sand. Muds occur at the top of this facies in places. The fine sand facies may be the result of carbonate dissolution or may represent channels where higher energy flow regimes overwhelmed carbonate deposition. The fine grained sand facies occurs in wells MWD 2A, 3A, 5A, and BTP 12C. Heavy minerals are conspicuous in both the fine grained sand and the calcareous facies. Green mud beds are sometimes present near the base of the siliciclastics. The average thickness of the Santee-Tinker section is about 10 m at the MWD Well Field. Sediments and abundant fossils indicate a middle-to-inner neritic environment for the Santee and inner neritic, littoral, barrier, and lagoonal environments for the Tinker.

Dry Branch Formation

In the study area the Dry Branch Formation (Huddlestun and Hetrick, 1986; Nystrom and Willoughby, 1982) is a tan-to-yellowish-orange, coarse-to-medium grained muddy sand, with mud content increasing up-section. The formation can be mapped at the MWD Well Field as two distinct units. The upper unit has a higher mud content than the lower, with common, thin, tan mud lenses and laminae, some up to 1 m thick. The upper unit is an aquitard at the MWD Well Field. The contact between the upper and lower units of the formation, picked at the base of the lowest tan mud bed, is fairly uniform across the study area, although individual mud beds generally can not be correlated from well to well. The contact between the upper Dry Branch and the overlying Tobacco Road Sand is marked by a change from yellowish-orange to red and the occurrence of a coarse sand bed containing pebbles at the base of the Tobacco Road. This contact occurs at about 30 m below land surface at the MWD Well Field and corresponds to a pronounced gamma ray spike on geophysical logs of some wells (Figure 4). The average thickness of the Dry Branch is 17 m at the MWD Well Field, and the average thicknesses of the upper and lower portions of the formation are 9 and 8 m respectively.

The calcareous Griffins Landing Member (Huddlestun and Hetrick, 1986) of the Dry Branch is present at well clusters IDB 2 and BTP 6. The member also occurs at well NPN 1A about 610 m west of the MWD Well Field. Where the Griffins Landing is present the Dry Branch is unusually thick, and the upper contact of the Dry Branch is higher in elevation than normal. At well BTP 6C the member is 21 m below ground surface. In the study area the unit consists of bioherms of oyster shells within a matrix of mud which are probably local barriers to ground water flow. Dry Branch sands were probably deposited in inner neritic and littoral environments, with muds and carbonates forming in lower energy, possibly lagoonal, environments.

Tobacco Road Sand

The Tobacco Road Sand (Huddlestun and Hetrick, 1978, 1986; Nystrom and Willoughby, 1982) consists of red, purple, and pink, coarse-to-medium grained, poorly-to-moderately sorted sands and muddy sands. A 3-m thick, pink, fine grained, silty sand layer occurs in the middle of the formation in the MWD Well Field. The presence of this layer allows division of the formation into upper, middle, and lower units in this area. The middle layer may support a perched water table at the MWD Well Field. The upper and lower units have similar textures and mud content and contain some thin mud beds (<10 cm). Average thickness of the formation is 20 m at the MWD Well Field, and average thicknesses of the upper, middle, and lower units are 9, 3, and 8 m respectively.

In places where the formation crops out, *Ophiomorpha* burrows are commonly observed, and in some places bioturbation has been intense enough to obscure bedding. Burrows are rarely recognized in core samples at the SRS. Gentle cross-bedding is also common within the formation (Nystrom and others, 1986; Dennehy and others, 1989). Sedimentary facies patterns suggest deposition of the Tobacco Road in shallow neritic, barrier island, and tidal flat environments.

"Upland" unit

A poorly sorted, coarse grained sand and gravel facies with mud lenses, common at higher elevations at the SRS, has been mapped as the "upland" unit by Nystrom and Willoughby (1982) and Nystrom and others (1986). In the study area it consists of multicolored muds, sandy muds, and muddy sands. Red is the dominant color. The unit is not well dated. Huddlestun (1988) and Nystrom and Willoughby (1992) proposed a Miocene age, and Colquhoun (1992) suggested Eocene-Oligocene. Two distinct facies of the formation are present in the MWD Well Field (Figure 4). One

Table 1.-Average statistical measures for sieved samples.

Formation	Number of samples	Mean grain size phi	Sorting	Skewness	Kurtosis
Tobacco Road	35				
average		1.46 +/- 0.20	1.02 +/- 0.09	0.04 +/- 0.05	1.19 +/- 0.09
standard deviation		0.58	0.25	0.16	0.26
verbal classification		medium sand	poorly sorted	near symmetrical	leptokurtic
Dry Branch	27				
average		1.48 +/- 0.14	0.88 +/- 0.06	-0.02 +/- 0.05	1.07 +/- 0.05
standard deviation		0.40	0.18	0.13	0.14
verbal classification		medium sand	moderately sorted	near symmetrical	mesokurtic
Santee/Tinker	21				
average		2.29 +/- 0.20	0.80 +/- 0.09	-0.03 +/- 0.05	1.13 +/- 0.08
standard deviation		0.58	0.26	0.13	0.22
verbal classification		fine sand	moderately sorted	near symmetrical	leptokurtic
Congaree	44				
average		1.08 +/- 0.13	0.80 +/- 0.06	-0.02 +/- 0.06	1.10 +/- 0.06
standard deviation		0.38	0.17	0.18	0.17
verbal classification		medium sand	moderately sorted	near symmetrical	mesokurtic
Fourmile Branch	17				
average		0.77 +/- 0.33	1.00 +/- 0.08	-0.13 +/- 0.06	1.31 +/- 0.10
standard deviation		0.96	0.23	0.18	0.29
verbal classification		coarse sand	moderately-poorly sorted	fine skewed	leptokurtic

+/- = 95% confidence for the mean of the statistical parameters

is a poorly sorted sand with weathered feldspar which occurs in the western half of the study area and at the top of the formation in the eastern half of the field. The other facies is a multicolored, massive mud facies in the eastern half of the area. A gravelly channel facies is exposed along a dirt road a few hundred feet north of the IDB 2 well cluster outside the study area. Large scale cross-bedding and scour and fill are commonly observed in surface exposures at the SRS. "Upland" sediments have the characteristics of fluvial deposits.

TEXTURAL ANALYSIS

Sieve Analysis

The textural characteristics of the sediments beneath the MWD Well Field were determined by 144 sieve analyses and by examination of cores. One hundred and eight sieve analyses were conducted as part of this study, and 36 analyses were done by M. K. Harris (written communication, 1988) prior to this investigation.

Samples collected as part of this study were taken at approximately 3-m intervals from wells MWD 1A, 2A, 3A, and 5A. Only sediment with a visually estimated mud content of less than 10% was selected for sieving. The "upland" and Warley Hill units were not sampled. At the desired sample interval an approximately 7-cm long piece of half-core was scraped to remove drilling mud. The sample was dried, disaggregated, split, weighed, and dry sieved at half phi intervals. Sieve sizes used in this investigation included U. S. Stan-

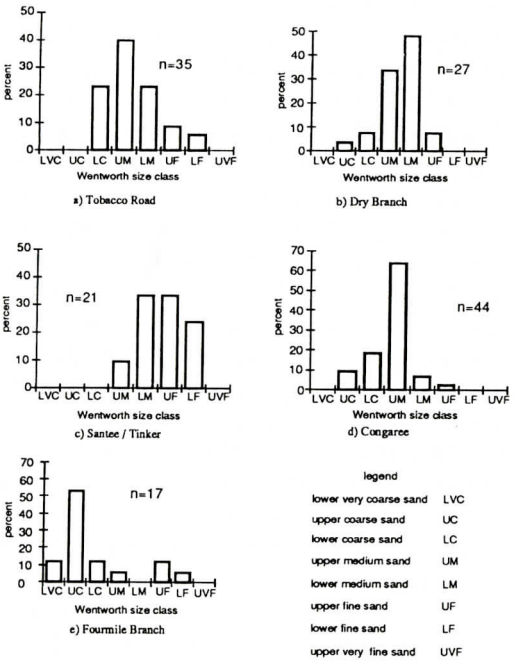

Figure 6.-Mean grain size distribution for stratigraphic units in the MWD Well Field as determined from sieve analysis.

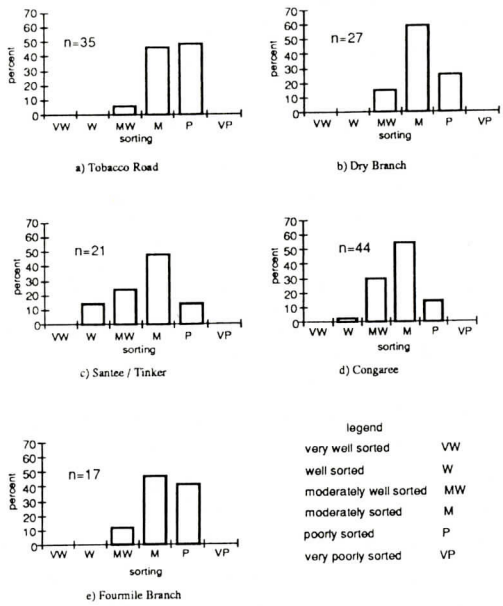

Figure 7.-Distribution of inclusive graphic standard deviation for stratigraphic units in the MWD Well Field as determined by sieve analysis. Sorting is equal to inclusive graphic standard deviation of Folk and Ward (1957).

dard Sieve Mesh numbers 10, 14, 18, 25, 35, 60, 80, 120, 170, and 230. With coarser material U. S. Standard Sieve Mesh numbers 5 and 7 were used. Size analyses were not done for sediment finer than 4.0 phi. Sieving procedures in Folk (1980) were used.

Statistical measures of Folk and Ward (1957) indicate that each stratigraphic unit at the MWD Well Field has a distinct textural composition (Table 1). Because texture and its distribution are the primary properties influencing permeability, each stratigraphic unit should have a distinct permeability distribution.

Histograms of textural parameters of each stratigraphic unit (Figures 6 through 9) reveal heterogeneity at two scales. Heterogeneity caused by textural differences between individual beds within a formation is indicated by the distribution spread within histograms. Heterogeneity between formations is indicated by distribution differences between histograms. The histograms indicate that the permeability distribution should be unique for each formation. The sample set is somewhat biased, however, because only sands with a visually estimated mud content of less than 10% were chosen for analysis.

Visually Estimated Mud Content

Because the distribution of silt and clay size material can have a large impact on permeability, the percent mud in each unit at the MWD Well Field was estimated by inspection with a binocular microscope of core at 0.3-m intervals by M. K. Harris (written communication, 1988). The mud percentages include mud occurring as matrix and as discrete beds, lenses, and laminae. Average percent gravel, sand, and mud are shown for each unit in Table 2.

For the most part, mud content within each unit has little variation between wells. Notable exceptions to this are the "upland" unit and the Warley Hill Formation. The mud content in the "upland" unit ranges from 47% mud at well MWD 1A to 70% mud at well MWD 5A. This increase is caused by a clay facies in well MWD 5A (Figure 4). The mud content of the

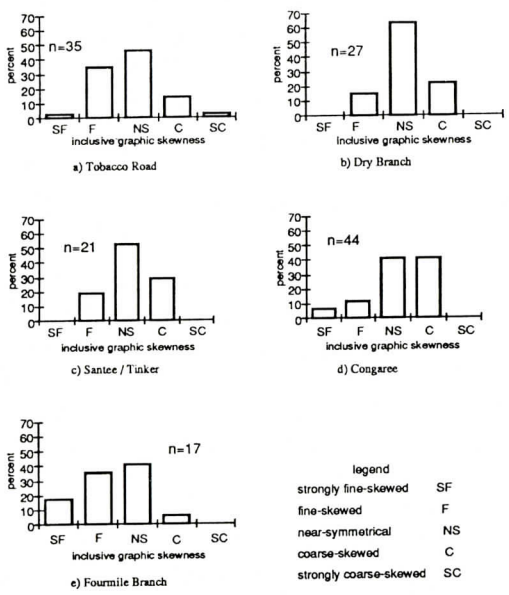

Figure 8.-Distribution of inclusive graphic skewness (Folk and Ward, 1957) for stratigraphic units at the MWD Well Field as determined by sieve analysis.

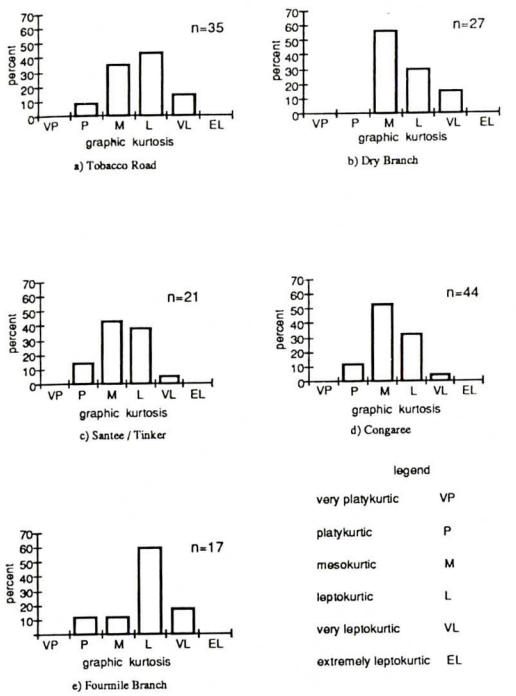

Figure 9.-Distribution of graphic kurtosis (Folk and Ward, 1957) for stratigraphic units at the MWD Well Field as determined by sieve analysis.

Warley Hill Formation is about 40% except in well MWD 3A where it is 18%.

PERMEABILITY DETERMINATIONS

Methods

A significant breakthrough in the study of permeability distribution is the use of a minipermeameter (Weber, 1982). A minipermeameter measures gas permeability of a small volume of rock. The instrument can measure permeability of cores, hand specimens, and outcrop faces and can make a large number of nondestructive measurements over a short period of time. Detailed studies using a minipermeameter have been conducted by Weber and others (1972), Goggin (1988), Chandler and others (1989), Dreyer and others (1990), and Tyler and others (1991).

A large number of closely spaced measurements is needed to study distribution of permeability within a ground water system; conventional methods, however, are too time consuming and costly to be used effectively; using a minipermeameter provides a solution to this problem. The instrument is designed to make a large number of rapid, localized, nondestructive permeability measurements. One measurement usually takes less than a minute. The equipment consists of a compressed nitrogen supply tank, flow rate measurement unit, and injection tip. The flow rate measurement unit is composed of a pressure gauge, regulator, series of flow meters, pressure transducer, and digital display (Temco, Inc., 1991), powered by a 12-volt battery. The injection probe consists of a valve and a silicone rubber tip. The tip is soft enough to conform to moderately irregular rock surfaces yet firm enough to resist severe deformation under compression. The tip size used for this study was 4 mm outside diameter and 1 mm inside diameter which

Table 2.-Visually estimated percent gravel, sand, and mud based on microscopic examination of core samples (M. K. Harris, written communication, 1988).

WELL	MWD-1A			MWD-2A			MWD-3A			MWD-5A		
Percent	Gravel	Sand	Mud	Gravel	Sand	Mud	Gravel	Sand	Mud	Gravel	Sand	Mud
"upland" unit	2	51	47	1	35	64	1	53	46	1	29	70
Tobacco Road	2	73	25	2	73	25	2	76	22	1	69	30
Upper Tobacco Road	1	76	23	1	79	20	2	80	18	1	73	26
Middle Tobacco Road	2	64	34	1	67	32	1	68	31	0	62	38
Lower Tobacco Road	2	74	24	2	71	27	2	75	23	2	68	30
Dry Branch	1	76	23	1	76	23	1	77	22	1	75	24
Upper Dry Branch	1	72	27	1	71	28	1	75	24	1	63	36
Lower Dry Branch	1	80	19	1	83	16	1	80	19	1	83	16
Santee / Tinker	1	74	25	1	78	21	0	84	16	0	72	28
Warley Hill	0	57	43	1	59	40	1	81	18	1	59	40
Congaree	1	90	9	1	93	6	1	93	6	2	93	5
Fourmile Branch	2	83	15	2	84	14	3	76	21	7	72	21

note: These averages are taken from unpublished core descriptions by M. K. Harris (1988), Westinghouse Savannah River Company.

provided a good seal for most samples encountered in this study.

At the sample point an approximately 5-cm length of half-core was placed in an aluminum drying pan and oven dried at 50°C for 24 hours. Because drying disintegrates core consisting of montmorillonite clays and clay-sand laminae, these sediments were not sampled. This problem precluded the testing of much of the upper Dry Branch unit. Compressed nitrogen is forced to flow under a constant pressure through the injection tip pressed against the rock surface. The gas flows into and through a small volume of rock beneath the inside diameter of the tip, then in all directions including back around the outside diameter of the tip (Goggin and others, 1988). The gas is allowed to flow until both flow rate and pressure readings stabilize, usually less than 1 minute. The flow rate, injection tip pressure, and atmospheric pressure are recorded and permeability is calculated using a modified form of Darcy's law for gases. The form of Darcy's law used is

$$k = 2\mu QPb/rG_o(P_1^2 - P_2^2) \quad (1)$$

where:

k = permeability (darcies),
μ = gas viscosity (0.0178 centipoise),
Q = gas flow rate (cm^3/s),
Pb = standard reference pressure for mass flow meters (1atm),
r = inside radius of tip (cm),
G_o = geometrical factor (dimensionless).
P_1 = upstream pressure (atm),
P_2 = downstream pressure (atm),

The geometrical factor is a function of the sample dimensions and inside diameter of the tip and is used to account for the radial flow geometry. This parameter was developed to eliminate the need for equipment-specific calibration curves (Goggin and others, 1988).

In our study the minipermeameter was used to determine the spatial distribution of permeability from core samples from the MWD Well Field. Core was analyzed at 0.3-m intervals for the entire length of the geologic section cored in wells MWD 1A, 2A, 3A and 5A. A total of 4,200 measurements was made. In some instances core was missing or too unconsolidated to sample. Two horizontally oriented and two vertically oriented measurements per sample were usually taken. If the two measurements taken either horizontally or vertically did not agree, two more measurements were made to ensure that the discrepancy was caused by sample heterogeneity and not by a bad tip seal. At every tenth sample, five measurements were made in both directions to evaluate repeatability and representativeness of measured values. Occasionally, multiple measurements differed because of small-scale heterogeneity. In most cases horizontal measurements were taken first and vertical measurements were taken last. Because most samples were unconsolidated, they would often break during the horizontal measurement and the vertical measurement probably was not as accurate. The two horizontal values were averaged and this value was taken to represent horizontal permeability at that interval. The vertical permeability measurements were treated in the same manner. These single point values were used to make permeability profiles and in statistical analysis.

Permeability measurements made with the minipermeameter and calculated with equation (1) are generally accurate within the 20 to 500 millidarcy range (Goggin and others, 1988). Outside this range two significant deviations can occur. For low permeability samples, measurements are greater than values from conventional procedures because of gas leakage around the injection tip (Goggin and others, 1988). For high permeability samples, calculated permeabilities are less than true permeability because of high velocity flow effects (Goggin and others, 1988). Nothing can be done to improve the accuracy of low permeability measurements, but high velocity flow effects can be taken into consideration to improve the measurement accuracy for high permeability samples.

High velocity flow results in a pressure drop greater than that proportional to velocity (Firoozabadi and Katz, 1979), a drop caused by turbulent flow in pores. The additional pressure drop is accounted for by incorporating an addi-

tional term into the flow equation. The equation used to correct for high velocity flow is:

$$k=-v\mu(dP/dl+\alpha\rho v^2)^{-1} \qquad (2)$$

where:

k = the intrinsic permeability (L^2),

v = the measured flow velocity (L/t),

μ = nitrogen viscosity ($F\text{-}t/L^2$),

dP/dl = pressure gradient

α = high velocity flow coefficient (L^{-1}),

ρ = the density of the fluid (m/L^3).

The equation is based on empirical data and a theoretical justification does not exist. In the equation there are two unknowns, k and α. Experimental data demonstrate that log of α is proportional to log of k, thus log α can be expressed as a function of log k (Firoozabadi and Katz, 1979).

Most samples examined in this study had permeabilities well over 0.5 darcies and required correction for high velocity flow; a correction was made for these samples using a computer program developed by Goggin (1988). In order to gain insight into the validity of lower permeability values, measurements were made on a glass plate; the instrument measured a permeability of 0.002 to 0.004 darcies. This value results from gas leakage around the tip and not gas flow through the glass. Some of the clay material, cemented sand, and limestones tested in our study had measured permeabilities in this range and were below the level of quantification of the minipermeameter.

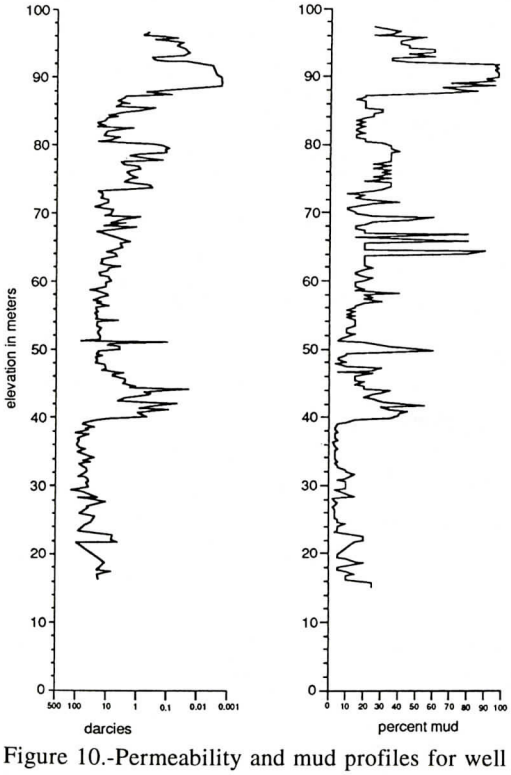

Figure 10.-Permeability and mud profiles for well MWD 2.

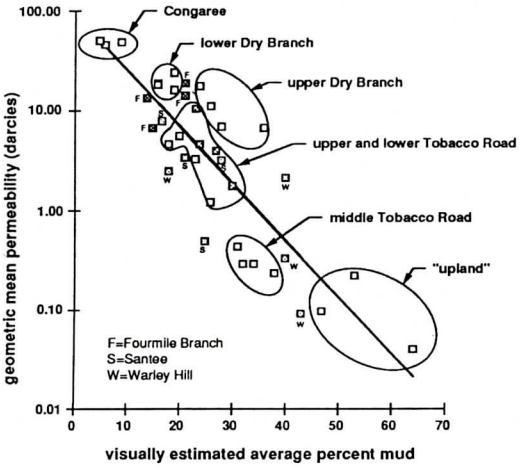

Figure 11.-Plot of visually estimated mud content versus geometric mean permeability.

Results

Permeability profiles with visually estimated percent mud were made for wells MWD 1A, 2A, 3A, and 5A, Figure 10 being an example. The mud percentages represent clay and silt existing as individual beds and as matrix material filling pore spaces between the sand grains. The measured horizontal permeability ranges from a low of 0.002 darcies for silicified sands of the Fourmile Branch Formation to a high of 154 darcies in well-sorted sands of the Congaree Formation. Lower permeability values correspond to muddy intervals, with the exception of carbonate in the Santee in well MWD 1A (41 to 47 m amsl) and silicified zones within the Fourmile Branch in wells MWD 1A (18 m amsl) and MWD 5A (17 m

amsl). The permeability profiles indicate that mud content is the dominant sediment property controlling permeability. The interval between 60-70 m amsl contains montmorillonite beds of the upper Dry Branch Formation. Because these clays could not be measured by the minipermeameter, the permeability curves do not correspond to the mud profile for this interval. An undisturbed sample taken from an upper Dry Branch clay bed had a measured permeability of 2.9 X 10^{-5} to 1.3 X 10^{-4} darcies (Westinghouse Savannah River Company, 1991).

Figure 11 is a plot of visually estimated average percent mud and the geometric mean permeability for each unit within each well. In general, units with high mud content have a lower permeability than units with low mud content. A regression analysis of the best fit curve yields a correlation coefficient of -0.92 using the log of the permeability. Figure 11 shows that data points from the same unit plot in close proximity to each other; this is because at the megascale level the units are fairly homogeneous. Subsurface units that have scattered data points are more heterogeneous. Because much of the muddy portion of the upper Dry Branch unit could not be tested, the data points for this unit plot higher than would be expected. If permeability measurements were available for the muddy portions of the upper Dry Branch unit, the geometric mean permeability would be lower and data points would plot lower. The Warley Hill data points are of questionable accuracy because of poor condition of the core and the low number of permeability measurements in this interval.

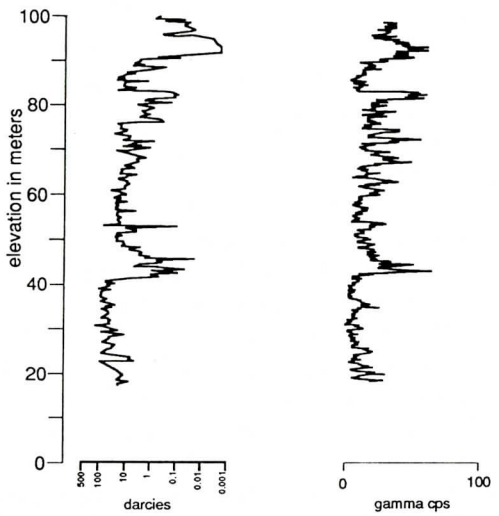

Figure 12.-Permeability profile and gamma ray log for well MWD 2.

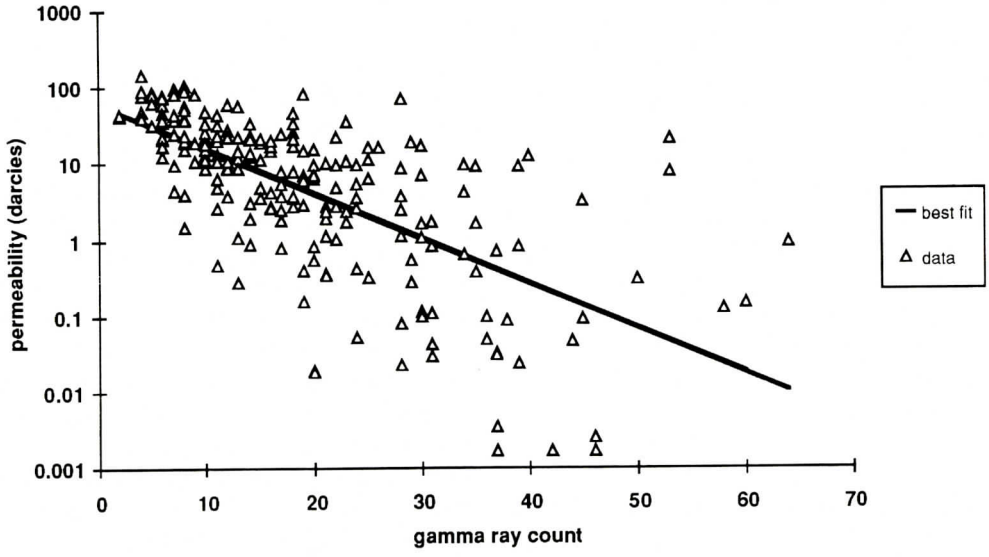

Figure 13.-Plot of permeability versus gamma ray count for well MWD 2.

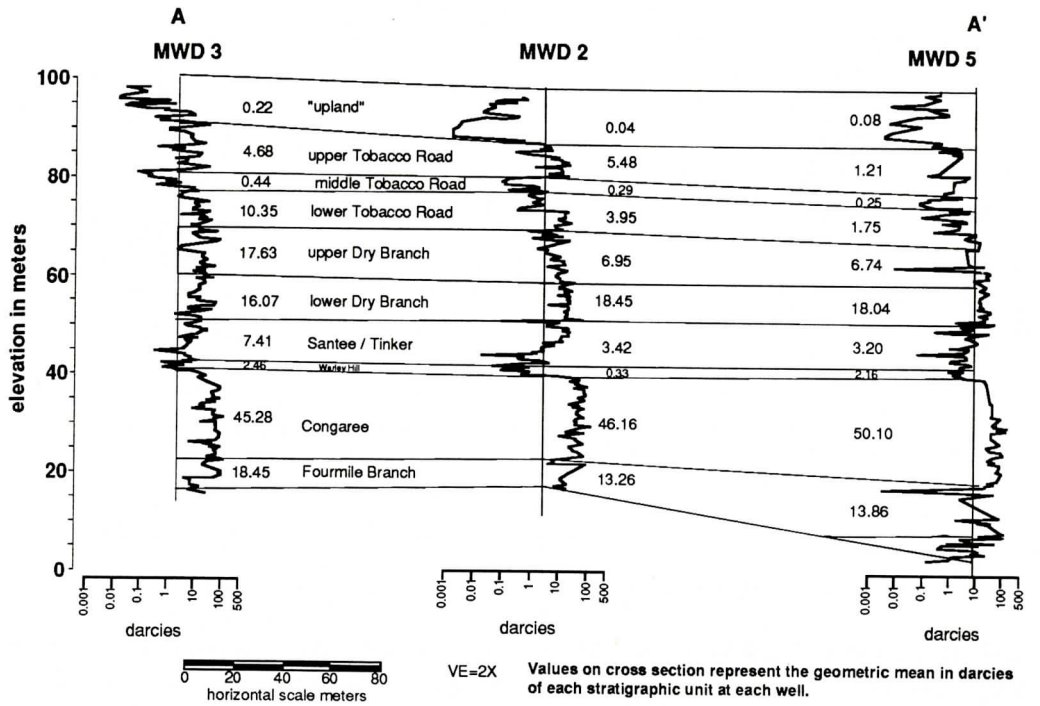

Figure 14.-Permeability cross-section for the MWD Well Field.

There is a remarkable similarity between gamma ray logs and permeability profiles (Figure 12), a similarity caused by the presence of fine grained material. Constituents of fine grained sediment, such as micas and clay minerals, are rich in potassium, but the coarse grained sediment is composed primarily of quartz. Clay minerals will also preferentially absorb metals, thereby accumulating radionuclides and emitting more gamma radiation than adjacent sands. Clays reduce permeability by filling pore spaces between sand grains and by being barriers to flow between sand beds where clay layers are present. The relationship between permeability profiles and gamma ray logs suggests that these logs could be useful tools for defining hydrostratigraphic units and predicting spatial distribution of permeability. A plot of permeability versus gamma ray count for well MWD 2 (Figure 13) shows a general increase in permeability with decrease in gamma ray count. A regression analysis yields a correlation coefficient of -0.67 using the log of the permeability values. The gamma ray counts were taken from the gamma ray log and do not correspond to the exact sample which was measured for permeability, and the mineralogy of the clays is probably different for each stratigraphic unit. The various clays within each unit emit different levels of gamma ray energy. The correlation coefficient would improve if gamma radiation energy were measured at the exact locations where permeability measurements are made.

Figure 14 shows permeability profiles, using geometric mean permeability data, along the line of section in Figure 2. Correlation lines in Figure 14 were determined by lithology and are the same as in the Figure 4 cross section. Similarity of permeability profiles is not surprising considering that permeability is controlled by textural properties of rock and that these textural properties are more or less distributed as discrete, somewhat horizontal intervals which correspond to lithology. This observation suggests that the permeability profiles can be divided into units of similar permeability based on lithology. Permeability units

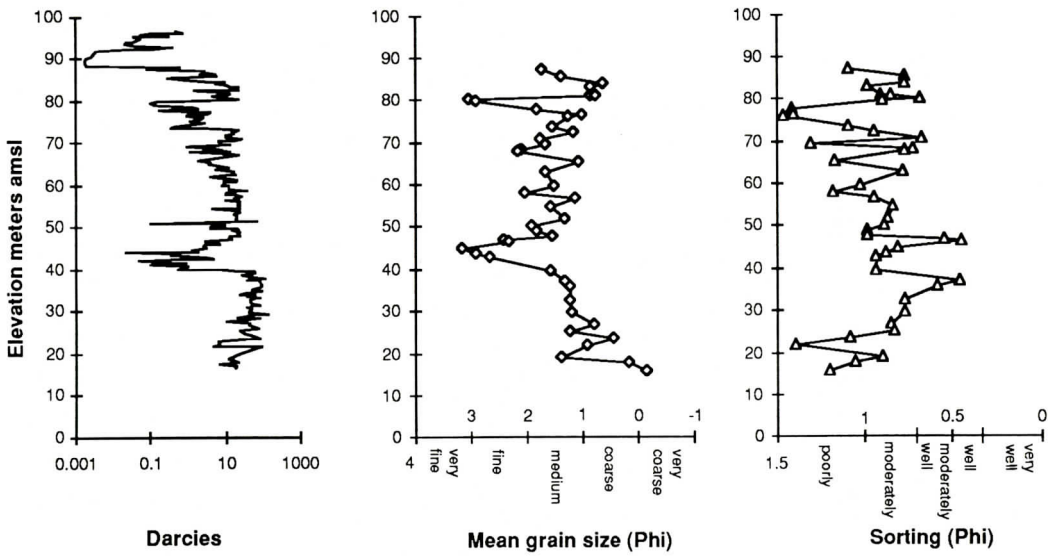

Figure 15.-Permeability profile for well MWD 2 with mean grain size and sorting profiles.

have been correlated with lithologic units by many authors including Weber and others (1972), Chandler and others (1989), Dreyer and others (1990), and Tyler and others (1991). Similarity of permeability profiles in Figure 14 indicates reasonably good permeability correlation between wells spaced approximately 150 m apart. Figure 14 also illustrates spatial variability of permeability at the inter-formational level.

Figure 15 is the permeability profile for well MWD 2 plotted with mean grain size and sorting values determined from sieve analysis. In general, permeability decreases as mean grain size decreases and as sorting becomes poorer.

Qualitative results from the minipermeameter analysis indicate that the Eocene and Miocene(?) section in the MWD Well Field can be divided into discrete units based on permeability. The boundaries for the these units are determined by lithology; the lithologic units, therefore, are also permeability units.

Statistical Analysis

Statistical values for the horizontal measurements are in Table 3, and the arithmetic mean, standard deviation, and geometric mean for the vertical measurements are compared to the horizontal values in Table 4. There are no systematic differences between the vertical and horizontal values, and most values are remarkably close; the average difference between the means is about one darcy.

Figures 16 and 17 show the frequency distribution of the natural log of permeability. More heterogeneous units, such as the "upland", and Santee/Tinker, are composed of contrasting lithologies and have a broad and irregular distribution, but the lower Dry Branch and Congaree units, composed of fairly uniform lithologies, have narrow and smooth distributions.

Figure 18 is a plot of percent mud (Table 2) and coefficient of variation for permeability (Table 3) for each unit investigated. The data indicate heterogeneity at inter-formational and intra-formational scales. Heterogeneity at the intra-formational scale is indicated by the scattering of the data points within each unit. The lithology of the Congaree is fairly uniform and the data points plot close together, whereas the lithology of the "upland" is characterized by discontinuous beds of clayey sand and clay affected by intense weathering, and the data

Table 3.-Statistical measures for the MWD Well Field.

Formation/Well	number of samples	arithmetic mean darcies	arithmetic standard deviation darcies	variation coefficient sd/mean	geometric mean darcies	confidence of the mean at 95%
"upland" unit						
MWD 1A	25	0.29	0.77	2.66	0.09	0.16 - 0.06
MWD 2A	24	0.14	0.20	1.46	0.04	0.08 - 0.02
MWD 3A	19	1.16	2.34	2.02	0.22	0.58 - 0.08
MWD 5A	20	0.26	0.27	1.07	0.08	0.21 - 0.03
all wells	88	0.43	1.22	2.84	0.08	0.13 - 0.06
Tobacco Road						
MWD 1A	62	6.45	7.75	1.20	2.77	4.16 - 1.84
MWD 2A	56	6.76	7.09	1.05	2.98	4.48 - 1.98
MWD 3A	61	8.97	9.76	1.08	4.34	6.62 - 3.01
MWD 5A	52	2.19	2.66	1.22	1.05	1.52 - 0.73
all wells	231	6.23	7.74	1.24	2.55	3.12 - 2.09
Upper Tobacco Road						
MWD 1A	29	6.60	5.66	0.86	3.30	6.31 - 1.73
MWD 2A	23	8.55	6.99	0.82	5.48	8.88 - 3.39
MWD 3A	27	7.70	8.34	1.08	4.68	7.10 - 3.08
MWD 5A	19	1.75	1.32	0.75	1.21	1.97 - 0.75
all wells	98	6.42	6.72	1.05	3.37	4.43 - 2.57
Middle Tobacco Road						
MWD 1A	8	0.38	0.33	0.85	0.29	0.55 - 0.16
MWD 2A	9	0.52	0.60	1.15	0.29	0.69 - 0.13
MWD 3A	10	0.81	0.91	1.12	0.44	1.04 - 0.19
MWD 5A	10	0.49	0.75	1.52	0.25	0.57 - 0.11
all wells	37	0.56	0.69	1.23	0.31	0.44 - 0.22
Lower Tobacco Road						
MWD 1A	25	8.22	9.98	1.21	4.63	7.38 - 2.91
MWD 2A	24	7.39	7.38	0.99	3.95	6.76 - 2.31
MWD 3A	24	13.81	10.56	0.76	10.35	14.56 - 7.36
MWD 5A	23	3.29	3.47	1.06	1.75	3.08 - 1.00
all wells	96	8.42	9.03	1.07	4.46	5.79 - 3.46
Dry Branch						
MWD1A	34	21.90	17.41	0.79	15.78	21.19 - 11.75
MWD 2A	54	14.49	10.73	0.74	10.92	13.72 - 8.70
MWD 3A	50	22.18	17.83	0.80	16.89	18.03 - 15.83
MWD 5A	35	18.65	10.66	0.57	12.87	20.78 - 7.98
all wells	173	18.95	14.81	0.78	13.39	15.69 - 11.44
Upper Dry Branch						
MWD 1A	18	16.66	16.63	0.99	10.86	17.49. - 6.74
MWD 2A	29	9.01	5.53	0.61	6.95	9.55 - 5.06
MWD 3A	27	24.02	20.45	0.85	17.63	24.49 -12.69
MWD 5A	12	14.49	11.21	0.77	6.74	27.66 - 1.64
all wells	86	16.08	15.72	0.98	10.18	13.11 - 7.90
Lower Dry Branch						
MWD 1A	16	27.79	16.82	0.61	24.02	32.14 - 17.95
MWD 2A	25	20.86	11.83	0.58	18.45	22.80 - 14.93
MWD 3A	23	20.03	14.29	0.71	16.07	21.56 - 11.97
MWD 5A	23	20.82	6.94	0.33	18.05	32.32 - 10.07
all wells	87	21.90	13.19	0.60	18.56	21.08 - 16.34
Santee / Tinker						
MWD 1A	22	2.15	3.18	1.48	0.49	1.24 - 0.20
MWD 2A	28	7.82	7.78	0.99	3.42	6.69 - 1.75
MWD 3A	35	10.01	7.06	0.71	7.41	10.00 - 5.50
MWD 5A	27	5.16	5.35	1.04	3.20	5.14 - 1.99
all wells	112	6.75	6.86	1.02	2.93	4.05 - 2.12
Warley Hill						
MWD 1A	2	0.09	0.00	0.05	0.09	0.14-0.06
MWD 2A	7	0.50	0.35	0.70	0.33	0.97 - 0.11
MWD 3A	10	3.29	2.44	0.74	2.46	4.56 - 1.33
MWD 5A	6	2.39	1.04	0.43	2.16	3.74 - 1.24
all wells	25	2.04	2.04	1.00	1.05	1.86 - 0.58
Congaree						
MWD 1A	15	54.47	27.53	0.50	48.53	63.97 -36.81
MWD 2A	47	53.02	27.22	0.51	46.16	54.26 - 39.26
MWD 3A	50	54.47	28.32	0.52	45.28	54.77 - 37.44
MWD 5A	38	56.69	30.69	0.54	50.10	58.63 - 42.82
all wells	150	54.58	28.27	0.52	47.06	51.66 - 42.87
Fourmile Branch						
MWD 1A	11	17.28	11.66	0.67	6.73	45.31 - 1.00
MWD 2A	5	26.61	37.48	1.41	13.26	62.76 - 2.80
MWD 3A	13	33.81	37.80	1.12	18.45	36.95 - 9.21
MWD 5A	14	44.08	42.60	0.97	13.86	66.61 - 2.88
all wells	43	32.09	35.30	1.10	12.50	24.19 - 6.45

Table 4.-Comparison of statistical measures for vertical and horizontal measurements at the MWD Well Field.

	Arithmetic mean		Standard Deviation		Geometric mean	
	Horizontal	Vertical	Horizontal	Vertical	Horizontal	Vertical
"upland" unit						
MWD 1A	0.3	0.1	0.8	0.2	0.1	0.1
MWD 2A	0.1	0.2	0.2	0.6	0.0	0.0
MWD 3A	1.2	1.4	2.3	3.9	0.2	0.2
MWD 5A	0.3	0.3	0.3	0.3	0.1	0.1
all wells	0.4	0.5	1.2	1.9	0.1	0.1
Tobacco Road						
MWD 1A	6.5	5.0	7.8	6.3	2.8	1.8
MWD 2A	6.8	6.0	7.1	6.3	3.0	2.6
MWD 3A	9.0	10.7	9.7	16.4	4.3	3.1
MWD 5A	2.2	2.1	2.7	2.5	1.1	1.0
all wells	6.2	6.1	7.7	10.0	2.6	2.0
Upper Tobacco Road						
MWD 1A	6.6	5.4	5.7	7.1	3.3	1.8
MWD 2A	8.6	5.8	7.0	5.5	5.5	4.1
MWD 3A	7.7	9.3	8.0	14.3	4.7	5.1
MWD 5A	1.7	2.8	1.3	2.6	1.2	1.6
all wells	6.4	5.9	6.7	8.8	3.4	2.8
Middle Tobacco Road						
MWD 1A	0.4	0.2	0.3	0.1	0.3	0.2
MWD 2A	0.5	0.7	0.6	1.0	0.3	0.2
MWD 3A	0.8	1.6	0.9	3.1	0.4	0.3
MWD 5A	0.5	0.7	0.8	1.3	0.2	0.2
all wells	0.6	0.9	0.7	1.9	0.3	0.2
Lower Tobacco Road						
MWD 1A	8.2	6.3	10.0	5.7	4.6	4.0
MWD 2A	7.4	8.5	7.4	7.1	4.0	5.1
MWD 3A	13.8	17.0	10.6	20.1	13.4	6.0
MWD 5A	3.3	20.7	3.5	10.3	1.8	17.6
all wells	8.4	8.6	9.0	12.2	4.5	3.5
Dry Branch						
MWD 1A	21.9	18.5	17.4	19.3	15.8	12.1
MWD 2A	14.5	13.1	10.7	8.7	10.9	9.3
MWD 3A	22.2	23.9	17.8	22.2	16.9	17.3
MWD 5A	18.7	17.4	10.7	10.8	12.9	11.1
all wells	19.0	18.1	14.8	16.6	13.4	12.1
Upper Dry Branch						
MWD 1A	16.7	17.8	16.6	24.7	10.9	9.3
MWD 2A	9.0	8.4	5.5	7.1	7.0	5.5
MWD 3A	24.0	23.9	20.5	22.2	17.6	17.3
MWD 5A	14.5	10.5	11.2	8.8	6.7	4.5
all wells	16.1	16.0	15.7	21.3	10.2	8.4
Lower Dry Branch						
MWD 1A	27.8	19.3	16.8	10.8	24.0	16.6
MWD 2A	20.9	18.4	11.8	7.3	18.5	16.9
MWD 3A	20.0	17.0	14.3	20.1	16.1	6.0
MWD 5A	20.8	20.7	6.9	10.3	18.0	17.6
all wells	21.9	20.2	13.2	9.8	18.6	17.5
Santee/Tinker						
MWD 1A	2.2	2.0	3.2	3.3	0.5	0.3
MWD 2A	7.8	6.4	7.8	7.4	3.4	2.5
MWD 3A	10.0	9.6	7.1	7.0	7.4	6.9
MWD 5A	5.2	4.5	5.4	3.7	3.2	2.5
all wells	6.8	6.0	6.9	6.4	2.9	2.2
Congaree						
MWD 1A	54.5	44.9	27.5	18.8	48.5	42.3
MWD 2A	53.0	51.7	27.2	26.1	46.2	43.4
MWD 3A	54.5	49.3	28.3	26.6	45.3	41.4
MWD 5A	56.7	57.9	30.7	30.6	50.1	48.3
all wells	54.6	51.7	28.3	27.0	47.1	43.7
Fourmile Branch						
MWD 1A	17.3	17.9	11.7	13.4	6.7	6.4
MWD 2A	26.6	12.3	37.5	8.8	13.3	8.6
MWD 3A	33.8	32.5	37.8	28.9	18.5	21.7
MWD 5A	44.1	35.9	42.6	40.2	13.9	9.5
all wells	32.1	25.7	35.3	27.0	12.5	10.9

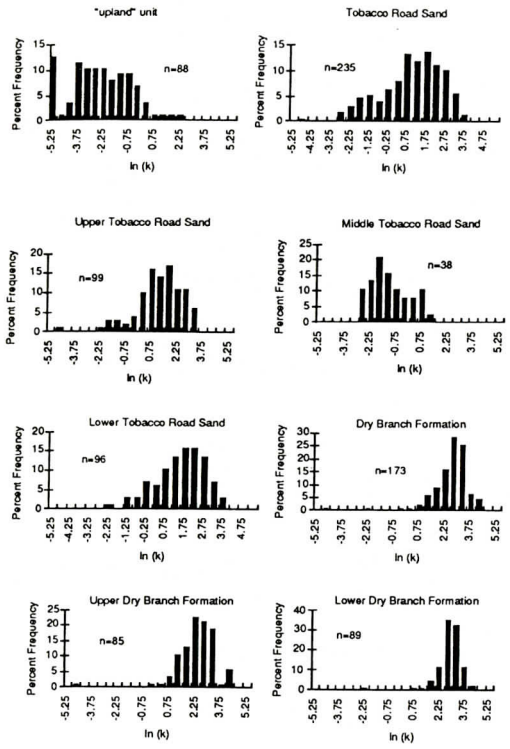

Figure 16.-Permeability distribution in the upper units in the MWD Well Field.

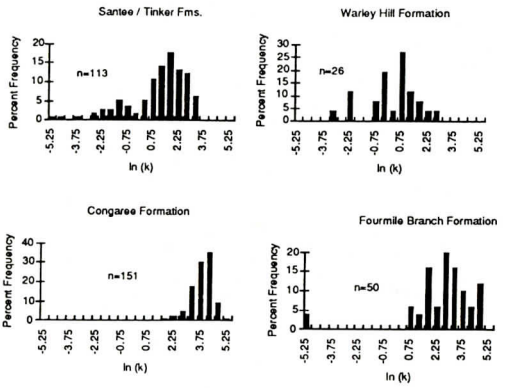

Figure 17.-Permeability distribution in the lower units in the MWD Well Field.

points for individual wells are widely spaced.

Because use of the variation coefficient normalizes the data points in Figure 18 with respect to the arithmetic mean, data from a unit with high mean permeability can be compared to a unit with low mean permeability. In general, the data support the conclusion that fine grained and poorly sorted units are more variable than coarse grained units. The Warley Hill Formation could not be adequately tested with the minipermeameter because of the poor condition of the cores. The upper Dry Branch data in Figure 18 do not account for the montmorillonitic clay beds in this unit.

The geometric mean permeability (Table 3) of each unit is shown in Figure 19. The error bars associated with each geometric mean represent the 95% confidence interval. The figure reveals heterogeneity within units as shown by varying ranges of confidence intervals, and heterogeneity between units as shown by fluctuation of geometric mean permeability. The geometric mean value for the upper Dry Branch represents permeability measurements taken from sand beds and does not include measurements from adjacent clay beds and laminae. If the permeability of clay beds were included in the study, the geometric mean for the upper Dry Branch would be much less than 10.2 darcies. The Warley Hill could not be adequately tested because the core was in poor condition.

Figures 20 through 22 show the geometric mean with the 95% confidence interval for each permeability unit in each well. The low geometric mean for the Santee/Tinker at well MWD 1 (Figure 21) is caused by carbonate. In places dissolution of carbonate has formed secondary porosity within the Santee, and overall permeability in well MWD 1 may be much higher than indicated in Figure 21.

Significance tests were performed to determine if geometric mean permeability is different between vertically adjacent units and if geometric mean permeability is the same for individual units between wells. The tests were conducted at the 5% level of significance. Because permeability distribution is controlled by lithology, it is expected that vertically adjacent units with different lithologies should have significantly different mean permeabilities; likewise, units which consist of uniform lithologies should have nearly the same mean permeability from well to well.

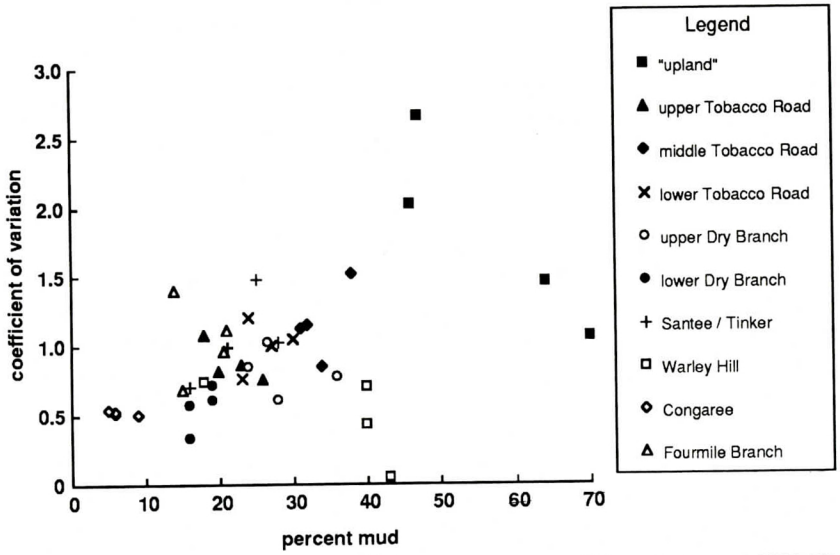

Figure 18.-Plot of permeability distribution coefficient and percent mud for units in the MWD Well Field.

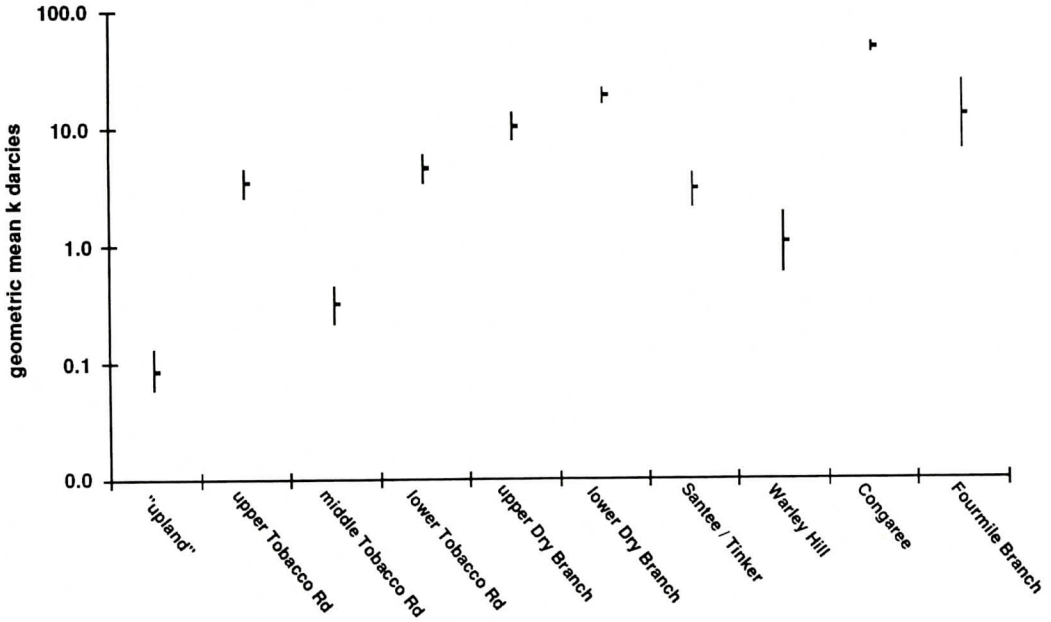

Figure 19.-Geometric mean permeability for units in the MWD Well Field. Error bars represent 95% confidence interval.

Tests performed for vertically adjacent units indicate that, with few exceptions, all geometric mean permeabilities were significantly different between adjacent units (Table 5). The log-transformed mean permeabilities which tested the same for vertically adjacent units include: the upper and lower Dry Branch units in wells MWD 3 and MWD 5; the Santee/ Tinker and the Warley Hill in well MWD 5; and the Congaree and Fourmile Branch units in well MWD 5. These similarities are probably caused by lack of sampling of mud beds and a

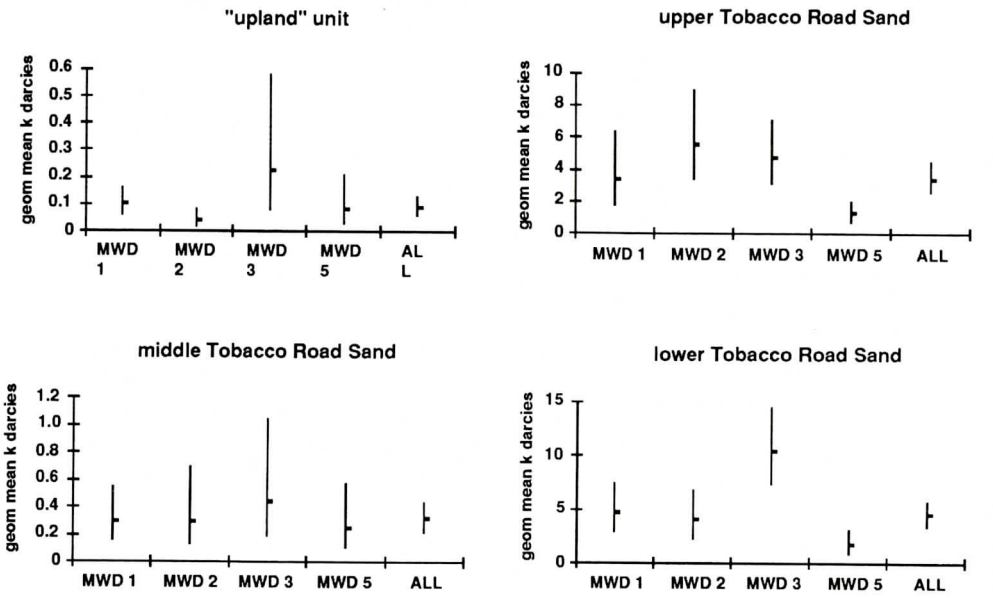

Figure 20.-Geometric mean permeability of the upper units in the MWD Well Field. Error bars represent 95% confidence interval.

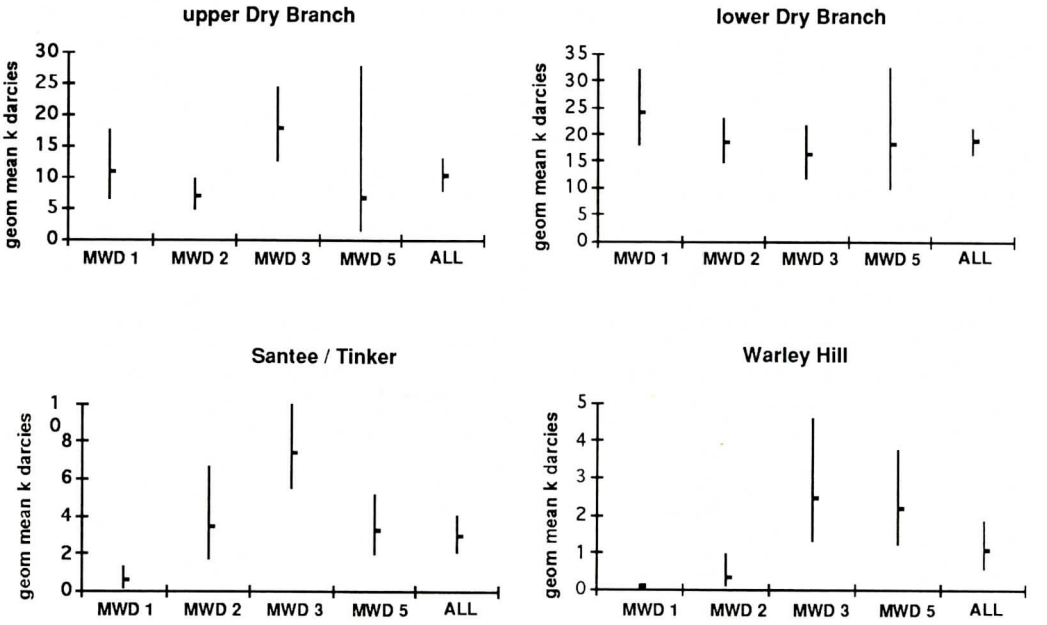

Figure 21.-Geometric mean permeability of the middle units in the MWD Well Field. Error bars represent 95% confidence interval.

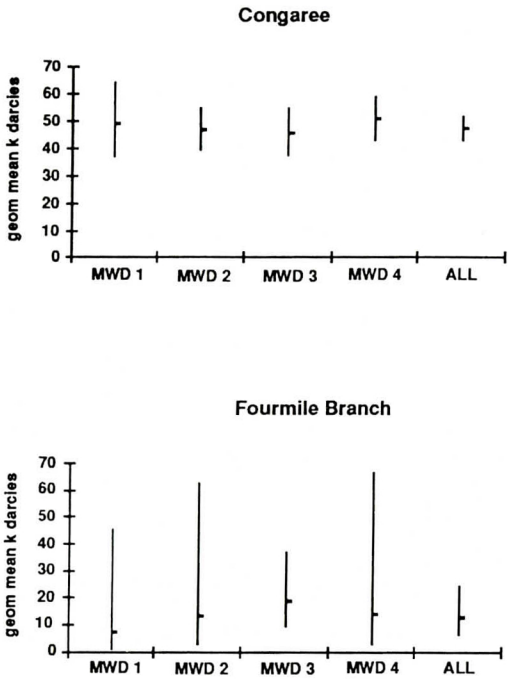

Figure 22. Geometric mean permeability of the lower units in the MWD Well Field. Error bars represent 95% confidence interval.

small number of samples from some units.

Permeabilities for individual units from well to well are in Table 6. In some cases dissimilarity of mean permeabilities from well to well is caused by changes in lithology within the unit. In other cases the dissimilarity may be caused by sparse sampling due to poor condition of the core or lack of core recovery. Some dissimilarities can not be explained by facies changes, inadequate number of samples, or lack of core recovery. The cause of the difference in means for the lower Tobacco Road between wells MWD 2 and MWD 3, for example, is unknown; the unit had nearly continuous core recovery and was sampled at 0.3-m intervals.

CONCLUSIONS

In the Tertiary section at the Savannah River Site, well permeability profiles can be correlated with one another to define zones of similar permeability in the same manner that lithologic and geophysical logs are correlated to define stratigraphic horizons. Permeability profiles show a remarkable correlation between visually estimated percent mud and gamma ray logs. In general, permeability decreases as the mud content and gamma ray count increase. A correlation coefficient of -0.92 was calculated for visually estimated mud versus the log of the permeability, and a correlation coefficient of -0.67 was calculated for gamma ray count versus the log of the permeability.

Statistical analyses indicate that each lithologic unit has a distinctpermeability distribution. In general, units consisting of poorly sorted sands and alternating lithologies have wide 95% confidence intervals for the geometric mean; but units exhibiting more uniform textural properties have relatively small confidence intervals. Significance tests indicate that geometric mean permeability within the same

Table 5.-Results of significance tests of geometric mean permeabilities between vertically adjacent units.

Formation	Well MWD 1	Well MWD 2	Well MWD 3	Well MWD 4
"upland" unit/ upper Tobacco Road	different	different	different	different
upper Tobacco Road/ middle Tobacco Road	different	different	different	different
middle Tobacco Road/ lower Tobacco Road	different	different	different	different
lower Tobacco Road/ upper Dry Branch	different	different	different	different
upper Dry Branch/ lower Dry Branch	different	different	same	same
lower Dry Branch/ (Santee/Tinker)	different	different	different	different
(Santee/Tinker)/ Warley Hill	different	different	different	same
Warley Hill/ Congaree	different	different	different	different
Congaree/ Fourmile Branch	different	different	different	same

Table 6.-Results of significance tests of geometric mean permeabilities for the same unit between wells.

Formation	Wells MWD 1-MWD 2	Wells MWD 1-MWD 3	Wells MWD 1-MWD 5	Wells MWD 2-MWD 3	Wells MWD 2-MWD 5	Wells MWD 3-MWD 5
"upland" unit	same	same	same	same	same	same
Upper Tobacco Road	same	same	same	same	different	different
Middle Tobacco Road	same	same	same	same	same	same
Lower Tobacco Road	same	same	same	different	different	different
Upper Dry Branch	same	same	same	different	same	same
Lower Dry Branch	same	same	same	same	same	same
Santee / Tinker	different	different	same	same	same	different
Warley Hill	different	different	same	different	different	same
Congaree	same	same	same	same	same	same
Fourmile Branch	same	same	different	same	same	same

lithologic unit is the same between wells, but permeability distribution is different between vertically adjacent units. There is no systematic difference between the horizontal and vertical measurements, the average difference between the measurements being about 1 darcy.

ACKNOWLEDGMENTS

We thank Mary K. Harris for making available unpublished results of 36 sieve analyses and several descriptions of core. Darryll T. Pederson made valuable suggestions which improved the manuscript. Funding for our research was provided by the United States Department of Energy and Westinghouse Savannah River Company through the South Carolina Universities Research and Education Foundation (SCUREF Task Order #26).

REFERENCES CITED

Beard, D. C., and Weyl, P. K., 1973, Influence of texture on porosity and permeability of unconsolidated sand: American Association of Petroleum Geologists Bulletin, v. 57, p.349-369.

Chandler, M. A., Kocurek, G., Goggin, D. J., and Lake, L. W., 1989, Effects of stratigraphic heterogeneity on permeability in eolian sandstone sequence, Page Sandstone, Northern Arizona: American Association of Petroleum Geologists Bulletin, v. 73, p. 658-668.

Cooke, C. W., and MacNeil, F. S., 1952, Tertiary stratigraphy of South Carolina: U. S. Geological Survey, Professional Paper 243-B, 29 p.

Colquhoun, D. J., 1992, Observations on general allostratigraphy and tectonic framework of the southeastern Atlantic coast regional cross section (DNAG E-5 corridor) Georgia and South Carolina as they relate to the Savannah River Site, *in* Fallaw, W. C., and Price, V., eds., 1992, Carolina Geological Society field trip guidebook, November 13-15, 1992, Geological investigations of the central Savannah River area, South Carolina and Georgia: U. S. Department of Energy and South Carolina Geological Survey, p. CGS-92-B-I-1-8.

Dennehy, K. F., Prowell, D. C., and McMahon, P. B., 1989, Reconnaissance hydrogeologic investigation of the Defense Waste Processing Facility and Vicinity, Savannah River Plant, South Carolina: U. S. Geological Survey Water Resources Investigation 88-4221,74 p.

Dreyer, T., Scheie, A., and Walderhaug, O., 1990, Minipermeameter-based study of permeability trends in channel sand bodies: American Association of Petroleum Geologists Bulletin, v. 74, p. 359-374.

Fallaw, W. C., and Price, V., 1992, Outline of stratigraphy at the Savannah River Site, *in* Fallaw, W. C., and Price, V., eds., 1992, Carolina Geological Society field trip guidebook, November 13-15, 1992, Geological investigations of the central Savannah River area, South Carolina and Georgia: U. S. Department of Energy and South Carolina Geological Survey, p. CGS-92-B-II-1-33.

Firoozabadi, A., and Katz, D. L., 1979, An analysis of high-velocity gas flow through porous media: Journal of Petroleum Technology, v. 31, no. 2, p. 211-216.

Folk, R. L., 1980, Petrology of sedimentary rocks: University of Texas Press, Austin, Texas, p.42-53.

Folk, R. L., and Ward, W. C., 1957, Brazos River Bar: a study in the significance of grain size parameters: Journal of Sedimentary Petrology, v.27, p. 3-26

Fraser, H. J., 1935, Experimental study of the porosity and permeability of clastic sediments: Journal of Geology, v. 43, p. 910-1010.

Goggin, D. J., 1988, Geologically sensible modeling of the spatial distribution of permeability in eolian deposits: Page Sandstone (Jurassic) northern Arizona: Unpublished Ph.D. dissertation, University of Texas at Austin, Austin, Texas, 417 p.

Goggin, D. J., Thrasher, R. L., and Lake, L. W., 1988, A theoretical and experimental analysis of minipermeameter response including gas slippage and high velocity flow effects: In-Situ , v.12, no. 1 & 2, p. 79-116.

Huddlestun, P. F., 1988, A revision of the lithostratigraphic units of the Coastal Plain of Georgia the Miocene through Holocene: Georgia Geological Survey Bulletin 104, 162 p.

Huddlestun, P. F., and Hetrick, J. H., 1978, Stratigraphy of the Tobacco Road Sand--a new formation: Georgia Geologic Survey Bulletin 93, p 56-76.

Huddlestun, P. F. and Hetrick, J. H., 1986, Upper Eocene stratigraphy of central and eastern Georgia: Georgia Geological Survey Bulletin 95, 78 p.

Krumbein, W. C., and Monk, G. D., 1943, Permeability as a function of size parameters of sedimentary particles: American Institute of Mining and Metallurgical Engineering, Technical Publication 1492, p. 153-163.

Logan, R. W., and Euler, G. M., 1989, Geology and ground-water resources of Allendale, Bamberg, and Barnwell counties and part of Aiken County, South Carolina: South Carolina Water Resources Commission, Report 155, 76 p.

Marine, I. W., and Siple, G. E., 1974, Buried Triassic basin in the central Savannah River area, South Carolina and Georgia: Geological Society of America Bulletin, v. 85, p. 311-320.

McClelland, S. A., 1987, Surface and subsurface stratigraphy of Cretaceous and younger strata along the Savannah River from southern Richmond County through Burke County, Georgia: Unpublished master's thesis, University of South Carolina, Columbia, South Carolina, 123 p.

Nystrom, P. G., Jr., and Willoughby, R. H., 1982, Cretaceous, Tertiary, and Pleistocene(?) stratigraphy of Hollow Creek and Graniteville quadrangles, Aiken County, South Carolina, *in* Nystrom, Jr., P. G., and Willoughby, R. H., eds., 1982, Geological investigations related to the stratigraphy in the kaolin mining district, Aiken County, South Carolina: Carolina Geological Society Field Trip Guidebook 1982, South Carolina Geological Survey, Columbia, South Carolina, p. 80-113.

Nystrom, P. G., Jr., and Willoughby, R. H., 1992, The upland unit in the Savannah River Site: distribution, lithology, depositional environment, and age: Geological Society of America 1992 Abstracts with Programs, v. 24, no. 2, p. 56.

Nystrom, P. G., Jr., Willoughby, R. H., and Kite, L. E., 1986, Cretaceous-Tertiary stratigraphy of the upper edge of the Coastal Plain between North Augusta and Lexington, South Carolina: Carolina Geological Society Field Trip Guidebook 1986, South Carolina Geological Survey, Columbia, South Carolina, 82 p.

Prowell, D. C., Christopher, H. A., Edwards, L. E., Bybell, L. M., and Gill, H. E., 1985, Geologic section of the updip Coastal Plain from central Georgia to western South Carolina: U. S. Geological Survey Miscellaneous Field Studies Map MF-1737, 11 p.

Pryor, W. A., 1973, Permeability patterns and variations in some Holocene sand bodies: American Association of Petroleum Geologists Bulletin, v. 57, p. 162-189.

Reineck, H. E., and Singh, I. B., 1980, Depositional sedimentary environments: Springer-Verlag, New York, 549 p.

Robertson, C. G., 1990, A textural, petrographic, and hydrogeological study of the Congaree Formation at the Savannah River Site, South Carolina: Unpublished master's thesis, University of North Carolina at Wilmington, Wilmington, North Carolina, 65 p.

Siple, G. E., 1967, Geology and ground water of the Savannah River Plant and vicinity, South Carolina: U. S. Geological Survey Water Supply Paper 1841, 112 p.

Sloan, E., 1908, Catalogue of the mineral localities of South Carolina: South Carolina Geological Survey, series V, Bulletin 2, The State Co., Columbia, S. C. Reprinted by South Carolina Geological Survey, Columbia, South Carolina, 1979, 506 p.

Snipes, D. S., Stieve, A., Price, V., Fallaw, W. C., Kegley, W. P., and Daggett, J. S., 1992, Middle Eocene "green clay interval" at the Savannah River Site, South Carolina: Geological Society of America Abstracts with Programs, v. 24, no. 2, p. 65.

Snipes, D. S., Fallaw, W. C., Price, V., Jr., and Cumbest, R. J., 1993, The Pen Branch Fault: documentation of Late Cretaceous-Tertiary faulting in the Coastal Plain of South Carolina: Southeastern Geology, v. 33, p. 195-218.

Temco Inc., 1991, Manual for minipermeameter: Temco, Inc., Tulsa, Oklahoma, 19 p.

Tyler, N., Barton, M. D., and Finley, R. J., 1991, Outcrop characterization of flow unit and seal properties and geometries, Ferron Sandstone, Utah:

Society of Petroleum Engineers Annual Technical Conference and Exhibition, SPE 22670, p. 127-134.

Weber, K. J., 1982, Influence of common sedimentary structures on fluid flow in reservoir models: Journal of Petroleum Technology, v. 34, p. 665-672.

Weber, K. J., Leijnse, D., and Moens, C., 1972, Permeability distribution in a Holocene distributary channel-fill near Leardam (The Netherlands), permeability measurements and in-site fluid-flow experiment: Geologic En Mijndoun, v. 52, no. 1, p. 53-62.

Westinghouse Savannah River Company, 1991, Site hydrology/geotechnical characterization report for Site B, Site, v. 1, document no. WSRC-RP-91-392: Westinghouse Savannah River Company, Aiken, South Carolina.